MOLECULAR AND CRYSTAL ORBITAL STUDIES OF ORGANIC CRYSTAL FORMATION

By

ARTËM   EDUARDOVICH   MASUNOV

A dissertation submitted to the Graduate Faculty in Chemistry in partial fulfillment of the requirements for the degree of Doctor of Philosophy, The City University of New York.

2000

8 2000

ARTËM   EDUARDOVICH   MASUNOV

This manuscript has been read and accepted for the Graduate Faculty in Chemistry in

satisfaction of the dissertation requirements for the degree of Doctor of Philosophy.

_____   _____

Date   Chair of Examining Committee

_____   _____

Date   Executive Officer

Prof. J. J. Dannenberg

Prof. Max Diem

Prof. Richard Franck

Prof. Louis Massa

Prof. Jerome Schulman

Supervisory Committee

THE CITY UNIVERSITY OF NEW YORK

Abstract

MOLECULAR AND CRYSTAL ORBITAL STUDIES OF ORGANIC CRYSTAL FORMATION

by

Artem Masunov

Adviser: Professor J. J. Dannenberg

Ab initio molecular orbital and crystal orbital methods are applied to the study of the geometry of hydrogen-bonded organic crystals and to predict the relative stability of polymorphic modifications. Cluster calculations of para-benzoquinone, of urea and of thiourea at HF, DFT, and AM1 levels with pseudotranslational constraints allow for the analysis of the energies for each type of H-bonds and their dependence on the cluster size. Periodical calculations on infinite systems are in good agreement with the results of cluster calculations. The cooperative components of intermolecular interaction, which are neglected in the most empirical force-field models account for up to 30% of the total interactions in the systems considered. This non-additivity is shown to lead to experimentally observed differences in crystal packing between urea and thourea, and can be successfully reproduced at the practically justified approximations.

One important application of MO calculations is to build simple yet accurate models for intermolecular interactions. Modifications of the basis set by optimizing the centroid positions of each basis function (floating basis set) combined with

semiempirical values for exponent factors are suggested for this purpose. Such a wavefunction satisfies the Hellman-Feynman theorem and its electron density can be exactly represented by point charges.

The methodology developed in this work, may be applied to the rational design of crystals with required properties. This will be useful to solve practical problems of crystal engineering, and material science.

TABLE OF CONTENTS

Chapter   **Page**

LIST OF FIGURES

Figure   **Page**

LIST OF TABLES

CHAPTER 1

1. INTRODUCTION

The purpose of this thesis is to apply *ab initio* molecular orbital (MO) and crystal orbital (CO) methods to interpret geometry of organic crystals. The methods are also applied to prediction of relative stability of polymorphic modifications. Success in the interpretation and prediction of organic crystal structures will assist material science in synthesizing the materials with particular properties. It will also advance the understanding of the structure for other condensed phases such as liquids and biopolymers. The results are discussed in the framework of the contemporary state of the field. In this study the supermolecular (cluster) and periodical approaches were applied to crystals with H-bonds at different levels of theory: semiempirical, Hartree-Fock (HF), and post-HF. It will be shown that the cooperative component of intermolecular interaction can be as large as 30% of the total interaction. On the example of urea and thiourea we will show how this cooperativity can lead to experimentally observable differences in crystal packing, and can be successfully reproduced with practically justified approximations.

Chapter 2 gives a brief overview of the methods for solid-state simulations. The existing methods of organic crystal structure predictions require a large number of energy evaluations, making the application of the empirical force field method a necessity. In many cases additive approximations are used for simplification. Some ofthem employ *ab initio* calculations to fit the force field parameters. The empirical

force-field approach has proved effective, but its applicability to the novel system types is uncertain. *Ab initio* methods of crystal calculation (both periodical and cluster approach) are far more reliable. At present no code for calculation of analytical derivatives for the periodic system is publically available, which makes geometry optimization unfeasible. The cluster approach makes the use of existing program packages for molecular *ab initio* calculations, and allows to analyze components of molecular interactions in details. However, this approach yields results for finite aggregates and it is applicable to periodical systems in asymptotic limits only.

Chapter 2 also summarizes the data on the molecular, cluster, and crystal structures of urea and thiourea. It addresses the consistency of *ab initio* calculations and experiments on energies and geometries of these systems. The joint application of single-point cluster and periodical calculations based on known crystal structure is applied in Chapter 3 to the case of crystalline benzoquinone, urea, and thiourea. When the crystal structure is not experimentally known, single point calculations are no longer applicable. This necessitates a thorough investigation based on constrained geometrical optimization of molecular clusters of different sizes. The results of such an investigation applied to urea and thiourea are reported in Chapters 4, 5 and 7 (for dimers, one- and two/three-dimensional clusters respectively).

One of the important applications of MO calculations at the high level of theory is to build simple yet accurate models for intermolecular interactions. Our attempts to build such a model in order to simulate *ab initio* data, as well as our suggestions for its improvements, are described in Chapter 6. According to the Hellman-Feynman theorem, forces on nuclei in the molecular system can be calculated classically from the charge density of the molecule. Therefore, when building an

electrostatic model, one has to make sure that (a) wavefunction complies with the Hellman-Feynman theorem, and that (b) electron density is reproduced by classical charge distribution to an acceptable approximation. By comparing classical charge distribution schemes in the form of different partial atomic charge separation methods, we found that the *ab initio* values on interaction energy in the urea chain dimer are best reproduced by Mulliken charges. This charges are used to describe polarization effects in larger chain clusters. Chapter 6 also describes the modifications to the basis set by optimizing centroid positions of each basis function. This, in turn, allows the wavefunction to satisfy Hellman-Feynman theorem. The resulting charge distribution is also significantly improved so that the residual electric field in the nuclei of the optimized molecule vanishes. Since the existing codes are not well suited to handle the floating basis sets, these calculations present a computational challenge. However, floating basis set alows to decrease the number of the basis functions N to the minimum, thus greatly reducing computational costs while maintaining built-in polarization flexibility of the basis set. We suggest a semiempirical approach to optimizing parameters of this minimal floating basis set. The ability of the wavefunction in the form of a minimal floating basis set to be exactly represented by point charges opens the possibility of building classical and combined models based on the described wavefunction. Finally, we discuss some donor-acceptor models, alternative to the electrostatic description of H-bonds.

The methodology developed in this work could be applied to the rational design of crystals with desirable properties to solve practical problems of crystal engineering and material science.

CHAPTER 2

2. RECENT ADVANCES IN CRYSTAL STRUCTURE SIMULATION AND UREA/THIOUREA STRUCTURE

In this Chapter we will review the methods presently applied to simulate crystal structure at empirical and *ab initio* levels. We will also consider the relevant data available at present in the literature on the structures and energies of molecular and crystalline urea and thiourea.

2.1 Empirical force-field potentials

The first simulations of molecular crystals were done by means of analog modeling: molecules were represented as a collection of overlapping atomic solid spheres.[1] Digital extension of this model is called force-field and employs smooth potentials with simple analytical expressions, including number of empirically adjusted parameters. The most widely used form of nonbonded potential is the Buckingham potential (1-6-exp):

$$V(r_{ij}) = A \exp(B\ r_{ij})\ B\ C\ r_{ij}^{-6}\ B\ q_i q_j\ r_{ij}$$

where i and j are force centers of the different molecules. The repulsion exponent term is sometimes replaced with softer r_{ij}^{-12} or r_{ij}^{-10} dependence. The last term of this

expression is the Coulomb interaction of two point charges. The form of this function

is justified by intermolecular perturbation theory (IMPT).[2] If one ignores overlap

between molecular wavefunctions and treats the influence of the second molecule as a

perturbation, an electrostatic term appears in the first order, while the dispersion r_{ij}^{-6}

term appears in the second order along with polarization, which will be discussed

below. To obtain the repulsion term one has to include overlap. This brings exchange

repulsion in the first order, and cross-terms in the second order. The part of

polarization term containing electronic excitations from occupied orbitals of one

molecule into vacant orbitals of another is often regarded as charge transfer term. The

resulting expression for energy becomes more complex, but at present, it is well-

studied and coded in computer programs such as SAPT[3] and CADPAC.[4]

At early stages of force-field development, force centers were associated with

atoms and parameters *A, B,* and *C,* as well as the charges were adjusted to fit empirical

data. Later the charges were obtained from population analysis of molecular

wavefunction (for instance, by Mulliken) or by fitting the molecular electrostatic

potential. At present there are several techniques applied for this purpose. Different in

details, they all based on the set of point charges (PC) and multipoles distributed in

space (not necessary on atoms). The values for these charges (multipoles) are obtained

directly from the wave function with a projection technique or indirectly via a

procedure of fitting values to the molecular electrostatic potential in the region of

interest (usually in the range from 1 to 2 Van der Waals distances form any atom). We

will compare these schemes in Chapter 6.

Additive transferable force-fields are the most computationally efficient representation of molecular electronic structure, and for this reason they are widely used for simulation of the structure and properties of condensed matter. However, they are not the most accurate and reliable way to describe molecular interactions. The necessity to develop models with polarizable potentials is clearly understood.[5,6] The traditional way to improve the force field method is to add polarizable centers to the model. Each of these centers is characterized by polarizability tensor α, proportionality constant between the external electric field F and the induced dipole moment μ:

$$\mu = \alpha\, F$$

Polarization allows the interaction energy to be a nonlinear function of the field strength. Dipolar (or second) polarizability is the derivative of the energy with respect to the field strength. The derivatives of the energy with respect to the field gradient (quadrupole polarizability, hyperpolarizability) makes description even more precise, but they are usually neglected for practical purposes.[7] The potential function has to be modified so that it includes the interaction of these induced dipole moments with point charges and with other dipole moments. Since energy has quadratic dependence on field strength, the appearing cross-terms result in 3-body interactions. The force field is no longer pairwise additive, as it includes the interaction energy of the molecule A with dipoles on the molecule B, induced by the molecule C. However, if no mutual polarization is considered, this model is three-body additive. Accounting for back polarization will introduce many-body effects.[7]

In some implementations both polarizabilities and magnitudes of PCs are

considered empirical parameters. In such a case these parameters absorb inaccuracies introduced in other parts of the potential function. A more rigorous approach requires the use of accurate molecular electric properties. The reasonable choice of polarizable centers makes the polarizable model transferable at least for some classes of molecules.[8] The non-pairwise (cooperative) feature of polarization means that it can play a crucial role in reducing intermolecular separation with increasing aggregation. This is important for construction of the force fields suited for both small clusters and condensed phases. However, accounting for polarization will be efficient only if it is the primary reason for the change in molecular electronic structure.[7]

Another way to describe polarization, called fluctuating charge, was suggested by Berne, Freisner et al.[9,10] In this approach atomic charges are considered to be variables, depending on molecular environment. Parameterization is done by electronegativity equalization[11,12] (which was modified to emulate *ab initio* results). However, there are cases (such as the out-of-plane polarization of a planar molecule or of a bifurcated H-bond to oxygen),[10] where a PC-only model is not sufficiently flexible. This made necessary the introduction of inducible atomic dipoles.[13] It is, however, possibile to retain an attractive and efficient PC scheme by using several point charges close to the atomic position. A model containing nine PCs for each heavy atom was constructed by Clark and Rauhut.[14] The positions and magnitudes of the charges are associated with centroids of each lobe of the natural atomic hybrid orbitals, which eliminates any fitting. A procedure involving numerical integration of the Slater-type functions was incorporated into the semiempirical package VAMP.[15]

Another approach is to keep the magnitude of the charge constant, but to allow the position of the charge to vary. This possibility will be further discussed in Chapter 6.

We should note here that any model including PC needs to explicitly account for long-distance interactions. By contrast, models including only distributed dipoles (and higher multipoles) allow for small cutoff radii.[16] In Chapter 7 we will show, that one has to include interactions at 50 Å in order to obtain convergence in electrostatic energy. Fortunately, the fast multipoles methods have recently been developed to avoid this problem.[17]

Precise intermolecular force fields have to be individually constructed for each molecule. They are usually based on supermolecule or on intermolecular perturbation theory calculations. The latter are used more often, as IMPT gives separate values for exchange, polarization, and dispersion terms, whereas supermolecule calculation gives only total interaction energy. Some of the examples will be mentioned later in this Chapter. It is necessary to note that perturbation theory treatment beyond the second order yields nonadditive terms not only in the electrostatic components of the energy but also in dispersion attraction and exchange repulsion.[18]

2.2 Force-field periodical calculations and prediction of molecular packing

In typical prediction of crystal structure, hundreds of thousands of starting points are used and hundreds of energy evaluations are necessary for optimization

from each of these starting points. Such a large number of energy evaluations make direct application of MO methods to the problems of this kind impractical. The conventional approach here is to represent the energy by an analytical function with adjustable parameters (create a force-field) and perform optimization of that function.

Whereas optimization of molecular crystal structure using empirical potentials is not a problem, it is much more difficult to predict this structure *a priori*. The very possibility of organic crystal structure prediction is still uncertain.[1] There are several reasons for these difficulties: (a) The shape of a potential surface is complex, with multiple local minima. The complexity here is close to the problem of protein folding. (b) Kinetics may play an important role in crystallization, so that the real structure may not be the global minimum on the potential surface. (c) Empirical force fields may be well fit to represent one region of the potential surface, but not the others. Despite the difficulties, several attempts have been made to predict crystal structures.[19] At present, there are two major approaches to crystal structure prediction. The first could be briefly described as stepwise increasing dimensionality. This method was introduced and used for analog simulations by Kitaigorodskii (*aufbau* algorithm).[1] Gavezzotti later published the computer program PROMET, based on similar ideas.[20] The program optimizes finite-size molecular clusters with the constraints of single crystallographic symmetry operations (including translations, screw axes, and glide planes). The optimization is repeated, starting with different operation or different orientation of the molecule with respect to the symmetry operation. The final geometry represents finite or 1D-cluster. The structures corresponding to the lower energy are

accepted as rigid units to the next step, where 2D-clusters are built. The best structures are used on the third step to build 3D-structures. After final 3D-optimization, a few hypothetical crystal structures are obtained. Unfortunately, only structures with one molecule in an asymmetric unit are considered in PROMET. Successful applications of this program have, however, been published.[21] We will adopt this step by step dimensionality increase for our cluster calculations.

Another approach was introduced by Gdanitz[22] and employs brute computer force. The first step is Monte-Carlo sampling of the configuration space (made of unit cell parameters, molecular center coordinates, orientations, and internal rotation angles for all independent molecules). The second step includes rough optimization and filtering out equivalent structures. In the third step simulated annealing is used to get rid of the shallow minima. Finally, after fine optimization and filtration, a set of nonequivalent polymorph structures is obtained. The final version of the software became the POLYMORPH module in the Cerius[2] package,[23] commercially available from MSI. A program based on a similar approach is called UPACK[24] and uses a regular grid instead of Monte-Carlo sampling in the configurational space. In principle, if the search starts with a large enough unit cell in P1 group, all space group symmetries may be obtained. However, because of computer time considerations the search is restricted to the most common space groups.

Finally, another program by Perlstein, called PACK,[25] which is commercially available from Chemical Design Inc., applies Monte-Carlo sampling and simulated annealing to construct low-dimensional periodical structures. This combines the two

approaches described above. The reduction of dimensionality makes it practically

possible to treat of up to three symmetrically independent molecules with up to twelve

intramolecular degrees of freedom. The program has been successfully applied to the

packing of polymer chains and monolayers.[26] Some new programs,[27] as well as new

versions of older programs such as LMIN[28] and others, perform a single 3D-

optimization in which the predicted crystal structure depends on the starting point

used.

Some of the latest crystal packing suites, such as MPA by Williams[29] and

GULP by Gale,[30] have the option of optimizing finite clusters, as well as 1,2,3D-

periodicals, and of fitting force field parameters to the set of experimental data.

2.3 *Ab initio* and semiempirical periodical calculations

Fortunately, even optimization with an arbitrary force field (like solid spheres)

leads in most cases to a reasonable crystal structure because of the close packing of

organic molecules. To obtain a correct energy for this structure, more precise (and

computationally expensive) MO methods could be applied. Historically, Crystal

Orbital calculations of solid state were undertaken using (oversimplified)

semiempirical zero-overlap non iterative approximations based on hybrid atomic

orbitals, such as tight-binding[31] and Fenske-Hall[32] models. One the other hand, metals

(as opposed to covalent crystals) were historically treated using electron gas models,

from which density function theory was eventually developed. Some examples of

computer programs that implement non-iterative methods are YAeHMOP,[33] the

extended Hückel method (suitable for CO calculations but not for geometry

optimization), and VEH[34] (parameterized to reproduce bond lengths in 1D-polymers).

Though computationally light, these models still attract some attention as linear

scaling methods for large systems and MD simulations.[35] The introduction of various

population-dependent iterative schemes into these methods allows one to build

semiempirical DFT schemes.[36] Unfortunately, standard semiempirical packages are

not well suited to 3D-periodical calculations (if implemented). For instance,

MOPAC6[37] (which has 3D-capability, and not only 1D-, as it is stated in the manual)

uses only one point for integration in the Brillouin zone and therefore needs the

generation of a large supercell in order to give reasonable results.

Recent advances in DFT methods, such as gradient corrections to exchange-

correlation functional and hybrid functionals including exact HF exchange, have made

possible the accurate description of H-bonding. For instance, these methods were

reported to give the interaction energies for the water dimer as good as or better than

second order Møller-Plesset (MP2) calculations.[38,39,40] While electron-correlation is

accounted for in DFT methods, these methods have not been successful in calculating

dispersion interactions,[41] which makes them an imperfect tool for the study of organic

crystals. In this work we used two hybrid functionals: the B3PW91 method combining

Becke's 3-parameter functional[42] with the non-local correlation provided by the

Perdew-Wang expression,[43] and B3LYP, combining the same Becke functional with

the correlation functional of Lee, Yang and Parr.[44]

Most of the modern DFT packages, although they allow optimization and even molecular dynamics (MD) calculations on solid state systems, still use plane wave basis sets, and this makes comparison with molecular MO calculations rather difficult. Although the plane-wave basis set is more suitable for description of highly delocalized electronic structures typically found in metals, molecular crystals are described reasonably well. The recent MD study of HBr crystal phases at high pressure[45] employing the program CPMD[46] reproduced orientational ordering, symmetrization of H-bonds, transition from the FCC to the HCP, and molecular dissociation as the pressure increased.

Among the packages that implement plane-wave DFT treatment, areVASP,[47] CP-PAW,[48] FHIMD98,[49] and CASTEP.[50] To allow the comparison, some of the packages (Wien95,[51] and ADF[52]) offer plane-wave calculations for isolated molecules. To date, only a few programs use atom-centered gaussian basis functions, usual for MO calculations: DMol3[53] (DFT only), PLH[54] (1D-periodicals only), GAPSS,[55] and CRYSTAL[56] (DFT and HF calculations). CRYSTAL can be used to perform infinite periodic calculations in three (crystals), two (slabs), one (polymers), or zero (molecules) dimensions. The periodic nature[57] of the calculations dictates certain approximations, as well as certain basis sets. In our calculations, described in Chapter 3, we chose the 6-21G** basis set, as it is also a standard GAUSSIAN[58] basis set and similar to the 6-31G** basis set generally used. The use of better basis sets for 3D-periodical calculations, including more diffuse primitive gaussian functions with exponent factors below 0.2 (not necessarily A+@ functions), often results in SCF

convergence problems,[59,59a] due to pseudo linear dependence. Unfortunately, the

procedure of eliminating linear dependent functions from the basis set, implemented in

GAUSSIAN 98, was not yet incorporated into CRYSTAL. As analytical derivatives

are not available in CRYSTAL 95/98, geometry and basis set optimizations, as well as

frequency calculations can be done numerically using a Unix shell script.[60] This is

feasible for systems with only a few geometrical variables, like ice VIII.[41]

A major disadvantage of using the gaussian basis set for Crystal Orbital

calculations is basis set superposition error (BSSE). The essence of BSSE is the

nonphysical stabilization of one molecule in the presence of basis functions located on

the other molecules in the system. The BSSE is particularly large for small basis sets,

but vanishes upon approaching complete-basis limit. In supermolecule calculations,

the customary (but controversial[61]) way to account for BSSE is counterpoise (CP)

procedure:[62]

$$CP = E(A, basis\ A) - E(B, basis\ AB) + E(B, basis\ B) - E(B, basis\ AB)$$

All energies should be calculated in the geometry optimal for the dimer, if the

optimization is performed.[63] It was shown,[64] that generalization for larger clusters does

not give unique results (which is sometimes regarded as a Dannenberg-Turi paradox),

unless one uses the sum of individual CP corrections calculated for each monomer in

the basis of all monomers in the cluster:

$$CP(M) = E(M, basis\ M) - E(M, basis\ M_n)$$

CP procedure was recently extended by Duran, Dannenberg et al.[65] to gradients and

Hessians using consecutive executions of GAUSSIAN from the Unix shell script,

which allows for geometry optimization on BSSE corrected potential energy surfaces. There are at least two other alternatives to BSSE corrected optimizations. One is the SCF-MI method introduced by Gianinetti, Raimondi et al.[66] And implemented in GAMESS-UK,[67] which modifies SCF equations to keep MOs localized on different monomers. The resulting wavefunction is close to an artificial state with charge transfer turned off, which was built in Kitaura-Morokuma[68] analysis (electrostatic, polarization, and exchange interactions remain). To bring back this meaningful part of intermolecular interaction, it was suggested to explicitly correlate the orbitals that form H-bonds via valence-bond formalism.[69] Mayer's Chemical Hamiltonian method[70] modifies the Fock matrix to exclude elements responsible for BSSE. It was implemented[71] in the POLYGAUSS program for periodical *ab initio* calculations. An alternative method for BSSE elimination at MP2 level, based on local MP2 treatment, was recently developed and implemented in the MOLPRO package by Werner, Schutz et al.[72] Full CP corrected optimization for the HF part of the energy is implemented in the latest version of this program.

Since full CP is impossible for the infinite crystal, only basis functions of the nearest atoms are used for CP calculations in CRYSTAL.[55] Our attempts to find the distance limit to select the nearest neighbors run into limitations in computational resources sooner than convergence in CP values was reached. In most cases CP evaluations were computationally more expensive than the 3D-calculation itself. A possible solution to this problem is to select only those basis functions that have sizable amplitude on the atoms of the monomer.

Post-HF periodical calculations have also been published, including the MP2/MP4 study on layers of formamide (using POLYGAUSS),[73] chains of water molecules[74] and HCN crystals[75] (using customized algorithms). Coupled-cluster (CC) methods were applied for 1,2D-systems of He atoms and implemented in the PNO-CEPA code.[76] Analytical derivatives for 1D-periodical systems made possible frequency calculations on chains of HF molecules.[77] Analytical first derivatives for 2,3D-periodical systems were also derived.[78] Periodical capability is expected to be added to the CC code ACES II, and to the HF/DFT part of GAUSSIAN 2000.

2.4 *Ab initio* cluster calculations

Another approach to the theoretical description of the crystals is applied in cluster calculations. The crystal environment of the molecule is usually simulated by point charges (PC)[79] and/or by a finite (usually small) number of neighboring molecules[80] (supermolecule calculations). Earlier approaches assumed pairwise additivity and estimated lattice energy as the sum of dimeric interactions.[81] We will assess the limitations of this approach in Chapters 3 and 5. A combined PC/supermolecule approach is consistently used by Van Alsenoy et al.[82] They have been able to perform optimizations and frequency calculations on relatively large clusters (15 molecules) using a multiplicative integral approximation that treats four-center integrals as a linear combination of three-center integrals. This approach is implemented in the BRABO package. The cluster is embedded in a field of point

charges representing a finite number (usually hundreds) of distant neighbors. As Madelung sums are known to converge slowly, even hundreds of distant neighbors may not be enough to simulate the infinite crystal environment. This is why a special fitting procedure for the values and positions for the limited number of point charges designed to efficiently simulate infinite crystal seems to be useful.[83]

Unfortunately, the point charge method has certain limitations. Sublimation energies were not considered in the papers referenced above and are not well evaluated by point charges method even with the nearest neighbors taken into account explicitly. Also, only the crystal field effects on intramolecular geometry and vibrational frequencies were studied. Intermolecular geometry was not optimized. A wider range of properties can be evaluated if isolated (or implicitly solvated) molecular clusters are considered.

Probably the most attention was paid to study of the water clusters. Here we briefly mention just one paper, since OH...O bonds are not considered in our study. Water cyclic clusters up to the hexameter were optimized[84] at HF and MP2/aug-cc-pVDZ and TZ level of theory, and many-body effects in the interaction energy were analyzed. Three-body effects were found to be up to 30% of the total interaction (depending on the point on a potential surface), whereas four-body and higher order terms were found negligible. Correlation correction was found to account for a 10-20% increase in two-body terms and for a 75% increase in three-body terms.
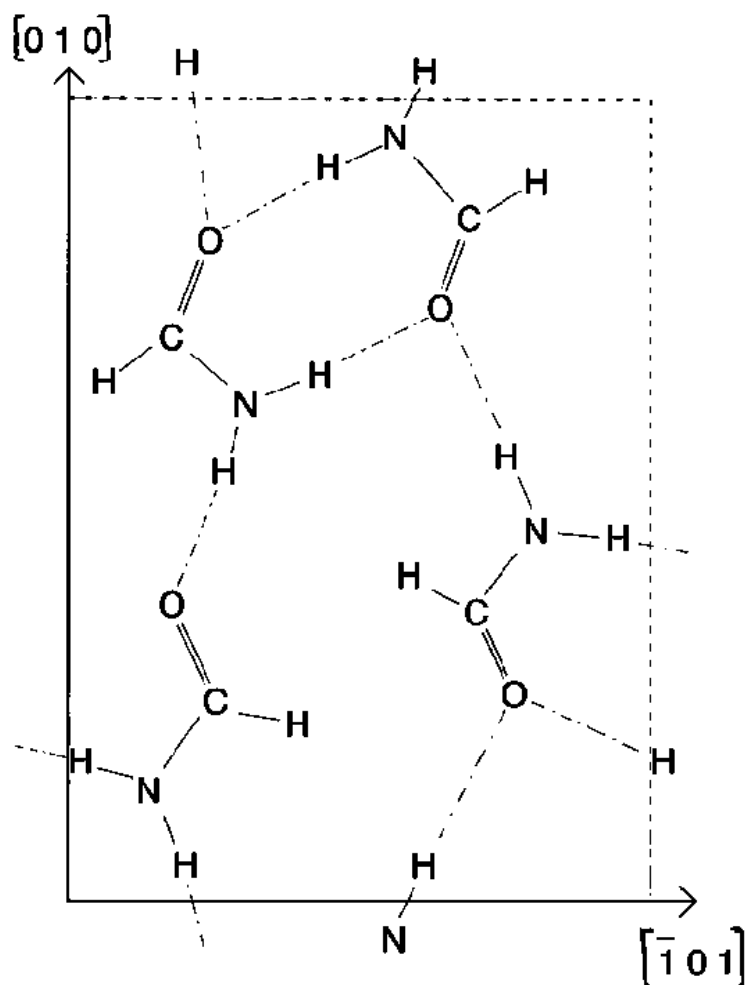
Figure 2.1. 2D H-bonded network in crystal structure of formamide. Cyclic H-bonded dimeric units are joined by H-bonds in a puckered layer. Alternative description: zigzag chains of the molecules parallel to Y-axis are connected by cyclic H-bonds. Reproduced from ref. 85.

A comparisons of cluster and periodical HF, DFT, and MP2/MP4 calculations (with total optimization of geometry) was recently done by Suhai[85] on the example of formamide. The molecular and crystal structures of this compound are closely related to those of urea (Figure 2.1), so the obtained results are important for our study. The results showed C=O and N-H bond elongation, and C-N shortening upon H-bond

formation. At all levels, the energy of the last H-bond in the infinite chain of head-to-tail structure was 60% greater than in the dimer, due to cooperative effects. However, the formation of 2D-infinite structures leads to weakening of the H-bonds in the cyclic dimeric units, compared to isolated dimers. The author found, that convergence of geometrical and energetic parameters is slow (even pentamer recovers only 60-70% of the energy changes observed between the dimer and the infinite chain). The basis set was found to have greater effect on DFT results than on those for HF and even MP2. The TZ(2d,2p) basis was necessary to achieve agreement with the experimental bond lengths. BLYP was found to agree with the MP2 results better than many other DFT functionals (including B3LYP).

Intermolecular perturbation theory was also applied to formamide dimers.[86] Five minimum energy conformations were found, with the cyclic centrosymmetric dimer being the most stable. An accurate polarizable potential was constructed to reproduce these results. When this potential was applied to calculate clusters up to eight molecules, the last H-bond in the linear clusters was found to have 25% cooperativity. The preference of linear chains over cyclic dimers in the liquid phase[87] was attributed to this cooperativity.

Linear chains $(HCN)_n$, n=2-7 considered by King and Weinhold[88] are other examples of cluster calculations. 40% of the last H-bond energy in the heptamer at HF/6-31+G* level was found to be due to cooperativity. An average dipole moment per molecule was found to increase from 3.3 D for the monomer to 3.6 D for the dimer, to 4.1 D for the heptamer. The calculation results agree well with geometrical

parameters, and with vibrational and nuclear quadrupole resonance spectra. No

comparison with crystals or periodical calculations was made. Employing the

nonpolarizable electrostatic model, and considering the interactions only between the

nearest neighbors, the authors argued that only a charge transfer can give a correct

description of the cooperative effects. In a comment on this paper, a quantitative

electrostatic description including distributed atomic multipoles and polarizabilities

for the same system was used by Stone and Buckingham.[89] These authors showed that

nonpolarizable treatment yields 15% of the last H-bond strength cooperativity due to

distant interactions. If polarization is included, 30% cooperativity is obtained. The

average dipole moment per molecule was found to increase from 3.0 D for the

monomer to 3.4 D for the dimer to 3.8 D for the octamer. Similar results were

obtained with a polarizable force field constructed to reproduce IMPT results for HCN

dimers: 27% cooperativity, and dipole moment from 3.0 D for the monomer to 3.3 D

for the dimer to 3.7 D for the octamer.[90] In an *ab initio* study by Karpfen,[91] both linear

and cyclic clusters of hydrogen cyanide and cyanoacetylene up to decamers were

examined at HF, B3LYP, and MP2 levels with different basis sets. Cyclic clusters

(Figure 2.2) were found to exhibit stronger cooperativity (up to 70%) and to be more

stable beginning from tetramer for both species. This is an opposite trend to the one

observed from the formamide clusters described above. Stacking clusters with parallel

and antiparallel orientations of cyanoacetylene molecules, typical of crystals, were

found[92] to have stability comparable to that of cyclic clusters.

A similar energy preference of cyclic to linear clusters was found in an MP2/6-
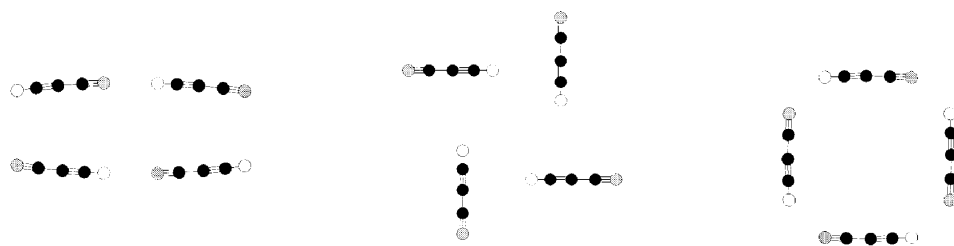
Figure 2.2.Structures of cyanoacetylene tetramers: antiparallel stacking arrangement of two linear dimers (left), pinwheel structure (center), and cyclic structure (right). Reproduced from ref. 90.

31+G** study on trimers consisting of methanol and water molecules.[93] A donor-acceptor orbital description was again used to rationalize these results. The authors referred to an earlier study[94] of water trimers, in which many-body polarization effects were able to recover only 60% of non-additivity. In another MP2/6-311++G** study on trimers consisting of methanol and trifluoromethanol[95] cooperative effects were found for both energies, H-bonding distances, O-H bond lengths, shifts in the stretching frequencies of the donor O-H bond, and electronic charge densities at the bond critical points. Similar cooperative effects on these properties were also found in a B3LYP/6-311G** study of ethanol[96] and 1-propanol[97] clusters.

Clusters of up to four molecules of methylamine were considered in another study.[98] At HF, B3LYP, and MP2/6-31+G* levels non-additive contribution to the interaction was found to be in the range of 12-18%. N-H distances and vibrational frequencies were found to change with the cluster size, in accord with the gas phase experimental data.

Ab initio cluster calculations were also found useful for statistical

thermodynamic evaluation of the physical properties and spectra of liquids by means

of Quantum Cluster Equilibrium theory, as shown in the example of N-methyl

formamide.[99] In this theory the equilibrium populations of the dimers, trimers,...,

hexamers were evaluated at a certain temperature based on *ab initio* calculated

interaction energies for each cluster. This approach allows one to derive the equation

of state for liquids and non-ideal gases and to describe phase transitions. However, it is

limited to equilibrium phenomena. Kinetics and non-equilibrium phenomena require

molecular dynamics simulations, when individual trajectories of nuclei are described

classically or semiclassically. As the size of the system in the MD approach must be

sufficient to simulate long-distance disorder, *ab initio* treatment is too expensive in

most cases. At present, MD simulations are done at the empirical force field level

(with or without polarizable potentials). The search for inexpensive methods for

improving the results of MD simulations includes some variations of the simplified

cluster approach. This would describe the electronic structure of the system on each

step of the nuclear motion (Aon the fly@), instead of calculation potential energy

function before the calculation. For example, a modification of the valence bond

method named Adiatomics-in-molecules@ applied to $(HF)_n$, n=3-6 system was shown to

give energies for sixteen cluster conformations closer to MP2/6-311+G(2d,2p) results

then to those achieved using a polarizable force field.[100] Unfortunately, the diatomics-

in-molecules method treats the contributions of ionic states as empirical parameter.

Using the same parameter for the different molecules in a cluster and for clusters of

different size is likely to underestimate cooperative effects.

Imposing translational symmetry can significantly simplify large cluster calculations. In HF calculations of large (500 heavy atom) clusters of diamond and ZnS[101] translational symmetry allowed one to reduce the number of necessary integrals. Even periodical constraints on intra- and intermolecular geometrical parameters help to achieve convergence in cases too large for full optimization. Such calculations were performed by Dannenberg and Turi on clusters of acetic acid,[102] cyclohexane-1,3-dione,[103] and nitroanilines.[104] However, the relative stability of organic polymorphs has not been studied at *ab initio* level. Comparison of two polymorphic structures could reveal a predictive strength of cluster calculations, using no empirical parameters. This explains our interest in the systems described below.

2.5 Urea molecular structure and vibrational spectra in the gas phase and in crystals

Urea and thiourea provide interesting and contrasting examples of how small changes in molecular structure can have a large influence on crystal structure. Investigating the basis of these effects can be of singular importance for understanding and designing intermolecular interactions that dictate crystal packing. This understanding will eventually play important role in crystal engineering.

Urea crystals attract the attention of both theoreticians and experimentalists

due to their nonlinear optical and piezoelectric properties.[105] The intermolecular

interactions of urea molecules with water[106] and with hydrophobic molecules[107] have

received much attention in connection with protein denaturation and RNA folding.[108]

Most chemists have assumed that urea is a planar symmetrical molecule.

Indeed, the crystal structures that have been published have reinforced this assumption

(see Figure 2.5). Below we will refer to the most precise low temperature (12K)

neutron study by Swaminathan et al.[109] Moreover, Bowen,[110] Coussens,[111] Frenking,[112]

and Dixon[113] have recently published theoretical studies of urea using *ab initio* and

DFT calculations up to MP4/6-311G**//MP2/6-31G*. These studies show the parent

molecule to be nonplanar. The planar structure was reported to be a second order

saddle point connecting the two pairs of equivalent nonplanar minima. In fact, the

nonplanarity of urea had previously been suggested by King in his early vibrational

analysis of urea in an argon matrix.[114] We will refer to that paper below as the matrix

isolation experiment. Although several groups were aware of the reported nonplanarity

of urea, analyses of experimental vibrational and microwave spectra have assumed

planarity for simplicity. Only recently have these data been reassigned based on

possibly nonplanar conformational behavior. Gas microwave experimental data on the

geometrical parameters of nonplanar urea molecules were reported by Godfrey,[115] and

will be referred below to as MW data.

The most comprehensive study to date, that of Van Alsenoy et al.[116] deals with

the geometry and spectra of the urea molecule in the gas and in crystal phases. It

reports the results of HF/6-31++G** calculations for the free molecule and the

Table 2.1. Comparison between calculated (HF/6-31++G**) and experimental (MW in the gas,[115] and ND in the crystal phase[109]) bond lengths (Å), valent and dihedral angles (°) for the gas phase and the crystal phase of Urea. Reproduced from ref. 116.

	gas			crystal			gas vs. crystal	
bonds	r_e, calc.	r_s, MW	Δ	r_e, calc.	r_α, ND	Δ	calc.	exp.
CO	1.200	1.221	-0.021	1.242	1.265(1)	-0.023	0.042	0.044
CN	1.370	1.378	-0.008	1.331	1.349(1)	-0.018	-0.039	-0.029
NHs	0.999	1.021	-0.022	0.999	1.008(4)	-0.009	0.000	0.013
NHa	0.998	0.998	0.000	0.999	1.001(4)	-0.002	0.001	0.003
angles								
OCN	122.7	122.6	0.1	121.2	121.4(1)	-0.2	-1.5	-1.2
NCN	114.6	114.7	-0.1	117.6	117.2(1)	0.4	3.0	2.5
CNHs	114.1	112.8	1.3	119.3	119.1(1)	0.2	5.2	6.3
CNHa	118.7	119.2	-0.5	120.9	120.5(1)	0.4	2.2	1.3
HsNHa	115.3	118.6	-3.3	119.8	120.4(1)	-0.6	4.5	1.8
dihedrals								
OCNHs	-12.5	-10.8	-1.7	0	0	0	12.5	10.8
OCNHa	-153.7	-156.9	3.2	-180	-180	0	-26.3	-23.1
NCNHs	167.5	169.2	-1.7	180	180	0	12.5	10.8

for the molecule in the crystal environment (simulated by the 14 nearest neighbors, with 664 neighbors represented by point charges). In this environment, the molecule becomes planar. The comparison between calculated and experimental data (gas microwave[108] and crystal neutron diffraction[102] at 12K) is summarized in Table 2.1. HF calculations predict the correct trends in geometrical changes between the gas and crystal phases. The bond lengths are 0.01-0.02 Å shorter than experimental values. Valence and torsional angles are within 3° range of experiment (0.6° for crystal phase).

Table 2.2. Experimental (MW) rotational constants (MHz) and differences between experimental and calculated values obtained using the experimental r_s and calculated r_e structure.

	MW	Δ, exp	Δ, HF/6-31++G**
$(NH_2)CO(NH_2)$			
A	11,233	20	285
B	10,369	28	142
C	5,417	16	118
$(NH_2)CO(NHD)$			
A	11,225	24	287
B	9,590	23	130
C	5,197	15	111
$(NH_2)CO(NDH)$			
A	10,826	28	253
B	9,895	21	150
C	5,204	14	112
$(^{15}NH_2)CO(^{15}NH_2)$			
A	11,027	19	279
B	9,828	25	134
C	5,220	15	112
$(NH_2)C^{18}O(NH_2)$			
A	10,466	17	264
B	10.369	28	142
C	5,231	16	115

Calculated rotational constants are compared to experimental values in Table 2.2. They are about 3% too small. After the authors empirically corrected the calculated structure to shorten C=O and C-N bonds, the agreement became quantitative.

The gas phase vibrational spectrum of urea is hard to obtain due to the quick thermal decomposition of urea at sublimation temperature. Only one gas-phase spectrum, that of Langer et al,[117] has been published. Vibrational spectra in the solution were studied repeatedly, and we will refer below to the detailed IR study in acetonitrile by Hadzi.[118] The most comprehensive spectroscopic study in crystal phase was published again by Van Alsenoy.[119] This study combines Infrared and Raman spectra of solid urea at high pressure (up to 1 GPa) and low temperature (-196°C), with cluster frequency calculations. The comparison of experimental and calculated frequencies is presented in Tables 2.3-2.4. While comparing calculated and experimental frequencies for urea, the authors[119] had to introduce individual scaling factors for crystal and gas. In addition, they used individual scaling factors for the N-H stretch in the gas phase and for the C=O stretch in the solid phase, in order to get satisfactory agreement.

The changes in observed frequencies correspond to the weakening of N-H and C=O bonds and to the strengthening in C-N bonds from gas to solution to crystal at room temperature (Figures 2.3a-c) to crystal at low temperature (or to crystal at high pressure). Also, NH_2 rocking vibrations shift to a lower frequency and NH_2

Table 2.3. Vibrational frequencies for urea and deuterated urea molecules: experimental (solution, Ar matrix isolation, and gas-phase), calculated (HF/6-311++G**, two scaling factors), and difference between calculated and experimental (matrix isolation), cm^{-1}

assignment	S	^{1}H					^{2}D		
		soln.	matr	gas	calc.	δ	matr.	calc.	δ
$\nu_a(NH_2)$	A	3503	3548	3533	3542	-6	2648	2623	-25
$\nu_a(NH_2)$	B	3503	3548	3559	3541	-7	2648	2620	-28
$\nu_s(NH_2)$	A	3390	3440	3434	3425	-5	2505	2485	-20
$\nu_s(NH_2)$	B	3390	3440	3460	3431	-9	2505	2480	-25
$\nu(CO)$	A	1695	1734	1776	1731	-3	1723	1707	-16
$\delta_a(NH_2)$	B	1614	1594	1749	1600	6		1135	
$\delta_s(NH_2)$	A	1614	1594	1604	1589	-5	1223	1219	-4
$\nu_a(CN)$	B	1419	1394	1394	1386	-8	1408	1407	-1
$\rho_s(NH_2)$	A	1167		1157	1149			968	
$\rho_a(NH_2)$	B	1167	1014	1157	1027	13		839	
$\nu_s(CN)$	A	969	960	1023	934	-26	845	830	-15
$\omega(CO)$	B		790	775	785	-5		756	
$\delta(CO)$	B	576	578	572	567	-11	517	512	-5
$\omega_s(NH_2)$	A				518			410	
$\tau_a(NH_2)$	B	509			516			322	
$\delta(CN)$	A				466			390	
$\omega_a(NH_2)$	B		410		422	12		377	
$\tau_s(NH_2)$	A				347			247	

Table 2.4. Crystal-phase experimental and calculated frequencies (cm^{-1}) for urea and deuterated urea.

assign.	S	^{1}H			^{2}D		
		ν_{exp}	ν_{calc}	δ	ν_{exp}	ν_{calc}	δ
$\nu_a(NH_2)$	A1	3448	3460	12	2595	2573	-22
$\nu_a(NH_2)$	B2	3435	3452	17	2584	2563	-21
$\nu_s(NH_2)$	A1	3345	3347	2	2439	2423	-16
$\nu_s(NH_2)$	B2	3330	3326	-4	2431	2403	-28
$\nu(CO)$	A1	1598	1597	-1	1603	1601	-2
$\delta_a(NH_2)$	B2	1627	1631	4	1154	1147	-7
$\delta_s(NH_2)$	A1	1683	1658	-25	1251	1247	-4
$\nu_a(CN)$	B2	1471	1469	-2	1490	1506	16
$\rho_s(NH_2)$	A1	1149	1153	4	1002	991	-11
$\rho_a(NH_2)$	B2	1055	1062	7	855	843	-12
$\nu_s(CN)$	A1	1008	1013	5	891	885	-6
$\omega(CO)$	B1	790	797	7	779	787	8
$\delta(CO)$	B2	568	576	8	527	508	19
$\omega_s(NH_2)$	A2		463			361	
$\tau_a(NH_2)$	B1	727	730	3	550	533	-17
$\delta(CN)$	A1	532	540	8	466	459	-7
$\omega_a(NH_2)$	B1	508	512	4	379	388	12
$\tau_s(NH_2)$	A2		602			428	

deformation and CO wagging vibrations shift to a higher frequency. Therefore, force

constants for the urea molecule significantly change in different phases. The use of the

gas force constants for solid and solution was responsible for the incorrect assignment

of vibrational modes in earlier studies. The changes in the bond strengths were

attributed to H-bonding and illustrated using a simple resonance picture (Figure 2.3).
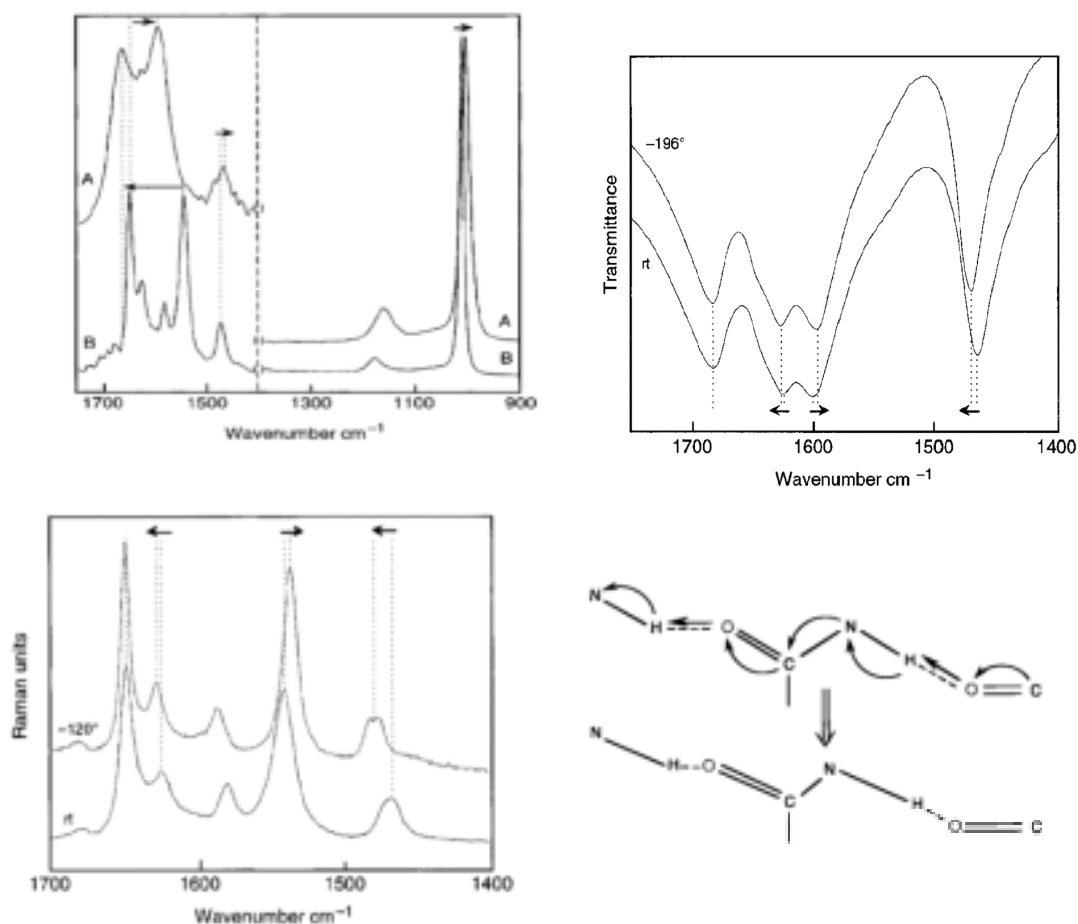
Figure 2.3 (top left) Raman spectra of urea in aqueous solution (A) and in crystal (B); (top right) Low-temperature shifts in the 1700-1400 cm^{-1} region of the infrared spectrum of urea; (bottom left) Low-temperature shifts in the 1700-1400 cm^{-1} region of the Raman spectrum of urea; (bottom right) Effect of H-bonding on the NH, CO, and CN strength (reproduced from Ref. 119)

2.6 Structure and spectra for dimers and trimers

To our knowledge, dimerization of urea molecules has only been studied theoretically. In earlier force field and intermolecular perturbation theory studies,[106] two dimers, cyclic and head-to-tail, were usually considered. Molecular geometry was assumed to be planar. Cyclic dimers were found to be the most stable. Their interaction energies of 22[106b] and 20[106d] kcal/mol were obtained from low-level *ab initio* calculations (HF/3-21G, no BSSE correction). Head-to-tail dimeric configuration and two trimers (head-to-tail and transverse, corresponding to **CAB** and **GAF** on Figure 3.4) were considered by Perez and Dupuis.[120] These authors performed single-point HF calculations in order to examine the additivity of (hyper) polarizabilities. Although five basis sets were considered for the monomer (D95 with various number of diffuse and polarization functions), the authors neglected to specify which one was used for cluster calculations. The dipole moment increased from 5.3 D in the monomer to 12.3 D for the dimer to 19.7 D for the head-to-tail trimer (a 25% increase from the monomeric value). For the transverse trimer, where molecular dipole moments are antiparallel and two of them cancel each other, they calculated a dipole moment of 4.5 D (a 15% decrease from the monomeric value). The interaction energy (without CP correction or molecular relaxation) was calculated to be 12.4 kcal/mol for the dimer, 27.8 kcal/mol for the head-to-tail trimer (so that the second H-bond is 25% stronger then the first), and 15.4 kcal/mol for the transverse trimer. The authors found significant cooperative effects of the individual components for polarizability and

hyperpolarizability tensor. However, the average values were additive to a good approximation.

After our present study was concluded, Belosludov, Li, and Kawazoe published a paper on *ab initio* calculations of trimers and dimers.[121] In their work the dimers were optimized using HF, MP2, BLYP, and BPW91 methods with 6-31G, 6-31G*, and 6-31++G** basis sets. The trimers were optimized at HF, BLYP, and BPW91 levels. Various starting geometries found in the crystal structures were used. Only two stable dimers were found: a head-to-tail dimer with two NH_2 groups of one molecule H-bonded to the O atom of another molecule, with an extra NH...N bond (see dimer **CB0** on Figure 4.2) and a cyclic dimer with two equivalent NH...O bonds (see dimer **R** on Figure 4.2). The interaction energies in these structures were calculated to be 9.0 and 11.5 kcal/mol at HF/6-31++G** level after CP correction. Neither orientation is observed in the experimental crystal structure. The global minimum among trimers consists of two cyclic dimeric units linked via one molecule (**CAB** on Figure 3.5), with interaction energy of 19.1 kcal/mol. Unlike the cyclic dimer, this trimer is planar, which was confirmed by frequency calculations. A similar arrangement (not planar, however) is observed in the hexagonal host structure of urea with different guest molecules (see Figure 2.5), but not in pure crystalline urea.

Considering vibrational frequencies, the authors found that the calculated spectra for the monomer are in agreement with available experimental data. They assigned vibrations at 1439, 1625, and 1700 cm^{-1}, experimentally observed for urea in the gas phase to the dimer, and the vibration at 227 cm^{-1} to the trimer.

The authors concluded that H-bonding interaction is important for stabilizing

planar geometry in small clusters, but not sufficient for forming this geometry in

crystals. They noted that the structures of the dimers and trimers are closely related to

the hexagonal than to the tetragonal structure of urea in the crystal phase. The results

of this paper will be discussed in Chapter 5 in connection with our own results.

2.7 Crystal structure of urea not based on the most stable dimer

The crystal structures of urea inclusion compounds were studied in detail.[122]

They can be described as spiral ribbons of 3_1 symmetry made of cyclic dimers and

packed in a honeycomb manner. The linear channels in this structure are occupied by

disordered solvent molecules or by other guest molecules which can sterically fit there.

This property is well known and is applied in industry to the separation of branched

and linear hydrocarbons.[115] The space group of the structure is *R-3c*. Ordering of the

guest molecules leads to the loss of the center of symmetry (*R3c*), or of the glide plane

(*R-3*), or both (*R3*). The projection of the spiral ribbons on axis X and their packing

along the hexagonal axis is shown in Figure 2.4. This structure is typical for inclusion

compounds of urea, thiourea and selenourea. The hexagonal polymorphic form of

selenourea,[123] crystallizing in the space group *P3₁*, is based on this structure. Instead of

guest molecules, it has spiral H-bonded thiourea ribbons of 3_1 symmetry filling the

channels without H-bonding to the host structure. These ribbons distort the

honeycomb network so that the body centered translational symmetry is lost and
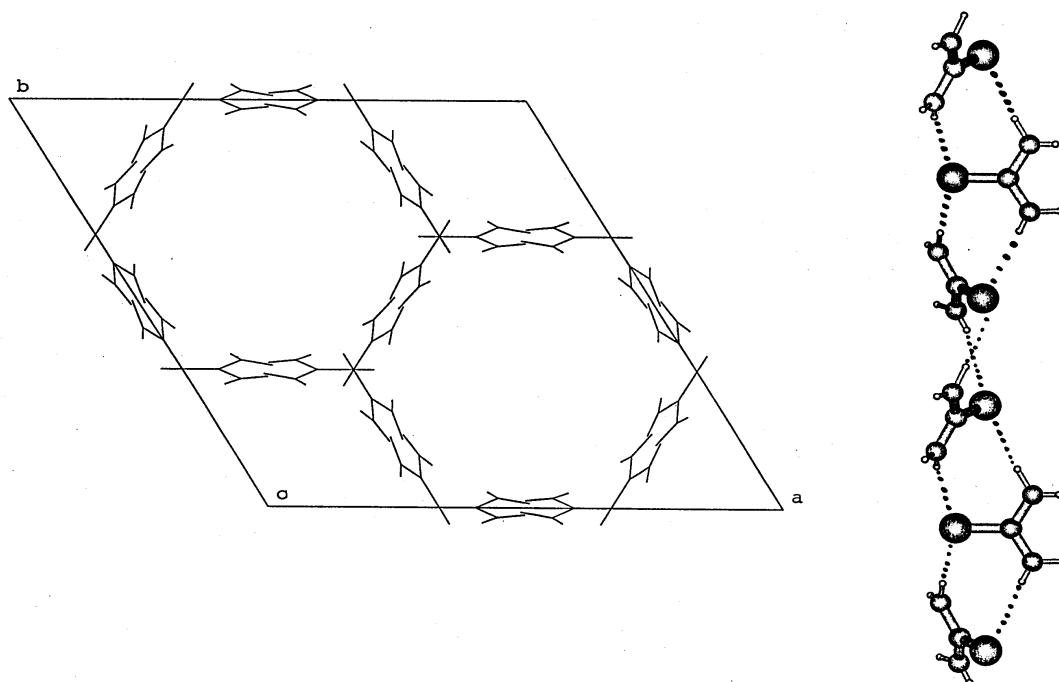
Figure 2.4. Crystal structure of hexagonal urea host frame from urea-CHCl$_3$ inclusion compound.

channels become symmetrically-independent. Host spirals are no longer 3_1

symmetrical nor equivalent. Consequently, selenourea has nine independent molecules

in the asymmetric unit cell -- a record among molecular crystals. However, for urea

and thiourea hexagonal structures without guest molecules have never been observed

in the experiment. Urea forms a tetragonal structure of *P-42$_1$m* symmetry (Figure 2.5),

in which the molecules form H-bonded chains in a head-to-tail manner. Each molecule

uses two hydrogen atoms to form H-bonds with one oxygen atom of the next

molecule. The chains are arranged in a herringbone motif, so that each molecule
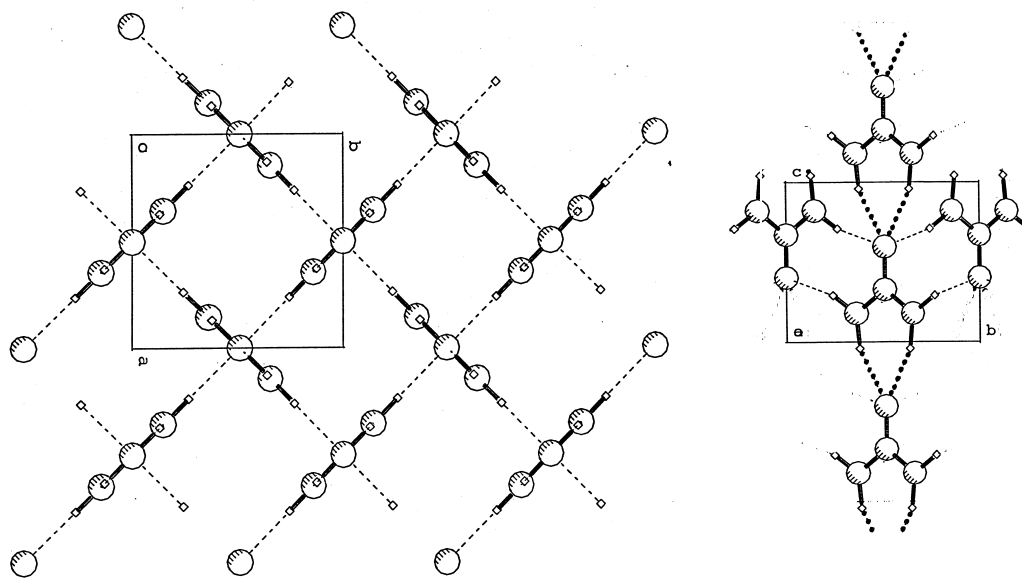
Figure 2.5. Crystal structure of urea in *P-42₁m* space group.

donates two H-bonds to two of the neighboring chains and accepts two H-bonds form two other chains. This is the only known structure with four H-bonds to one carbonyl group. Since the direction of the chains alternates, the structure is non polar overall.

The experimental enthalpy of sublimation for crystalline urea was reported to be 20.95 ± 0.21[124] and 23.3 ± 0.24 kcal/mol.[125] The first attempt to access this value by *ab initio* methods was the periodical HF/6-21G** calculation by Dovesi, Roetti, et al.[126] using CRYSTAL and experimental geometry. The value before CP correction was 33.5 kcal/mol, partial CP correction brings it to 21.4 kcal/mol, and relaxation of the monomer brings it to 16.3 kcal/mol. Due to the difficulties discussed in Section 2.3, only the nearest neighbors, those at a distance closer than 2.5 Å, were taken into

account. In Section 3.5 we will show that using this cutoff one recovers at most 60% of full CP correction. All atomic Mulliken charges were found to increase in absolute value in comparison with an isolated molecule. Bond populations decreased for C=O, and N-H bonds, and increased for C-N and O...H bonds, in accord with the resonance picture (Figure 2.3).

The urea crystal structure was optimized by Van Alsenoy et al. using the non-gradient corrected DFT method in the plane wave basis with pseudopotentials.[127] Instead of total energy, the enthalpy H=E+pV was minimized for different pressure values. The hydrogen bonds between the chains were found to shorten much faster than those within the chains upon the application of external pressure. Since single molecule calculations were done with a different basis set and a different DFT functional, the heat of formation was not estimated.

The molecular dipole moment of urea shows significant polarization, from 3.83 D in the gas phase[110] to 4.2 D in solution[128] to 4.66 D in crystal.[129] The latter value was obtained from X-rays diffuse scattering measurements interpreted with a model of longitudinal lattice dynamics. We should note that Raman spectra of the lattice vibrations yielded a much smaller value of 3.0 D.[130]

Model calculations show that refinement of atomic multipole moments from high-precision X-ray diffraction data for monocrystals is capable of quantitative retrieval of the electron density redistribution due to intermolecular interaction (interaction density).[131] In fact, experimental electron density distribution in the urea crystal was studied repeatedly by means of X-ray diffraction.[132] The results were

compared to molecular and periodical HF calculations and used to estimate the dipole

moment and sublimation enthalpy.[133] For the latter, the classical electrostatic part

derived from the interaction of experimental electron densities was supplemented by

an empirical a 6-exp force field. This simple scheme, which neglects relaxation and

polarization energy of the molecule in the crystal was suggested by Spackman.[133a] It

yields 15.7 kcal/mol, surprisingly close to our periodical HF/6-311G** result, reported

in Section 3.5. Close agreement between this scheme and the crystal orbital HF result

was also obtained by Abramov, Coppens et al. in their study of three crystalline amino

acids.[134] The scheme was further improved by Tsirelson, Feil et al.[133b] They introduced

an induction energy term depending on the deformation of the molecular electron

density upon crystal formation. To obtain this deformation, the HF electron density of

a single molecule was subtracted from the experimental electron density. The use of

the calculated HF electron density with this improved model yields interaction energy

of 21.8 kcal/mol, close to the experimental sublimation energy. However, compared to

HF interaction energy this value is highly overestimated. If the experimental electron

density is used, the electrostatic interaction is 10 kcal/mol weaker, mostly because of

the large differences between experimental and HF monopole populations (atomic

charges).[133b] However, the induction energy is calculated to be +7 kcal/mol, a positive

value with no physical sense. The authors see the reason for this failure in

experimental uncertainties in the phases of the structural factors for non-

centrosymmetric crystals,[135] and conclude that experimental interaction density is

unreliable in this case. It is interesting to note that, besides experimental errors,

molecular electron distribution depends on the refinement procedure. The dipole

moment values reported for the same set of data varied from 3.8 D[132c] to 4.2 D.[133b] A

stronger (three-fold) model dependence for molecular dipole moment obtained from

X-ray diffraction data was found in the case of 4-nitro-4'-aminobiphenyl.[136]
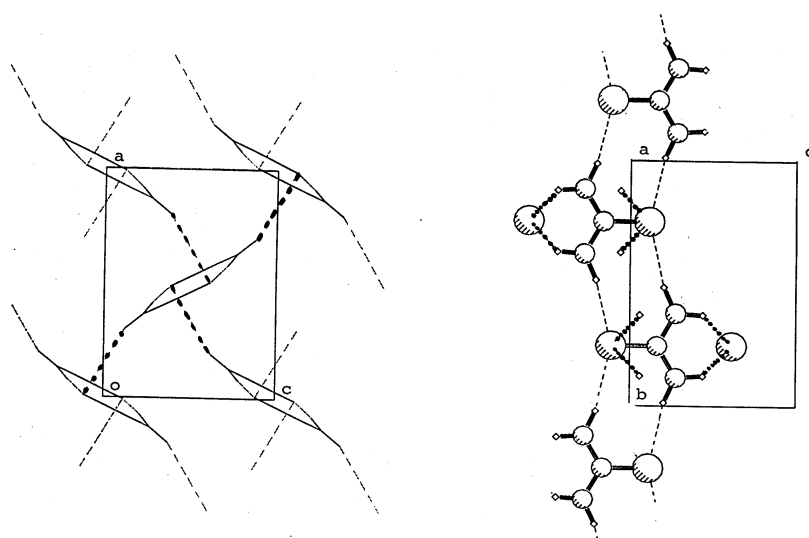
Figure 2.6. Crystal structure of thiourea in *Pmna* space group (high temperature modification).

2.8 Thiourea not isomorphic with urea

Unlike urea, thiourea forms orthogonal crystals[137] in space group *Pnma* (Figure

2.6). In these crystals, molecules are linked into ribbons by cyclic dimeric interactions.

These slightly nonplanar ribbons are packed in a herringbone motif. Each molecule forms two H-bonds with other ribbons. At low temperatures thiourea undergoes ferroelectric phase transition to another polymorph, $P2_1ma$, which is closely related to this structure.[138] It can be described as a deformed modification, in which the H-bonds between the ribbons are no longer equivalent (one is shorter then the other). As a result, the molecular planes within the ribbon are no longer parallel to each other and the unit cell contains two symmetrically-independent molecules.

The experimental enthalpy of sublimation for thiourea was reported as 22.4±2.4[139] and 26.8±0.36 kcal/mol.[140] To our knowledge, no previous attempts have been made to simulate this crystal structure with *ab initio* methods.

As one can see, the most stable dimer of urea has nothing in common with its crystal structure. Rather, it is closely related to the crystal structure of thiourea. To resolve this paradox, and to understand the reasons behind the differences in the urea and thiourea structures, we will apply *ab initio* methods, as described in the following Chapters.

References for Chapter 2.

[1.] Kitaigorodskii, A.I., Organic Chemical Crystallography, Consultants Bureau; New York, **1961**; pp 65-112.

[2.] Hayes, I.C.; Stone, A.J.: <u>Mol. Phys.</u>, **1984**, <u>53</u>, 107.

[3.] Jeziorski, B.; Moszynski, R.; Ratkiewicz, A.; Rybak, S.; Szalewicz, K.; Williams, H. L. In *Methods and Techniques in Computational Chemistry: METECC-94, Vol. B, Medium Size Systems*; Clementi, E., Ed.; STEF: Cagliari, 1993; p 79. http://www.physics.udel.edu/wwwusers/mas/group.htm

[4.] CADPAC: The Cambridge Analytic Derivatives Package. Amos, R.D.; Alberts, I.L.; Andrews, J.S., Colwell, S.M.; Handy, N.C.; Jayatilaka, D.; Knowles, P.J.; Kobayashi, R.; Laidig, K.E.; Laming, G.; Lee, A.M.; Maslen, P.E.; Murray, C.W., Rice, J.E., Scimandrias, E.D.; Stone, A.J.; Su, M.D.; Tozer, D.J. **1995**; http://ket.ch.cam.ac.uk/software/cadpac.html

[5.] Meng, E. C., Caldwell, J. W., Kollman, P. A., <u>J. Phys. Chem.</u>; **1996**, <u>100</u>(6), 2367.

[6.] Bursulaya, B.D.; Zichi, D.A.; Kim, H.J.: <u>J. Phys. Chem.</u>, **1996,** <u>100</u>**,** 1392.

[7.] Dykstra, C.E.: <u>Chem. Rev.</u>, **1993**, <u>93</u>, 2339.

[8.] van Duijnen, P. T., Swart, M., <u>J. Phys. Chem. A;</u> **1998**; <u>102</u>(14); 2399.

[9.] Rick, S.W.; Berne, B.J.: <u>J. Am.Chem. Soc</u>, **1996**; <u>118</u>(3); 672.

[10.] Banks, J.L; Kaminski, G.A.; Zhou, R.; Mainz, D.T.; Berne, B.J.; Freisner, R.A.: <u>J. Chem. Phys.</u>, **1999**, <u>110</u>, 741.

[11.] Rappe, A.K.; Goddard, W.A.III: <u>J. Phys. Chem.</u>; **1991**; <u>95</u>; 3358.

[12.] Allen, L.C.: Electronegativity and the periodic table. In: The Encyclopedia of Computational Chemistry, Ed. Schleyer, P.v.R., **1998**, <u>3</u>, 123.

[13.] Stern, H.A.; Kaminski, G.A.; Banks, J.L.; Zhou, R.; Berne, B.J.; Freisner, R.A.: <u>J. Phys. Chem.</u>, **1999**, <u>103</u>, 4730.

[14.] Rauhut, G.; Clark, T.: <u>J. Comput. Chem.</u>, **1993**, <u>14</u>, 503; Beck, B.; Rauhut, G.; Clark, T.: <u>J. Comp. Chem.</u>, **1994,** <u>15</u>, 1064.

15. Rauhut, G.; Alex, A.; Chandrasekhar, J.; Steinke, T.; Sauer, W.; Beck, B.; Hutter, M.; Clark, T.**: VAMP**, Oxford Molecular
http://www.oxmol.com/software/tsar3d/spec.shtml#vamp

16. Batista, E.R.; Xantheas, S.S.; Jónsson, H.: J. Chem. Phys., **1998,** 109(11), 4546.

17. Board, J.; Schulten, K.: Comput. Sci. Eng., **2000,** 2(1), 76.

18. Lotrich, V.F.; Szalewicz, K.: J. Chem. Phys., **1997**, 106(23), 9668.

19. Gdanitz, R.J., *Theoretical aspects and computer modelling of the molecular solid state,* Ed. Gavezzotti, A., John Wiley & Sons, New York, **1997**, 195.

20. Gavezzotti A., J. Am.Chem. Soc, **1991**, 113, 4622.

21. Braga, D., et. al., J.Chem. Soc, Dalton Trans., **1995,** 1215.

22. Karfunkel, H.R., Gdanitz, R.J., J. Comp.Chem., **1992,** 13, 1171.

23. Verwer, P.; Leusen, F.J.J.: Reviews in Computational Chemistry, K.B. Lipkowitz and D.B. Boyd, Eds., Wiley-VCH:New York, Volume 12, **1998,** pp.327-365.

24. (a) Van Eijck, B.P., Mooij, W.T.M., Kroon, J., Acta Cryst., **1995,** B51, 99; (b) Van Eijck, B.P., Kroon, J. J. Comput. Chem., **1999**, 103, 9872.

25. Perlstein, J., J. Am.Chem. Soc, **1994,** 116, 11420.

26. Roberts, K. J.; Sherwood, J. N.; Yoon, C. S.; Docherty, R.: Chem. Mater. **1994,** 6, 658; Chen et. al. Phys. Chem. **1994**, 98, 5138.

27. Chaka, A.M., Zaniewski, R., Youngs, W., Tessier, C. & Klopman, G.: Acta Cryst., **1996**, B52, 165.

28. Gibson, K.D., Scheraga, H.A.: J.Phys.Chem., **1995,** 99, 3752.

29. Williams, D.E.: Acta Cryst., **1996,** A52(2), 326.

30. Gale, J.D.: Phil. Mag. B, **1996,** 73, 3;
http://argon.ch.ic.ac.uk/gale/Research/gulp.html

31. Haugk, M.; Elsner, J.; Heine, Th.; Frauenheim, Th.; Seifert, G.: Comput. Mater.

<u>Sci.,</u> **1999**, <u>13</u>(4), 239.

32. Tan, A.; Harris, S.: <u>Inorg. Chem.,</u>**1998**, <u>37</u>, 2205.

33. Landrum, G.A.: Yet Another extended Hückel Molecular Orbital Package; http://overlap.chem.cornell.edu:8080/yaehmop.html

34. Themans, B.; Andre, J.M.; Bredas, J.L.: <u>Mol.Cryst. Liq. Cryst.,</u> **1985,** 118; http://www.chimie.fundp.ac.be/cta/docs/veh.html

35. Ordejon, P.: <u>Comput. Mater. Sci</u> **1998**, <u>12</u>(3), 157.

36. Frauenheim, T.; Seifert, G.; Elstner, M.; Hajnal, Z.; Jungnickel, G.; Porezag, D.; Suhai, S.; Scholz, R.: <u>Phys. Status Solidi B</u>., **2000**, <u>217</u>(1), 41.

37. Dewar, M.J.S.; Stewart, J.J.P. <u>Chem. Phys. Lett.,</u> **1984,** <u>111</u>, 416; http://www.ccl.net/cca/software/NT/mopac6/index.shtml

38. Kim, K.; Jordan, K. D.; <u>J. Phys. Chem.,</u> **1994**, <u>98</u>, 10089.

39. Simon, S.; Duran, M.; Dannenberg, J. J., <u>J. Phys. Chem. A</u>, **1999**, <u>103</u>, 1640.

40. Guo, H.; Sirois, S.; Proynov, E. I.; Salahub, D. R., in ATheoretical Treatments of Hydrogen Bonding,A Had i, D., Editor, **1997**, Wiley, 49.

41. (a) Kohn, W.; Meir, Y.; Makarov, D. E., <u>Phys. Rev. Lett.,</u> **1998**, <u>80</u>, 4153; (b) Dobson, J. F.; Dinte, B. P. <u>Phys. Rev. Lett.,</u> **1996**, <u>76</u>, 1780; (c) Andersson, Y.; Langreth, D. C.; Lundqvist, B. I., <u>Phys. Rev. Lett.,</u> **1996**, <u>76</u>, 102.

42. Becke, A. D., <u>J. Chem. Phys.,</u> **1993**, <u>98</u>, 5648.

43. Perdew, J. P.; Wang, Y., <u>Phys. Rev.,</u> **1992**, <u>B 45</u>, 13244.

44. Lee, C.; Yang, W.; Parr, R. G., <u>Phys. Rev. B</u>, **1988**, <u>37</u>, 785.

45. Ikeda, T.; Sprik, M.; Terakura, K.; Parrinello, M.: <u>J. Chem. Phys.,</u> **1999**, <u>111</u>(4), 1595.

46. Car, R.; Parrinello, M.: <u>Phys. Rev. Lett.</u> **1985,** <u>55</u>, 2471; http://parrserv2.mpi-stuttgart.mpg.de; http://pages.nyu.edu/~mt33/abstracts/manual/manual.html

47. Kresse, G.; Furthmüller, J.: Comput. Mat. Sci. **1996**, 6, 15; http://tph.tuwien.ac.at/~vasp/

48. Blöchl, P.E.: Phys. Rev. B **1994,** 50, 17953; http://www.zurich.ibm.com/~blo/

49. Bockstedte, M.; Kley, A.; Neugebauer, J.; Scheffler, M.: Comp. Phys. Commun. **1997**, 107, 187; http://www.fhi-berlin.mpg.de/th/fhimd/

50. Payne, M.C.; et. al., Rev. Mod. Phys. **1992**, 64, 1045; http://www.tcm.phy.cam.ac.uk/castep/

51. Kurth, S.; Perdew, J.P.; Blaha, P.: Int.J.Quant.Chem. **1999,** 75, 889; http://info.tuwien.ac.at/theochem/wien97/

52. Guerra, C. F.; Snijders, J.G.; te Velde, G.; Baerends, E.J.: Theor. Chem. Acc. **1998,** 99, 391; http://www.scm.com

53. DMol User Guide, San Diego:MSI, **1995**; http://www.msi.com/materials/cerius2/dmol3.html

54. Andre, J.M.; Mosley, D.H.; Champagne, B.; Delhalle, J.; Fripiat, J.G.; Bredas, J.L.; Vanderveken, D.J.; Vercauteren, D.P.: in "METECC-94 Methods and Techniques in Computational Chemistry", E. Clementi Editor, Vol. B, Chapter 10, pp 423, STEF (Cagliari) (1993); http://www.chimie.fundp.ac.be/cta/docs/plh-93.html

55. Jaffe, J.E.; Hess, A.C.: J. Chem. Phys. **1996,** 105, 10 983; Anchell, C. *et al.*, "NWChem, A computational chemistry package for parallel computers, Version 3.2.1," Pacific Northwest National Laboratory, Richland, Washington 99352-0999, **1998.**

56. Pisani, C.: J. Mol. Struc. (THEOCHEM) **1999**, 463, 125; Dovesi, R.; Saunders, R.; Roetti, C.; Causà, M.; Harrison, N.M.;Orlando, R.; Apra, E.: CRYSTAL95 User=s manual, Univertity of Torino, Torino, **1996**; http://www.ch.unito.it/ifm/teorica/crystal.html

57. Pisani, C. Dovesi, R.; Roetti, C, Hartree-Fock ab-intitio treatment of crystalline systems, Lecture Notes in Chemistry, Vol. 48, Springer Verlag, Heidelberg, **1988.**

58. Frisch, M. J.; Trucks, G. W.; Schlegel, H. B.; Gill, P. M. W.; Johnson, B. G.; Robb, M. A.; Cheesman, J. R.; Keth, T. A.; Petersson, G. A.; Montgomery, J. A.; Raghavachari, K.; Al-Lahan, M. A.; Zakrzewski, V. G.; Ortiz, J. V.; Foresman, J. B.;

Cioslwski, J.; Stefanov, B. B.; Nanayakkara, A.; Challacombe, M.; Peng, C.Y.; Ayala, P. Y.; Chen, W.; Wong, M. W.; Andre, J. L.; Replogle, E. S., Gomperts, R.; Martin, R. L.; Fox, D. J.; Binkley, J. S.; Deefres, D. J.; Baker, J.; Stewar, J. P.; Head-Gordon, M.; Gonzalez, C.; Pople, J. A. Gaussian 94: Gaussian, Inc., Pittsburgh, PA, **1995.**

59. Ojamäe, L.; Hermansson, K.; Dovesi, R.; Roetti, C.; Saunders, V. R., <u>J. Chem. Phys.</u>, **1994**, <u>100</u>, 2128.

60. (a) Towler, M. D.; ›Hartree-Fock Theory of the Electronic Structure of Solids,= CRYSTAL Network School, September, **1995;** (b) http://www.tcm.phy.cam.ac.uk/~mdt26/crystal.html

61. (a) Schwenke, D. W.; Truhlar, D. G., <u>J. Chem. Phys.</u>, **1984**, <u>82</u>, 2418; (b) Frisch, M. J.; Del Bene, J. E.; Binkley, J. S.; Schaefer, H. F. III, <u>J. Chem. Phys.</u>, **1986**, 2279; (c) Szalewicz, K.; Cole, S. J.; Kolos, W.; Bartlett, R. J., <u>J. Chem. Phys.</u>, **1988**, <u>89</u>, 3662; (d) Gutowski, M.; van Duijneveldt-van de Rijdt, J. G. C. M.; van Duijneveldt, F. B, <u>J. Chem. Phys</u>, **1993**, <u>98</u>, 4728; (e) Cook, D. B.; Sordo, J. A.; Sordo, T. L., <u>Int. J. Quant. Chem.</u>, **1993**, <u>48</u>, 375; (f) van Duijneveldt, F. B.; van Duijneveldt-van de Rijdt, J. G. C. M.; van Lenthe, J. H., <u>Chem. Rev.</u> **94** (1994) 1873.

62.. (a) Boys, S. F.; Bernardi,F.: <u>Mol. Phys.</u>, **1970,** <u>19</u>, 553; (b) Meunier, A.; Levy, B.; Berthier, G.: <u>Theor. Chim. Acta</u>, **1973**, <u>29</u>, 49; (c) Jansen, H.B.; Ross, P.: <u>Chem. Phys. Lett.</u>, **1969,** <u>3</u>, 40.

63. Mayer, I.; Surjan, P. R., <u>Chem. Phys. Lett.</u>, **1992**, <u>191</u>, 497; Turi, L.; Dannenberg, J. J.: <u>J. Phys. Chem.</u>, **1993**, <u>97</u>, 2488.

64. Turi, L.; Dannenberg, J. J.: <u>J. Phys. Chem.</u> **1993**, <u>97</u>(11), 2488.

65. Simon, S.; Duran, M.; Dannenberg, J.J.: <u>J. Chem. Phys.</u>, **1996**, <u>105</u>, 11024; http://stark.udg.es/~perico/bbopt.html

66. Gianinetti, E.; Raimondi, M.; Tornaghi, E.: <u>Int. J. Quantum Chem.</u>,**1996,** <u>60</u>, 157; Gianinetti, E.; Vandoni, I.; Famulari, A.; Raimondi, M.: <u>Adv. Quantum Chem.</u>, **1998**, <u>31</u>, 251; Famulari, A.; Raimondi, M.; Sironi, M.; Gianinetti, E.: <u>Chem. Phys.</u> **1998**, <u>232</u>(3), 275.

67. M.W.Schmidt, K.K.Baldridge, J.A.Boatz, S.T.Elbert, M.S.Gordon, J.J.Jensen, S.Koseki, N.Matsunaga, K.A.Nguyen, S.Su, T.L.Windus, M.Dupuis, J.A.Montgomery <u>J.Comput.Chem.</u> **1993,** <u>14</u>, 1347; http://www.msg.ameslab.gov/GAMESS/GAMESS.html

68. Kitaura, K.; Morokuma, K.: Int.J.Quantum Chem. **1976,** <u>10</u>, 325; Kitaura, K.; Morokuma, K.: in "Chemical Applications of Electrostatic Potentials", P.Politzer,D.G.Truhlar, Eds.Plenum Press, NY, 1981, p. 215; Cammi, R.; Bonaccorsi, R.; Tomasi J.:<u>Theoret.Chim.Acta</u> **1985,** <u>68</u>, 271; Stevens, W.J.; Fink, W.H.: <u>Chem.Phys.Lett</u>., **1987,** <u>139</u>, 15; Chen,W.; Gordon; M.S.: <u>J.Phys.Chem.</u> **1996,** <u>100</u>, 14316.

69. Raimondi. M.; Famulari, A.; Gianinetti, E.: <u>Int. J. Quantum. Chem.</u>, **1999**, <u>74</u>(2), 11024.

70. (a) Halász, G.; Vibók, Á.; Valiron, P.; Mayer, I.: <u>J. Phys. Chem.</u>, **1996,** <u>100</u>(15), 6332; (b) Mayer, I. <u>Int. J. Quantum. Chem.</u> **1983**, <u>23</u>, 341.

71. Kieninger, M.; Suhai, S.; Mayer, I. <u>Chem. Phys. Lett.</u> **1994**, *230*, 485.

72. Schütz, M., Rauhut, G.; Werner, H.-J.: J. Phys. Chem. **1998,** <u>102</u>, 5997; Runeberg, N.; Schütz, M.; Werner, H.-J. :<u>J. Chem. Phys</u>. **1999,** <u>110</u>, 7210; http://www.tc.bham.ac.uk/molpro/

73. Suhai, S., <u>J. Chem. Phys</u>. **1995**, <u>103</u>(16), 7030.

74. Suhai, S., <u>J. Chem. Phys</u>. **1994**, <u>101</u>(11), 9766.

75. Alfredsson,M.; Ojamae L.; Hermansson, K: <u>Int. J. Quantum Chem.</u>, **1996**, <u>60</u>(3), 767.

76. Funk, K; Staemmler, V.; <u>J. Chem. Phys.</u>, **1995**, <u>103</u>(7), 2603.

77. (a) Hirata, S., Iwata, S., <u>J. Chem. Phys.</u> **1998**; *10*9; 4147; (b) Hirata, S., Iwata, S., <u>J.Phys.Chem. B</u>; **1998**; *102*(43); 8426.

78. Jaffe, J.E.; Hess, A.C.: <u>J. Chem. Phys.</u>, **1996**, <u>105</u>(24), 10983.

79. Saebo, S, Klewe, B., Samdal, S. <u>Chem. Phys. Lett.</u> **1983**, <u>97</u>, 499.

80. Sugano, S., Shulman, R. G., <u>Phys. Rev.</u>, **1963**, <u>130</u>, 517.

81. Smit, P.H.; Derissen, J.L.; Van Duijneveldt, F.B. <u>Mol. Phys.</u>, **1979**, <u>37(2)</u>, 501.

82. (a) Rousseau, B.; Alsenoy, C. Van; Keuleers, R.; Desseyn, H. O.,<u>J. Phys. Chem.</u> **1998**, *A.102(32),* 6540; (b) Peeters, A.; Van Alsenoy, C.; Lenstra, A.T.H.; Geise, H.J.

J. Chem. Phys. **1995**, 103(15), 6608; (c) Van Alsenoy, C., Peeters, A., J. Mol. Struc. THEOCHEM, **1993**, *286*, 125.

83. Stefanovich, E. V., Truong, T. N., J. Phys. Chem. B; **1998**; 102(16); 3018.

84. Xantheneas, S.S.: J. Chem. Phys., **1994**, 100(10), 7523.

85. Suhai, S.: J. Phys. Chem., **1996**, 100, 3950.

86. Cabaleiro-Lago, E.M.; Rios, M.A.: J. Chem. Phys., **1999**, 110(14), 6782.

87. Nielsen, O.F.; Christiansen, D.H.; Rasmussen, O.H.: J. Mol. Struct., **1991**, 242, 273.

88. King, B.F.; Weinhold, F.: J. Chem. Phys., **1995**, 103(1), 333.

89. Stone, A.J.; Buckingham, A.D.: J. Chem. Phys., **1997**, 107(3), 1030.

90. Cabaleiro-Lago, E.; Rios, M.: J. Chem. Phys., **1998**, 108(9), 3598.

91. Karpfen, A.: J. Phys. Chem., **1996**, 100, 13474.

92. Karpfen, A.: J. Phys. Chem., **1998**, 102, 9286.

93. Masella, M.; Flament, J.P.: J. Chem. Phys., **1998**, 108(17), 7141.

94. Chalaszinski, G.; Szczesniak, M.M.; Cieplak, P.; Scheiner, S.: J. Chem. Phys., **1991**, 94, 2873.

95. Parra, R.D.; Zeng, X.C.: J. Chem. Phys., **1999**, 110(13), 6329.

96. Gonzales, L.; Mo, O.; Yanez, M.: J. Chem. Phys., **1999**, 111(9), 3855.

97. Sum, A.K.; Sandler, I.S.: J.Phys.Chem.A, **2000**, 104(6), 1121.

98. Cabaleiro-Lago, E.M.; Rios, M.A.: J. Chem. Phys., **2000**, 112(5), 2155.

99. Ludwig, R.; Weinhold, F.; Farrar, T. C.: J. Chem. Phys., **1997**, 107(2), 499.

100. Grigorenko, B.L.; Moskovsky, A.A.; Nemukhin, A.V.: J. Chem. Phys.; **1999**; 101(10); 4442.

101. (a) Strout, D.L.; Scuseria, G.E., J. Chem. Phys., **1995,** 102, 8448 ; (b)

http://www.chem.joensuu.fi/people/juha_muilu/Research/ab_initio_method.html

[102.] (a) Turi, L.; Dannenberg, J. J.J. Phys. Chem. **1993**, 97, 12197; (b) Turi, L.; Dannenberg, J. J. J. Am. Chem. Soc. **1994**, 116, 8714.

[103.] (a) Turi, L.; Dannenberg, J. J. Chem. Mater. **1994**, *6*, 1313; (b) Turi, L.; Dannenberg, J. J. J. Phys. Chem. **1992**, *96*, 5819.

[104.] (a) Turi, L., Dannenberg, J. J., J. Phys. Chem.; **1996**; *100* (23); 9638; (b) Vinson, L. K.; Dannenberg, J. J. J. Am. Chem. Soc. **1989**, *111*, 2777.

[105.] Halbout, J.M.; Tang, C.: In: Nonlinear Optical Properties of Organic Molecules and Crystals. Chemla, D.S.; Zyss, J. Eds. Acad. Press, NY 1987, vol. 1, p. 385; Mestechkin, M. M.: Optics Spectrosc., **1996**, 81(5), 714.

[106.] (a) Tanaka, H.; Touhara, H.; Nakanishi, K.; Watanabe N.: J. Chem. Phys., **1984**, 80(10), 5170; (b) Tanaka, H.; Nakanishi, K.; Touhara, H.: J. Chem. Phys., **1985**, 82(11), 5184; (c) Astrand, P.O.; Wallqvist, A.; Karlstrom, G.; Linse, P.: : J. Chem. Phys.; **1991**; 95(11); 8419; (d) Astrand, P.O.; Wallqvist, A.; Karlstrom, G.: J. Chem. Phys.; **1994**; 100(2) 1262; (e) Hernandez-Cobos, J.; Ortega-Blake, I.; Bonilla-Marin, M.: J. Chem. Phys.; **1993**; 99(11) 9122; (f) Boek, E.S.; Briels, W.J.; van Eerden, J.; Feil, D.: J. Chem. Phys.; **1992**; 96(9) 7010; (g) Boek, E.S.; Briels, W.J.: J. Chem. Phys.; **1993**; 98(2) 1422.

[107.] Godínez, L.A.; Schwartz, L.; Criss, C.M.; Kaifer, A.E.: J. Phys. Chem. B, **1997**, 101(17), 3376; Shen, X.; Belletête,M.; Durocher, G.: J. Phys. Chem. B, **1997,** 101(41), 8212; Wallqvist, A.; Covell, D.G.; Thirumalai, D.: J. Am. Chem. Soc., **1998** 120(2), 427.

[108.] Castronuovo, G.; Elia, V.; Postiglione, C.; Velleca, F.: Thermochim. Acta **1999**, 339(1), 11; Shelton, V.M.; Sosnick, T.R.; Pan, T.: Biochemistry **1999**, 38(51), 16831; Griko, Yu.V.; Kutyshenko, V.P.: Biophys. J., **1994,** 67(1), 356.

[109.] Swaminathan, S.; Craven,B.M.; McMullan, R.K.; Acta Cryst., **1984**, B, 40, 300.

[110.] Kontoyianni, M.; Bowen, P., J. Comput. Chem., **1992**, 13, 657.

[111.] Meier, R. J.; Coussens, B., J. Mol. Struct., **1992**, 253, 25.

[112.] Gobbi, A.; Frenking, G., J. Am. Chem. Soc., **1993**, 115, 2362.

[113.] Dixon, D. A.; Matsuzawa, N., J. Phys. Chem., **1994**, 98, 3967.

[114.] King, S. T., Spectrochim. Acta, **1972**, 28, 165.

[115.] Godfrey, P.D.; Brown, R.D.; Hunter A.N.; J. Mol. Struct., **1997**, 413-414, 405; Brown, R. D; Godfrey, D.; Storey, J., J. Molec. Spect., **1975**, 58, 445.

[116.] Rousseau, B.; Van Alsenoy, C.; Keuleers, R.; Desseyn, H.O.: J. Phys. Chem., **1998**, A102, 6540.

[117.] Langer, J.; Schrader, B.; Bastian, V.; Jacob, E, Fresenius J. Anal. Chem., **1995**, 352, 489.

[118.] Hadzi, D.; Kidric, L.; Knezevic, Z.V.; Barlic, B.: Spectrochim. Acta, **1976**, A32, 693.

[119.] Keuleers, R.; Desseyn, H. O.; Rousseau, B.; Van Alsenoy, C.;,J. Phys. Chem., **1999**, *A.103,* 4621.

[120.] Perez, J.; Dupuis, M.: J. Phys. Chem., **1991**, 95, 6526.

[121.] Belosludov, R.V.; Li, Z.Q.; Kawazoe, Y. Molecular Engineering **1999**, 8, 105.

[122.] Harris, K.D.M.; Hollingworth, M.D. Urea, thiourea, and selenourea inclusion compounds, in J.-M. Lehn (Ed.), Comprehensive Supramolecular Chemistry, Vol. 6, Elsevier Science Ltd., Oxford, **1996**, 177.

[123.] Rutherford, J.S.; Calvo, C.: Z.Kristallogr., **1969**, 128, 229.

[124.] Suzuki, K.; Onishi, S.; Koide, T.; Seki, S. Bull. Chem. Soc. Jap., **1956**, 29, 127.

[125.] Kabo, G.Ya.; Miroshnichenko, E.A.; Frenkel, M.L.; Kozyro, A.A.; Simirskii, V.V.; Karsulin, A.P.; Vorob=eva, V.P.; Lebedev, Yu.A. Bull. Acad. Sci. USSR, Div. Chem. Sci. **1990**, 662.

[126.] (a) Dovesi, R.; Causa, M., Orlando, R., Roetti, C.; Saunders, V. R., J. Chem. Phys., **1990**, 92, 7402; (b) Gatti, C.; Saunders, V. R.; Roetti, C. J. Chem. Phys., **1994**, 101, 10686.

[127.] Miao, M.S.; Van Doren, V.E.; Van Alsenoy, C.; Martinis, J.L.: Proc. 5th Electronic Conf. On Comput. Chem. 1997; http://hackberry.chem.niu.edu/ECCC5/articles/article31/urea.html

[128.] Gilkerson, W.; Srivastava, K., J. Phys. Chem., **1960,** 64, 1485.

[129.] Lefebvre, J. Solid State Commun., **1973,** 13, 1873.

[130.] Lefebvre, J.; Fontaine, H.; Fouret, R.: J. Raman Spectrosc. **1975**, 4(2), 173.

[131.] Spackman, M.A.;Byrom, P.G.; Alfredsson, M.; Hermansson, K. Acta Cryst., **1988**, A55, 30.

[132.] (a) Mullen, D., Hellner, E. Acta Cryst., **1978,** B34, 1624.(b) Swaminathan, S., Craven, B. M., Spackman, M. A.; Stewart, R. F. Acta Cryst., **1984**, B40, 398; (c) Zavodnik, V., Stash, A., Tsirelson, V., Vries, R. de, Feil, D. Acta Cryst., **1999** B55, 45.

[133.] (a) Spackman, M.A.;Weber, H.P.; Craven, B.M. J. Am. Chem. Soc., **1988**, 110, 775; (b) Suponitsky, K.Yu.; Tsirelson, V., Feil, D. Acta Cryst., **1999** B55, 45.

[134.] Abramov,Y.A; Volkov, A.; Guang Wu, G.; Coppens, P.:*J. Phys. Chem. B*; **2000**; 104(9); 2183.

[135.] De Vries, R. Y., Feil, D.; Tsirelson, V. G.: Acta Cryst., **2000**, B56, 118.

[136.] Volkov, A., Wu, G.; Coppens, P.: J. Synchrotron Rad., **1999,** 6, 1007.

[137.] Kutoglu, A., Scheringer, C., Meyer, H., Schweig, A. Acta Cryst. **1983,** B38, 2626; Mullen, D. Acta Cryst. **1983**, B38, 2620; Gao, Y., Coppens, P. Acta Cryst. **1989,** B45, 298.

[138.] Takahashi, I.; Onodera, A.; Shiozaki, Y.: Acta Cryst.,B **1990**, 46, 661.

[139.] Ashcroft, S.J. J. Chem. Soc. A, **1970**, 1020.

[140.] Gomez, T.; Alfonso, L.; Sabbah, R. Thermochim. Acta **1982**, 57, 67.

CHAPTER 3

3. PERIODICAL AND CLUSTER CALCULATIONS ON EXPERIMENTAL CRYSTALLINE GEOMETRY

In this chapter we will apply single point periodical calculations on experimental crystalline geometry to the crystal of benzoquinone, compare the results to single point cluster calculations at different levels of theory, and consider the applicability of this approach to urea and thiourea.

3.1 Crystalline benzoquinone.

Para-benzoquinone forms stable crystals with a melting point of 116° C. A plane from the crystal structure is shown in Figure 3.1. All stabilizing interactions between the nearest neighbors within the plane are C-H...O hydrogen bonds. To understand the nature and the strength of the individual hydrogen bonds involved in the intermolecular interactions leading to crystal formation, and their cooperative effects, we applied *ab initio* cluster and periodical calculations to *para*-benzoquinone.

We performed *ab initio* calculations using the GAUSSIAN 94 and both CRYSTAL 92 and CRYSTAL 95 (CRYSTAL) suites of programs. Specific to the periodical calculations is that the coulomb and exchange integrals are evaluated
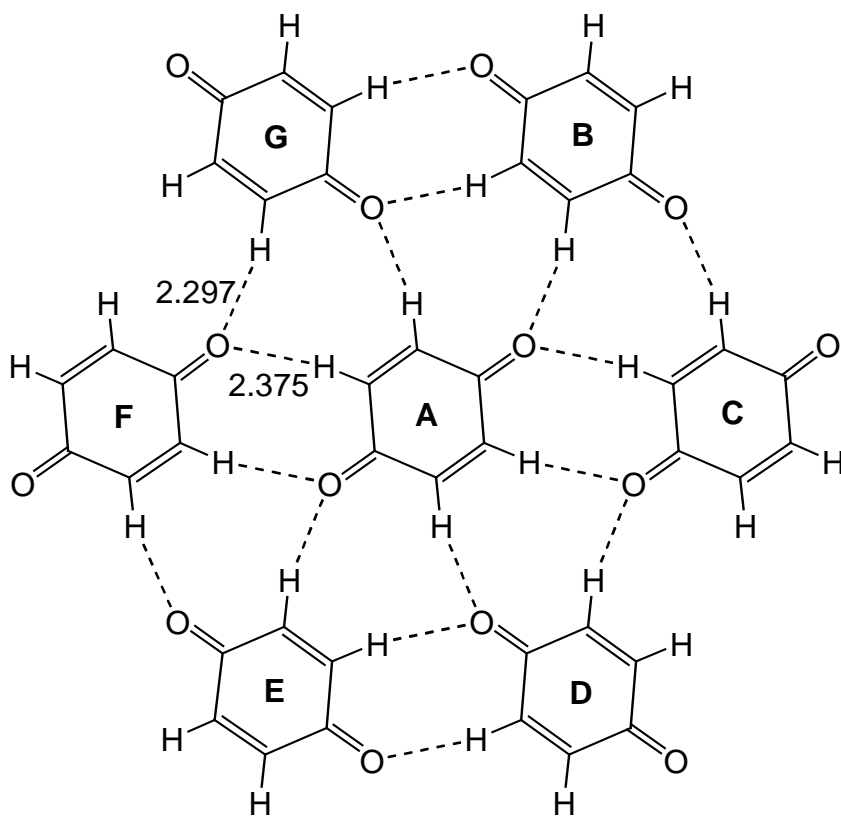
Figure 3.1. Seven molecules within a plane taken from the experimental crystal structure of *para*-benzoquinone.

exactly only when the overlap is larger then a given threshold and estimated from multipolar expansions by the Ewald method outside this inner zone.[1] Corresponding threshold levels (including coulomb overlap, coulomb penetration, and exchange overlap tolerances) were set to 10^{-6}, 10^{-8}, and 10^{-6}, respectively. Other tolerances (pseudo overlap) refer to different terms in the exchange summation series in reciprocal space and were left at their default levels (10^{-6} and 10^{-12}). Convergence criteria were 10^{-5} on eigenvalues and 10^{-6} on total energy. We found these values for

tolerances and convergence to be necessary to make the CRYSTAL calculations

consistent with GAUSSIAN 94 calculations on identical clusters. We changed the

conversion factor between Ångstroms and Bohrs in CRYSTAL 92 (where it is given to

five places) to the more precise value used in GAUSSIAN 94. Without this change,

there were slight (about 0.6 kcal/mol) differences in the internuclear repulsions for the

monomer. GAUSSIAN 94 uses six d-functions as the default for the polarization

functions, while CRYSTAL uses only five. The 6-21G** calculations performed with

GAUSSIAN 94 used the (non-default) value of five d-orbitals.

We used GAUSSIAN 94 to calculate aggregates of from 1 to 7 *para*-

benzoquinone molecules. Both Hartree-Fock and the density functional theory were

used with the 6-21G** and D95* basis sets. The DFT calculations employed the

B3LYP and B3PW91 functionals. In addition, we used the AM1 semiempirical

method[2] to calculate the aggregates for comparison. This method has been shown to

give accurate results for H-bonds other than those involving O-H...O[3] and C-H...O

interactions in dimeric H-bonding interactions,[4] The method also seems to give

reasonable results for aggregate calculations,[5] although no energetic comparisons for

these specific interactions are available. MP2 calculations of two stacking interactions

were also performed. These were limited to dimers.

We prefer to use neutron diffraction studies as input to our calculations, as

these directly provide the positions of the hydrogen atoms. However, no neutron

diffraction studies of *para*-benzoquinone crystals have been reported. The present

calculations use the experimental crystal geometry taken from the low temperature

(-160" C) X-ray diffraction study (R 0.074).[6] An earlier X-ray diffraction study at

room temperature had been reported.[7] The coordinates were taken directly from the

Cambridge Crystallographic Data Base.[8] The positions of the H-atoms were fixed at

1.08 Å from the carbon atoms in the crystal structure. *para*-Benzoquinone crystallizes

with a unit cell containing two molecules in space group $P2_1/a$. Both molecules of the

unit cell provided the repeating unit for 3D- (crystal) and 2D- (slab) calculations. One

molecule is sufficient for the repeating unit in one of the 1D-chains, while two

molecules are necessary for the other two (equivalent) chains. One should note that the

H-bonding sheets in the crystal slightly deviate from planarity.

The counterpoise[9] corrections to the basis set superposition error were

performed differently in the aggregate and periodic calculations. For the aggregates,

the counterpoise (CP) correction was evaluated from the calculation of each

monomeric unit in the presence of the ghosts of all the others. As it was described in

the Section 2.3, the counterpoise correction for the periodic calculation is usually done

using cluster calculations of the molecule in the presence of a limited number of

ghosts, representing the nearest atoms of other molecules. We found this approach

unsatisfactory. Instead, we considered all the ghosts located closer than a certain

distance to any atom of the monomeric unit. Gradually increasing this distance, we

monitored the change in the CP-correction. The distance of 4 Å was chosen as a

compromise between disk space and precision. CP-correction is particularly large for

the 6-21G** (5D) basis set used in the CRYSTAL calculations. However, after

correction, the interaction energies of the clusters for this basis that became

approximately equal to those calculated using the other methods.

No geometric optimizations were attempted for several reasons: (a) We wish to evaluate the interactions at the experimental geometry; (b) The large basis set superposition errors (BSSE) and consequent counterpoise corrections would be expected to adversely affect the reliability of the potential energy surface.[10]

3.2 Benzoquinone cluster calculations

The interaction energies for clusters containing up to seven benzoquinone molecules calculated five different ways are collected in Table 3.1. To simplify our discussion, we will use the B3LYP/D95* calculated values where individual energies are cited. These seem appropriate as they allow for electron correlation and are in reasonable agreement with three of the other methods, while the B3PW91 results seem to differ.

The energy of an individual hydrogen bond was taken as that of the **AB** dimer (see Figure 3.1), this being the only dimer containing only one hydrogen bond. The stabilization energy of 0.97 kcal/mol is consistent with other calculations on C-H...O interactions of this type. The results of the calculations on the **AC** dimer and other aggregates suggest that H bond cooperativity plays an important role in the crystal interaction energy. We approximated the cooperativity of each aggregate calculated using GAUSSIAN 94 by subtracting the appropriate number of individual hydrogen bond energies from the total interaction energy. Within the planar structure depicted

in Figure 3.1, one can trace several kinds of cyclic hydrogen bonding interactions.

One kind of ring involves two molecules, each providing hydrogen bonding donor and

an acceptor. Molecules **A** and **C** form such a cycle. These hydrogen-bonding rings

contain eight atoms and six π-electrons in a ring and provides the proper polarization

(alternating positive and negative) in the σ-system. A second kind of ring involves

three molecules. Molecules **A, B** and **C** form such a ring. Here, one molecule, **A**,

provides two acceptors, the second molecule, **B**, provides a donor and an acceptor

while the third molecule, **C**, provides two donors within the H-bonding ring. These H-

bonding rings also contain 6 π-electrons, but do not provide the proper polarization

(alternating positive and negative) in the σ-system as they contain an odd number of

atoms (nine). Consequently, the **AC** ring leads to a much larger cooperative interaction

than the **ABC** ring. Each aggregate composed of 3 or more molecules that contain an

ABC ring must also contain at least one **AC** type ring. The cooperativity due to the

ABC ring can be estimated as the difference between the total cooperativity in **ABC**,

less the cooperativity of the **AC**-ring. The data in Table 3.1 indicate the total **ABC**-

ring cooperativity (-0.13 kcal/mol) to be about 10% of the **AC**-cooperativity (-1.55

kcal/mol). Inspection of Figure 3.1 leads to identification of larger H-bonding rings

(each of which contains one or more of the smaller ones).

Aside from the **ABC** aggregate discussed above, two other trimers are

identifiable from Figure 3.1: **FAC** and **EAB**. **FAC** contains two **AC** interactions. The

central molecule, **A**, is polarized opposite of its two partners: **C** and **F**. As a result, the

additional cooperativity in the **FAC** aggregate (as compared to two **AC**s) is negligible

(-0.05 kcal/mol). The **EAB** aggregate is destabilized slightly (+0.05 kcal/mol) relative

to two **AB** interactions. The likely cause for this is a repulsive interaction of 0.04

kcal/mol (Table 3.1) between molecules **B** and **E** (due to their relative orientations)

combined with the uncooperative polarization of the central molecule, **A**. As there are

no cyclic H-bonding structures in **EAB**, no aromatic stabilization is possible.

Table 3.1. Energies of benzoquinone clusters calculated using GAUSSIAN 94
(kcal/mol).

M[a]	HB[b]	Type[c]	AM1	HF 6-21G**5D		B3LYP D95*	B3PW91	MP2
				Energy of interaction				
2	2	AC	-3.01	-3.03	-3.40	-3.49	-2.65	
	1	AB	-1.06	-0.71	-0.79	-0.97	-0.38	
	0	A'A						-0.73
	0	A'D						-1.62
	0	BE	0.03	0.04	0.06	0.04	0.04	
3	4	FAC	-6.07	-6.19	-6.90	-7.03	-5.36	
	2	EAB	-2.06	-1.27	-1.45	-1.89	-0.74	
	2	GAD	-2.03	-1.17	-1.36	-1.82	-0.67	
	4	ABC	-5.18	-4.61	-5.01	-5.56	-3.60	
4	7	ABCG	-9.31	-8.49	-9.18	-10.00	-6.71	
	6	ABCD	-7.54	-6.65	-7.08	-8.13	-5.04	
7	16	ABCDEFG	-21.16	-19.51	-20.85	-23.23	-15.48	
				Total cooperative interaction				
2	2	AC	-0.88	-1.61	-1.82	-1.55	-1.89	
	1	AB	0.00	0.00	0.00	0.00	0.00	
3	4	ACF	-1.81	-3.35	-3.73	-3.15	-3.84	
	2	ABE	0.07	0.15	0.13	0.05	0.02	
	2	ADG	0.09	0.25	0.22	0.12	0.09	
	4	ABC	-0.93	-1.77	-1.84	-1.68	-2.08	
4	7	ABCG	-1.86	-3.52	-3.63	-3.21	-4.05	
	6	ABCD	-1.16	-2.39	-2.33	-2.31	-2.76	
7	16	ABCDEFG	-4.14	-8.15	-8.16	-7.71	-9.40	
			Estimate of infinite sheet energy from aggregate					
	total		-5.44	-5.30	-5.44	-6.19	-4.33	
Cooperative component			-1.19	-2.46	-2.26	-2.31	-2.81	

[a]number of molecules in aggregate [b]number of H-bonds in aggregate [c]See Figure 3.1.

The total cooperative contribution to the seven-molecule aggregate (-7.71

kcal/mol) is roughly one-third the total interaction energy (-23.23 kcal/mol), about

10% more than would be expected from adding the cooperative contributions from

each of the dimers (-6.98 kcal/mol). We estimate the stabilization energy of an

individual molecule in an infinite sheet from the heptamer (-6.19 kcal/mol) by

subtracting the stabilization due to the eight H-bonds (two **AC** rings and four H-bonds)

that do not involve the central molecule, then dividing by two (as each hydrogen bond

involves two molecules). The cooperative contribution is 37% (-2.31 kcal/mol).

3.3 Benzoquinone periodical calculations

The results of periodic calculations on infinite chains, slabs, and the three

Table 3.2. Periodic calculations using CRYSTAL95 at the HF/6-21G** level. Cluster
calculations using trimers in place of infinite chains with the same basis set are
included for comparison.

	Periodic calculation			Aggregate calculation	
Chains	Uncorrected	CP-corrected	using MP2/D95** dimeric **A'D** and **A'A**	uncorrected	CP-corrected
ACF	-8.71	-3.35		-8.73	-3.35
ABE	-3.13	-0.85		-1.20[a]	-0.20[a]
ACF + 2 **ABE**	-14.97	-5.05		-10.13	-3.75
2D-slab	-15.20	-5.49		-15.49	-5.30
Stack **A'D**	-0.34	+1.78	-1.62		
Stack **A'A**	-0.64	+0.18	-0.73		
all chains	-16.28	-1.31			
3D-crystal	-15.17	-0.93	-9.46[b]		

[a]The average of **ABE** and **ADG** from table 1. [b]The MP2/D95* values for the dimers replace the two
stack **A'D** and stack **A'A** periodic HF calculations and are added to the corrected slab interaction.
dimensional crystal are collected in Table 3.2. Due to limitations in the CRYSTAL

programs, we were constrained to work at the HF/6-21** level, using five d-orbitals

(rather than the six used in the more common gaussian basis sets). Individual (finite)

aggregates were calculated using this procedure for comparison with the periodic

calculations. In the following discussion, all energies (including the cluster

calculations that are used for comparison) refer to the values obtained using this

procedure. The large CP corrections required to offset the BSSE have complicated the

analysis of these calculations. In many cases, the CP correction accounts for more than

half the (uncorrected) interaction energy. The fact that the CP-corrections are so large

combined with the substantially different procedures necessary for calculating CP in

CRYSTAL makes comparisons somewhat difficult.

In the crystal structure, one can identify four different types of chains formed

by the nearest neighbors in the benzoquinone crystal: two within the planar sheet

(formed by molecular contacts of **AB** and **AC** type), and two involving molecules in

adjacent sheets (stacking interactions). The different stacking interactions (Figure 3.2)

involve interactions of the type **A-D** (smmetrically equivalent to **A-E**) and **A-A**. The

stabilization/molecule of infinite chain **AC** before CP correction shows no additional

cooperative effect beyond the stabilization of the dimer (8.7 kcal/mol for both), but

roughly 10% additional cooperativity after CP correction (3.3 vs. 3.0 kcal/mol). This

result is consistent with the discussed above small additional cooperativity of the **FAC**

aggregate with respect to the two **AC**-s. The interaction energy per hydrogen bond of

chain **AB** is less than for the dimer (-3.1 vs. -3.3 kcal/mol) before CP correction. This
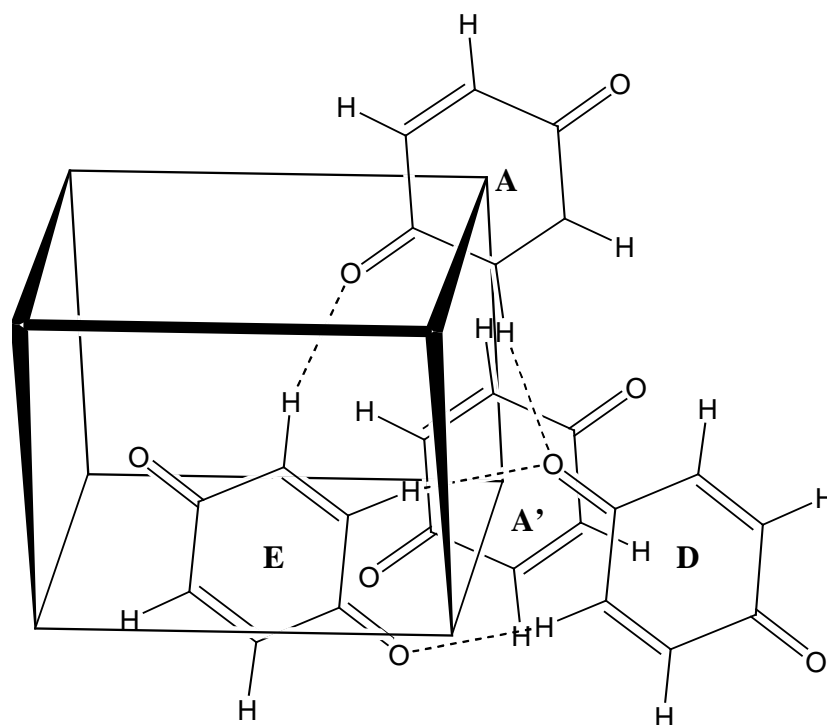
Figure 3.2. Four molecules forming stacking interactions in the experimental crystal structure of *para*-benzoquinone. Molecules **A**, **D** and **E** correspond to the same molecules in Figure 3.1. Molecule **A'** corresponds to a molecule equivalent to **A** in a plane behind that of **A**, **D** and **E**.

appears to be consistent with the calculation of the **EAB** aggregate (discussed above), where the interaction was slightly less than that of two **AB**=s. However, unlike the **BE** interaction which is repulsive, the **CF** interaction should be attractive. The chains that involve stacking interactions, **A**=**D** and **A**=**A**, have interaction energies of -0.34 and -0.64 kcal/mol, respectively. However, they both become repulsive after CP-correction (see Table 3.2). The sum of interaction energies over in-plane chains (taking into account that each molecule participates in one **AC** and two **AB** chains) is -15.0 kcal/mol before CP correction to be compared to -15.2 kcal/mol interaction energy per molecule of the infinite sheet. Nonadditivity of the CP correction makes BSSE

corrected values difficult to compare. The sum over all chains leads to the total

stabilization of 16.28 kcal/mol vs. 15.20 kcal/mol for the 3D structure. The apparent

negative cooperative effect could be due to repulsive 1-3 interactions between

molecules in different chains as well as the non-additivity of the BSSE.

Stabilization of the double infinite sheet is 15.20 before and 5.49 kcal/mol

after CP-correction, as calculated by this method. Thus, the sheets do not interact

before CP correction, but repel each other by 3.74 kcal/mol after correction. The

crystal stabilization after CP correction (0.9 kcal/mol) is consistent with the facts that

each sheet has two neighbors in 3D-structure and that there should be a repulsive

interaction between every second sheet. Clearly, the repulsion between adjacent sheets

must be an artifact of the calculation. There are several reasons for this repulsion: (1)

the intermolecular distances were not optimized for this basis set and fell into a

repulsive region of the potential curve; (2) the basis set gave large BSSE; (3) the HF

method systematically underestimated dispersion energy, which were important for π-π

stacking interactions. MP2/D95* calculations give stacking interactions between

sheets that are attractive by 3.97 kcal/mol (two **A=D** interactions of -1.62 and one **A=A**

interaction of -0.73 kcal/mol). If this stacking interaction is used to replace the 3.74

kcal/repulsion, the crystal interaction becomes -9.46, instead of -0.93 kcal/mol.   In

any case, we can conclude that stacking interaction between the sheets in the crystal

are weaker then the H-bonding interactions. This is consistent with weak stacking

energy.

For the discussion of stacking interactions it is useful to mention a recent work

on the dimer of *para*-benzoquinone and pyridine.[11] MP2 calculations overestimated

the stability of the stacking interactions before BSSE. Only after CP correction of the

MP2 energy, did the (experimentally observed) planar H-bonding interactions become

more stable than the stacking interactions. The best stacking interaction (before

vibrational correction) for benzoquinone/pyridine was reported to be 3.06 kcal/mol, or

about twice the apparent stacking in benzoquinone crystals as estimated above. The

calculations using HF or DFT methods show no stability for stacking of benzoquinone

and pyridine. This is no surprise, as interactions that are often attributed to dispersion

forces or time-dependant polarization are poorly treated by HF calculations. This effect

occurs for both H-bonds and stacking interactions but is hidden by much stronger

(usually) electrostatic components of H-bonds. If one neglects multipole/multipole

interactions, the stacking interaction between two nonpolar molecules at HF level

might be close to zero. DFT methods also have not been successful in calculating

dispersion interactions.

The experimental heat of sublimation for benzoquinone has been reported as

15.0 ± 0.8 kcal/mol.[12] This value is close to the uncorrected three dimensional periodic

value calculated by CRYSTAL and is about 1.5 times greater then the most reasonable

(corrected) calculated interaction energies. This overestimation holds even if one

replaces the repulsive stacking interactions with the attractive MP2/D95* values for

the **A≡D** and **A≡A** dimers, which leads to a crystal energy of 9.46 kcal/mol. If one

estimates the stacking interaction to be about 3 kcal/mol from benzoquinone/pyridine

stacking value, the calculated sublimation energy for benzoquinone becomes about 8.5

kcal/mol, a slightly lower value. One might assume that this value might become somewhat greater if one used the B3PLYP procedure instead of HF/6-21G**. The B3LYP calculation of the stabilization in the seven molecule aggregate is 17% greater than that calculated by HF/6-21G** for the same system. Applying this correction to the CRYSTAL slab calculation and using the MP2/D95* values for the stacking stabilization would yield an estimate of 10.4 kcal/mol for the heat of sublimation. These calculated interactions do not include vibrational corrections or relaxation of the geometry of the crystal to that of the monomer or the PΔV work done upon sublimation. The AM1 calculations performed for comparison gave results for the individual interactions that are similar to the *ab initio* aggregate values, although the cooperative components are somewhat lower.

3.4 Comparison of cluster and periodical calculations

Calculations using various *ab initio* and semiempirical methods gave similar results for the hydrogen bonds within aggregates containing up to seven p-benzoquinone molecules taken from the experimental crystal structure.

The disaccord between the experimental and theoretical results might be due to one or more of several factors: (1) The cooperative component of the crystal interactions might be poorly approximated by the CRYSTAL calculations. (2) The estimate of the stacking interaction or its cooperativity might be inadequate. To the extent that MP2 calculations on the dimer are used, no cooperativity is taken into

account. (3) There may be errors in the experimentally determined heat of sublimation.
Nevertheless the individual C-H...O hydrogen bonding energies are in accord with
those previously reported for other systems.

Cooperativity accounts for approximately half the interaction energy of the
heptamer aggregate. Since the capacity for cooperativity will be greater in the infinite
3D crystal, the cooperative component must be somewhat greater than that calculated
for this aggregate.

3.5 Crystal orbital HF calculations on urea and thiourea in experimental geometry

In order to analyze cooperative effects in crystals of urea and thiourea (Figure
3.3), we carried out periodical HF calculations in the experimental geometry. The
results are summarized in Table 3.3.
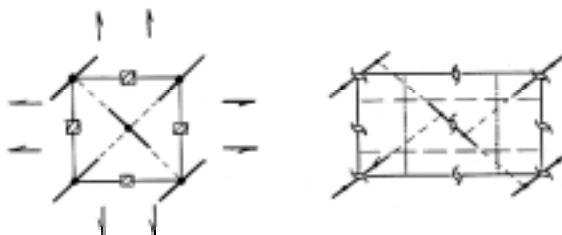
Figure 3.3. The schematic representation for tetragonal *P-42m* (left) and orthogonal
Pmna (right) crystal structures considered for urea and thiourea.

Table 3.3. Results for single-point 1,2,3D-periodical HF/6-311G** calculations on tetragonal urea and orthogonal thiourea in experimental geometry. Total energy in hartree, interaction energy (molecular relaxation is not included), and counterpoise correction CP in kcal/mol.

	E_{tot}	ΔE	ΔE_{cp}, 2.5A	ΔE_{cp}, 3.0A	ΔE_{cp}, 3.5A	ΔE_{cp}, 4.0A	cp 4.0A
				Tetragonal urea			
AB	-448.098968	-10.72	-9.44	-8.99	-8.97	-8.92	0.90
Z (**CAB**)	-224.065174	-15.21	-14.16	-13.82	-13.77	-13.72	1.49
2Z	-448.135170	-16.72	-14.62	-14.18	-13.88	-13.81	2.91
AD	-448.094288	-7.78	-6.69	-6.42	-6.32	-6.27	0.76
X (**EAD**)	-448.103135	-6.67	-5.57	-5.29	-5.20	-5.15	1.52
XY	-448.127326	-14.26	-14.26	-11.53	-11.38	-11.03	3.23
XZ	-448.136808	-17.23	-14.46	-14.00	-13.53	-13.41	3.82
XYZ (3D)	-448.151783	-21.93	-17.76	-17.19	-16.24	-16.12	5.81
3D, 6-21G**	-447.681065	-33.29	-20.99	-18.27	-16.44	-16.30	17.00
				Orthogonal thiourea			
AB	-1093.382983	-9.94		-9.49	-9.33	-9.31	0.64
AF	-1093.378284	-6.99		-6.41	-6.23	-5.93	1.07
AD	-1093.373880	-4.23		-4.23	-4.08	-3.99	0.24
XYZ (3D)	-2186.821710	-13.72		-12.43	-11.39	-11.03	2.69

Previously reported HF calculations by Dovesi, Roetti et al.[13] on urea crystal were done with the small basis set 6-21G** resulting in high BSSE. We used a 6-311G** basis set to minimize this error. Since basis with low exponential values lead to convergence problems, we had to modify standard 6-311G** by increasing the outermost exponent of SP-functions for the carbon atom from 0.18 to 0.22. Similar modification of the 6-31G** basis set for the periodical calculations were used by Abramov, Coppens et al.[14] They changed the outermost exponents for both C and H atoms to 0.20. In our case, this modification also improved convergence but it resulted in bigger increase in total energy; besides, there was a deviation of the basis set on H atom from the optimum value could affect H-bonding. That is why we preferred to

modify the exponent on the C atom only. After this modification, the convergence was stable. Since full counterpoise correction is impossible for an infinite system, we had to limit the number of ghost atoms used in CP correction to all atoms located at the distance closer than the fixed distance from any atom of the molecule. We used four distances in the range from 2.5 to 4.0 Å. The distance of 3.5Å was found sufficient, as the CP value did not change by more then 0.2 kcal/mol upon further increase.

Total cohesion energy for the urea crystal was found 16 kcal/mol (22 kcal/mol before CP correction). For the 6-21G** basis set, this value is 16.3 kcal/mol, which agrees with the bigger basis set but differs from the value of 21.5 kcal/mol previously reported by Dovesi, Roetti et al.,[13] because of incomplete CP correction in their paper. After adding molecular relaxation and pyramidalization energy (5.00 and 1.51 kcal/mol, obtained by geometry minimization using GAUSSIAN98 and the modified 6-311G** basis set) the energy is 9.5 kcal/mol, two times less then experimental enthalpy of sublimation. For the thiourea crystal after molecular relaxation (1.52 kcal/mol) and piramidalization (0.03 kcal/mol) the cohesion energy is 10 kcal/mol, also about a half of the experimental value. Underestimation the heat of formation in the periodical HF calculations was reported by Abramov, Coppens et al.[14] We should note, that calculated energy does not include zero-point vibration correction and is not directly comparable with enthalpy.

As one can see from the crystal structure (Figure 3.4), urea forms H-bonds with 2 neighbors within the chain (**AB** dimer, 9 kcal/mol) and with 4 neighbors from antiparallel chains (**AC** dimers, 6.6 kcal/mol). The sum of dimeric interactions yields
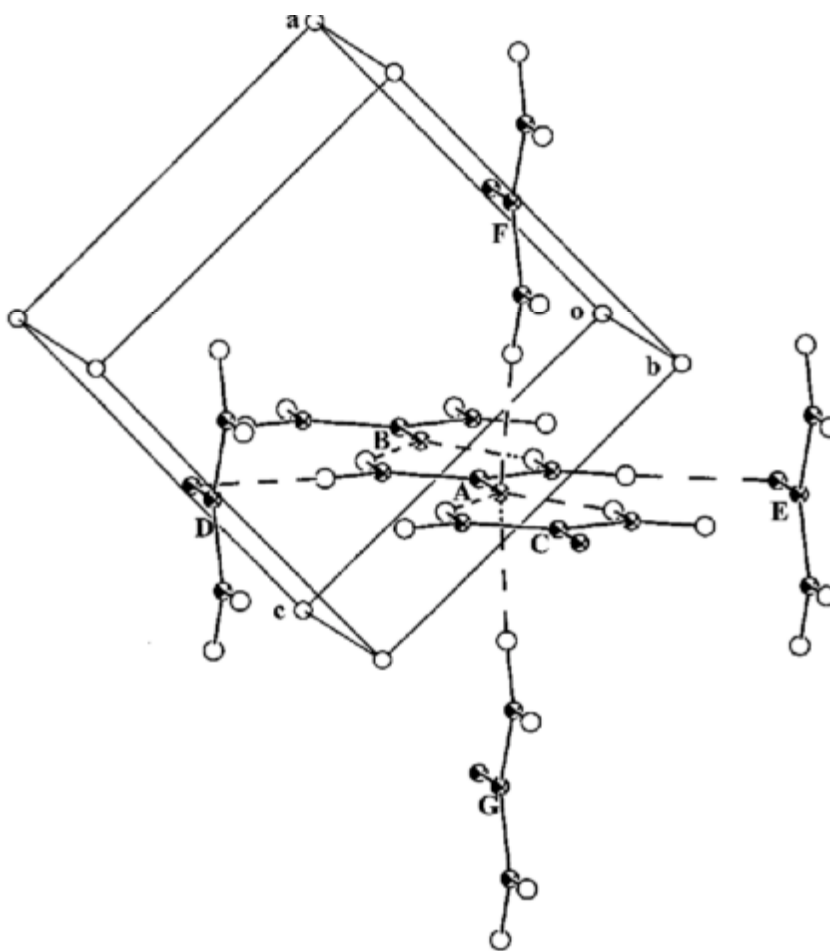
Figure 3.4. H-bonds between central molecule **A** and its nearest neighbors (**B-G**) in experimental crystal structure of urea.

22.2 kcal/mol, more than twice the result of 3D-calculation. For the thiourea (Figure

3.5) crystal sum of dimeric interactions **AB**, **AD**, and **AF** (9.3, 4 and 6 kcal/mol) is

19.3 kcal/mol, also twice of the periodical result. However, we did not include (often

repulsive) second-neighbor interactions in this estimate and neglected all cooperative

effects.
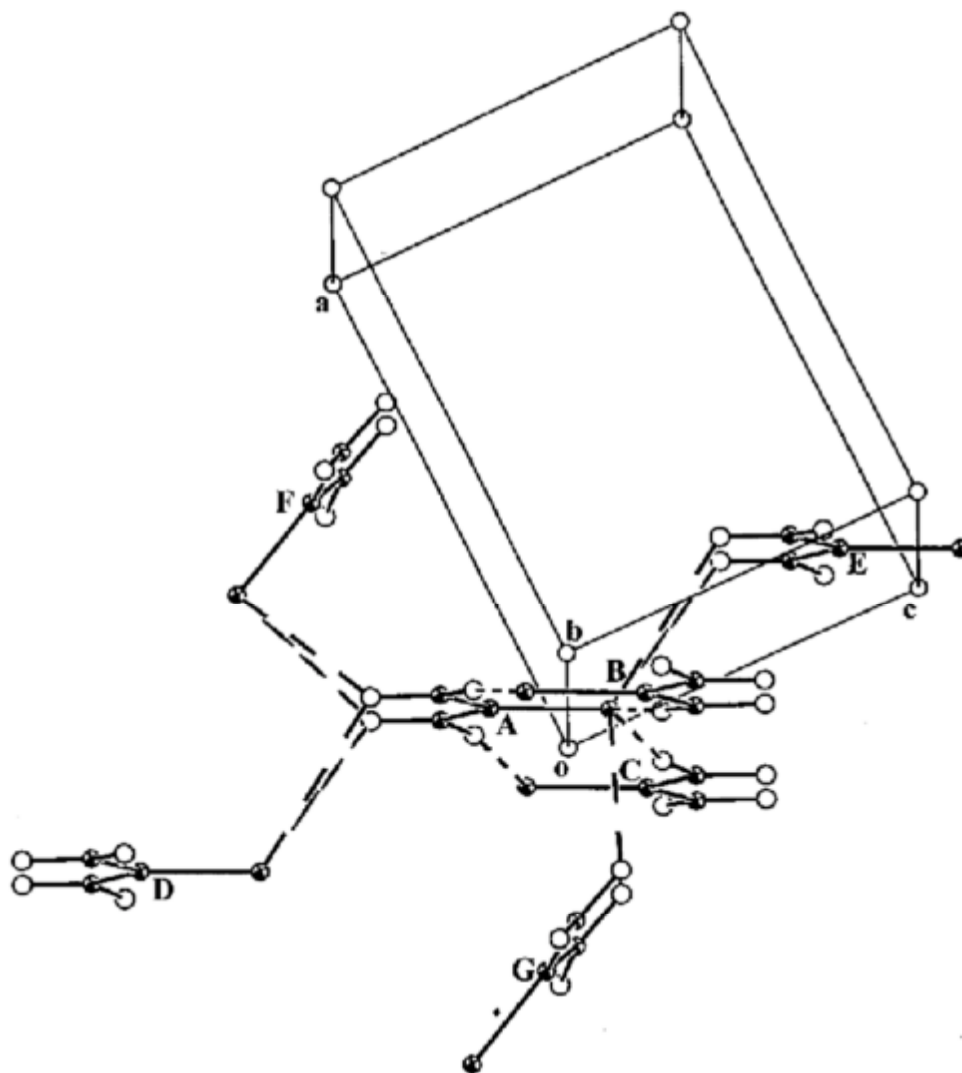
Figure 3.5. H-bonds between central molecule **A** and its nearest neighbors (**B-G**) in experimental crystal structure of thiourea.

We can also consider non-additive effects in different directions in the urea crystal. In Z-direction, H-bond energy increases more then 50% from dimer **AB** (9 kcal/mol) to an infinite chain (13.7 kcal/mol). Addition of an antiparallel chain stabilizes the system by only 0.1 kcal/mol (1.2 kcal/mol before CP correction), despite

the formation of one new H-bond of **AD** type per two molecules. This is due to repulsion between the molecules of antiparallel chains.

Similar weakening of H-bonds was found in periodical HF/6-31G** calculations of ice VIII.[15] Ice structure is a superposition of two 3D-networks of water molecules with opposite dipole moments. When these substructures are combined, electrostatic repulsion between molecules included into the different substructures results in the weakening of H-bonds.

An infinite layer of molecules in the XZ plane is slightly destabilizing with respect to isolated chains after CP correction (and 2 kcal/mol stabilizing before CP correction). The energy of the isolated H-bond in X-direction also decreases from 6.6 kcal/mol in **AD** dimer to 5.2 kcal/mol in the infinite chain. The formation of a second equivalent H-bond in Y-direction stabilizes the XY-layer so that is slightly cooperative with respect to X-chain (1 kcal/mol). As a result the 3D-structure is 3.5 kcal/mol more stable than the single chain in Z-direction, even though each molecule forms two H-bonds of **AD** type.

We should also mention, that part of non-additivity of intermolecular interaction comes from non-additivity in CP correction. The last column in Table 3.3 reports our best estimate for average CP correction per molecule in infinite structures and in dimers calculated with the same cutoff limit of 4 Å. Note that for the dimers the actual correction is twice the reported value. One can see for the Z-chain CP correction is 26% less then sum of corrections for **AB** and **AC** pairs, whereas for X-chain it is exactly equal to the sum for **AD** and **AE** pairs. This is because the addition of the

ghost **C** does not improve the wavefunction for **A** in the presence of ghost **B** as

efficiently as ghost **B** did. On the other hand, CP correction for the layer XY is 6%

greater then sum of two chains in X and Y directions. Similarly, CP correction for the

3D-structure is 22% greater than sum of the chains in X, Y, and Z directions due to the

presence of additional ghosts in 2D- and 3D-structure corresponding to diagonal

second-neighbors, which were not present in either of the chains.

3.6 Semiempirical optimizations of urea and thiourea tetragonal and orthogonal crystal structures

The application of single-point calculations to hypothetical polymorphic forms

is complicated by their unknown geometry. Although the structures for the tetragonal

forms of urea and orthogonal thiourea are known (see Figures. 2.3, 2.7, and 3.3), the

second polymorph is hypothetical. Therefore, crystal structures of orthogonal urea and

tetragonal thiourea must be qualitatively estimated.

A priori prediction of possible crystalline forms for urea and thiourea was

recently performed[16] using the POLYMORPH module of the Cerius^2 package,

commercially available from MSI. Dreiding force field[17] and rigid intramolecular

experimental geometry were used. Atomic charges were obtained by fitting to

molecular electrostatic potential distribution obtained in MNDO calculations. The

search was restricted to five space groups (*P2₁/c, P-1, P2₁2₁2₁, P2₁, C2/c*) with one

symmetrically independent molecule. These space groups cover 70% of the molecular

structures in the Cambridge Database. In some cases, the structure spontaneously

adopted higher symmetry. The local minima found in this search correspond to

possible polymorphic modifications. Atomic coordinates for the ten solutions of the

lowest energy are listed in Table 3.4. For urea, tetragonal structure was correctly found

to be the most stable, and orthogonal structure was among the the low-energy

polymorphs. For thiourea, the experimental orthogonal structure was not the most

stable, and tetragonal structure was not present among low-energy solutions.

Presumably, the reason for this failure was inaccuracy in the parameters of the additive

force field.

　　　We applied the semiempirical MO methods to predict the geometry of

orthogonal urea and tetragonal thiourea and compared their stability to the stability of

the experimentally observed structures. The periodical MO method with semiempirical

AM1[18] Hamiltonian as coded in MOPAC 6 (adapted[19] for Windows NT) was used.

Although only 1D- (polymer) capability is described in the manual, we have found that

this package gives reasonable results in all three dimensions for the test examples.

　　　The tetragonal structure of urea (described in Section 2.8) was modified. To

overcome inaccuracy of one-point Brillouin zone integration, translation vectors

should have values over 5 Å (as suggested in the MOPAC manual). For this purpose

,diagonal ($a=a+b$, $b=a-b$) coordinate transformation was applied to convert the

experimental tetragonal unit cell of $P\text{-}42_1m$ symmetry containing two molecules to a

supercell of *Cmm2* symmetry containing four molecules, and parameter c was doubled.

Consequently, the new unit cell contained four chain dimers, arranged in a cyclic

Table 3.4a. Space groups (number and axis setting option are given according to International Tables of Crystallography), optimized with Dreiding force field unit cell parameters and atomic fractional coordinates for ten the most stable structures, as predicted by Cerius2/POLYMORPH for urea.

	4 P 21		opt 1		14 P 21/c		opt 2		14 P 21/c		opt 2
abc	4.662	5.230	5.230	abc	5.208	5.208	10.687	abc	9.394	6.906	3.433
	90	90	90		90	119.166	90		90	90.004	90
N1	-0.3266	-0.1548	0.3880	N1	0.5536	0.1114	1.1650	N1	0.3894	0.3944	0.8061
C2	-0.1718	-0.0168	0.2500	C2	0.3373	0.2500	1.0873	C2	0.3118	0.2500	0.7500
N3	-0.3266	0.1212	0.1120	N3	0.2765	0.3886	1.1650	N3	0.3894	0.1056	0.6939
O4	0.0909	-0.0168	0.2500	O4	0.2061	0.2500	0.9561	O4	0.1815	0.2500	0.7500
H5	-0.2336	0.2350	-0.0018	H5	0.1163	0.5033	1.1196	H5	0.3463	-0.0141	0.6266
H6	-0.5281	0.1045	0.1287	H6	0.3943	0.3714	1.2656	H6	0.4892	0.1253	0.7169
H7	-0.2336	-0.2686	0.5018	H7	0.6229	-0.0033	1.1196	H7	0.3463	0.5141	0.8735
H8	-0.5281	-0.1381	0.3713	H8	0.6370	0.1286	1.2657	H8	0.4892	0.3747	0.7831

	14 P 21/c		opt 1		14 P 21/c		opt 2		14 P 21/c		opt 2
abc	3.89	8.745	8.159	abc	6.95	6.655	6.465	abc	4.675	13.317	3.891
	90	118.471	90		90	84.496	90		90	78.404	90
N1	0.3433	0.1464	0.1081	N1	0.5554	0.1657	0.3560	N1	0.8523	0.6846	0.0767
C2	0.4145	0.0694	0.2500	C2	0.5495	0.2988	0.2206	C2	0.6706	0.6176	0.1974
N3	0.6272	0.1464	0.3919	N3	0.3877	0.3829	0.2425	N3	0.8092	0.5471	0.3012
O4	0.2835	-0.0580	0.2500	O4	0.6787	0.3394	0.0847	O4	0.4041	0.6205	0.2335
H5	0.6956	0.1039	0.5105	H5	0.3649	0.4836	0.1444	H5	0.7085	0.4904	0.4113
H6	0.6990	0.2455	0.3723	H6	0.2974	0.3383	0.3523	H6	1.0147	0.5551	0.2666
H7	0.1746	0.1039	-0.0105	H7	0.6670	0.0836	0.3543	H7	0.7882	0.7448	-0.0144
H8	0.4545	0.2455	0.1277	H8	0.4444	0.1531	0.4520	H8	1.0504	0.6719	0.0857

	14 P 21/c		opt 2		14 P 21/c		opt 1		14 P 21/c		opt 2
abc	4.684	3.809	13.619	abc	4.657	7.003	6.917	abc	10.002	6.906	3.434
	90	72.601	90		90	86.228	90		90	69.922	90
N1	0.7453	0.2924	0.0488	N1	1.2831	0.3954	0.1122	N1	0.3894	0.1056	1.3046
C2	0.5221	0.2023	0.1210	C2	1.1282	0.2500	0.1047	C2	0.3118	0.2500	1.4382
N3	0.6117	0.0761	0.1915	N3	1.2831	0.1047	0.1122	N3	0.3894	0.3944	1.4167
O4	0.2613	0.2483	0.1235	O4	0.8725	0.2500	0.0737	O4	0.1815	0.2500	1.5685
H5	0.4675	-0.0099	0.2513	H5	1.1982	-0.0163	0.0910	H5	0.3463	0.5141	1.5272
H6	0.8215	0.0738	0.1813	H6	1.4830	0.1245	0.1242	H6	0.4892	0.3747	1.2939
H7	0.7160	0.4012	-0.0100	H7	1.1982	0.5163	0.0910	H7	0.3463	-0.0141	1.2803
H8	0.9356	0.2559	0.0583	H8	1.4830	0.3755	0.1242	H8	0.4892	0.1253	1.2278

	14 P 21/c		opt 2
abc	7.685	7.691	4.726
	90	89.037	90
N1	0.2672	0.3340	0.8207
C2	0.3676	0.2128	0.8845
N3	0.3092	0.1349	1.0988
O4	0.5004	0.1731	0.7541
H5	0.3754	0.0390	1.1644
H6	0.2061	0.1798	1.1852
H7	0.2969	0.4005	0.6584
H8	0.1663	0.3505	0.9367

Table 3.4b. Space groups (number and axis setting option are given according to International Tables of Crystallography), optimized with Dreiding force field unit cell parameters and atomic fractional coordinates for ten the most stable structures, as predicted by Cerius2/POLYMORPH for thiourea.

	14 P 21/c		opt 2		14 P 21/c		opt 2		14 P 21/c		opt 1
abc	11.613	7.334	3.929	abc	5.458	3.775	15.796	abc	5.483	7.679	7.763
	90	70.229	90		90	108.804	90		90	69.117	90
N1	0.3410	0.3836	0.7826	N1	0.2536	1.2232	0.0517	N1	1.2459	0.1073	0.6134
C2	0.4046	0.2500	0.8455	C2	0.4485	1.2948	0.1226	C2	1.1208	0.2500	0.6090
N3	0.3410	0.1164	1.0355	N3	0.3876	1.3906	0.1923	N3	1.2459	0.3927	0.6134
S4	0.5601	0.2500	0.6899	S4	0.7606	1.2652	0.1240	S4	0.8158	0.2500	0.5996
H5	0.3833	0.0131	1.0871	H5	0.5237	1.4539	0.2463	H5	1.1682	0.5040	0.6058
H6	0.2533	0.1248	1.1239	H6	0.2080	1.4007	0.1879	H6	1.4157	0.3842	0.6227
H7	0.3833	0.4870	0.6463	H7	0.2858	1.1535	-0.0025	H7	1.1682	-0.0040	0.6058
H8	0.2533	0.3752	0.8695	H8	0.0818	1.2418	0.0552	H8	1.4157	0.1158	0.6227

	14 P 21/c		opt 2		14 P 21/c		opt 2		14 P 21/c		opt 1
abc	5.495	14.96	4.051	abc	4.052	14.96	5.499	abc	5.495	14.961	4.051
	90	68.434	90		90	111.679	90		90	111.56	90
N1	1.3245	0.0542	0.3094	N1	0.8661	0.9459	0.1755	N1	0.9025	0.3195	0.4774
C2	1.2322	0.1185	0.1739	C2	1.0938	0.8816	0.2678	C2	0.7322	0.3816	0.3261
N3	1.4026	0.1805	0.0226	N3	1.0748	0.8195	0.0974	N3	0.8245	0.4459	0.1907
S4	0.9167	0.1215	0.1971	S4	1.3862	0.8785	0.5833	S4	0.4167	0.3785	0.3029
H5	1.3541	0.2314	-0.0843	H5	1.2302	0.7686	0.1459	H5	0.7136	0.4944	0.0676
H6	1.5773	0.1746	0.0211	H6	0.9017	0.8254	-0.0773	H6	1.0046	0.4427	0.2142
H7	1.2136	0.0056	0.4324	H7	0.8539	0.9944	0.2864	H7	0.8540	0.2686	0.5843
H8	1.5046	0.0573	0.2859	H8	0.7095	0.9427	-0.0046	H8	1.0773	0.3254	0.4790

	14 P 21/c		opt 1		14 P 21/c		opt 1		14 P 21/c		opt 2
abc	5.368	8.263	7.178	abc	5.416	13.636	4.617	abc	8.401	9.453	4.013
	90	71.023	90		90	114.279	90		90	98.591	90
N1	0.8768	0.0906	0.6888	N1	0.2527	0.9263	0.1474	N1	0.4266	0.3619	0.8212
C2	0.9144	0.2418	0.6378	C2	0.4593	0.8812	0.1348	C2	0.5602	0.2966	0.7942
N3	1.1519	0.2830	0.5314	N3	0.4084	0.8331	-0.1263	N3	0.5623	0.1642	0.8819
S4	0.6661	0.3801	0.7057	S4	0.7720	0.8808	0.4395	S4	0.7182	0.3789	0.6560
H5	1.1851	0.3926	0.4857	H5	0.5522	0.7970	-0.1502	H5	0.6546	0.1060	0.8634
H6	1.2921	0.2046	0.4932	H6	0.2285	0.8348	-0.2931	H6	0.4686	0.1275	0.9630
H7	0.7008	0.0538	0.7579	H7	0.2747	0.9651	0.3309	H7	0.4132	0.4595	0.7528
H8	1.0242	0.0173	0.6601	H8	0.0802	0.9205	-0.0308	H8	0.3423	0.3104	0.9059

	19 P 21 21 21		opt 1
abc	8.307	5.614	6.73
	90	90	90
N1	0.1771	0.8616	0.2449
C2	0.1083	0.8397	0.0726
N3	0.0349	1.0255	0.0021
S4	0.1178	0.5814	-0.0580
H5	-0.0166	1.0150	-0.1258
H6	0.0340	1.1734	0.0748
H7	0.2352	0.7272	0.2985
H8	0.1724	1.0105	0.3160

herringbone cluster.

The orthogonal structure of *Pmna* symmetry with four molecules in the unit cell was taken from the experimental crystal structure of thiourea, described in Section 2.9 (see Figure 2.6). The notations were rearranged (*a=c, b=a, c=b*) so that the ribbons were parallel to Z-directions, like the chains in the tetragonal structure. We constrained the molecules to planarity, which is not imposed by symmetry in this structure. We also constrained the ribbons to be planar by changing the NCS...S dihedral from 5.6^o to 0°. The unit cell consists of two cyclic dimers, forming one herringbone H-bond between them. The C=S...S and S...S=C angles along this H-bond are flexible, so that optimization of these values for clusters, layers and ribbons distorts them considerably. For instance, optimization of the cluster representing one unit cell changes the values from 17° and 70° observed in crystal to 3° and 178° in the cluster. Instead of fixing these angles at their experimental values, we idealized them to 0° and 90°, so that the planes of the ribbons were orthogonal to each other. Both changes were achieved by 17° rotation of the symmetrically independent molecule about the crystallographic Z-axis. We will refer to the new structure as an idealized orthogonal structure. The experimental and idealized structures are shown side by side in Figure 3.6.

The energies of experimental and optimized structures are presented in Table 3.6. We should mention, that optimization slightly changes the crystallographic parameters from *a* 5.485 Å, *b* 7.657 Å, *c* 8.588 Å to *a* 5.305 Å, *b* 7.396 Å, *c* 8.217 Å, and idealization increases them to *a* 6.653, *b* 7.584, *c* 8.217. The unit cell

Figure 3.6. Experimental (left) and idealized (right) molecular packing in orthogonal thiourea.

volume increases from 322 Å³ to 415 Å³. According to Kitaigorodskii≠s postulate,[1] the molecules in the crystals are closely packed. This insures a minimum of isotropic components of intermolecular interaction (mostly dispersion attraction). Only in rare cases, when strong directional intermolecular interactions dominate (such as in ice), does the close packing principle fail to hold. Clearly, idealization of orthogonal unit cell contradicts the close packing principle. However, idealization stabilizes the unit cell tetramer by 2 kcal/mol, and the crystal structure by about 6 kcal/mol. This is because the HF method and its semiempirical simplifications give poor description of dispersion interactions.

    We have to note that experimental crystal structure is not a local minimum on calculated potential energy. After one subtracts the energy of molecular relaxation, the experimental structure is 3.5 kcal/mol less stable then the structure obtained after the

Table 3.5. Results for optimized and experimental 1,2,3D-periodical AM1 calculations on tetragonal and orthogonal structures of urea and thiourea. Heat of formation ΔH, periodical stabilization of the unit cell ΔH_{int}, and enthalpy of sublimation ΔH_{sub} are in kcal/mol.

	ΔH	ΔH_{int}	ΔH_{sub}	ΔH	ΔH_{int}	ΔH_{sub}	ΔH	ΔH_{int}	ΔH_{sub}	ΔH	ΔH_{int}	ΔH_{sub}
tetragon.	experimental urea			optimized urea			optimized thiourea					
1 mon	-42.93			-44.08			9.89					
1 cell	-372.68	0.00	-3.66	-409.74	0.00	-7.14	6.57	0.00	-9.07			
Z-chain	-404.48	-31.80	-7.63	-435.50	-25.76	-10.36	-25.70	-32.27	-13.10			
X-chain	-382.09	-9.41	-4.83	-420.10	-10.36	-8.43	-1.71	-8.28	-10.10			
XY-layer	-391.51	-18.83	-6.01	-430.49	-20.75	-9.73	-16.45	-23.02	-11.95			
XZ-layer	-411.41	-38.73	-8.50	-446.81	-37.07	-11.77	-32.76	-39.33	-13.99			
3D	-420.66	-47.98	-9.65	-457.45	-47.71	-13.10	-40.64	-47.21	-14.97			
orthog.				optimized urea			optimized thiourea			experimental thiourea		
1 mon				-44.08			9.89			16.9		
1 cell				-197.79	0.00	-5.37	10.05	0.00	-7.38	34.80	0.00	-8.20
Z-chain				-211.14	-13.35	-8.71	-0.20	-10.25	-9.94	13.83	-20.97	-13.44
X-chain				-201.92	-4.13	-6.40	4.02	-6.03	-8.89	18.03	-16.77	-12.39
Y-chain				-202.20	-4.41	-6.47	7.27	-2.78	-8.07	30.59	-4.21	-9.25
D-chain				-200.81	-3.02	-6.12	2.00	-8.05	-9.39	32.42	-2.38	-8.79
XY-layer				-210.18	-12.39	-8.47	-8.78	-18.83	-12.09	9.80	-25.00	-14.45
XZ-layer				-215.11	-17.32	-9.70	-7.68	-17.73	-11.81	0.45	-34.35	-16.79
YZ-layer				-215.11	-17.32	-9.70	-7.68	-17.73	-11.81	10.39	-24.41	-14.30
DZ-layer				-213.58	-15.79	-9.32				13.25	-21.55	-13.59
3D				-219.05	-21.26	-10.68	-23.60	-33.65	-15.79	-4.02	-38.82	-17.91
3D, exp				-217.17	-19.38	-10.21	-18.05	-28.10	-14.40			

optimization for both urea and thiourea.

One can see that the total sublimation energies are underestimated by about 30% AM1 correctly predicts the tetragonal form to be more stable for urea, but incorrectly predicts the tetragonal form of thiourea to be more stable by about 0.5 kcal/mol.

It is also interesting to compare cooperative effects in different directions. In agreement with HF/6-311G** results, the interactions in the tetragonal structure are almost additive in X and Y-directions (the XY layer is twice as stabilizing as the X-

chain), and anticooperative (by about 5%) in X and Z directions. In the orthogonal structure, the X and Y directions are strongly cooperative (25%), additive in Y and Z directions, and 10% anticooperative in X and Z-directions. Discussions of this effect will be presented in Chapters 5 and 7 below.

References for Chapter 3.

[1.] Pisani, C. Dovesi, R.; Roetti, C, Hartree-Fock ab-intitio treatment of crystalline systems, *Lecture Notes in Chemistry*, Vol. 48, Springer Verlag, Heidelberg, **1988.**

[2.] Dewar, M. J. S.; Zoebisch, E. G.; Healy, E. F.; Stewart, J. J. P. J. Am. Chem. Soc., **1985**, 107, 3902.

[3.] Dannenberg, J. J., THEOCHEM, **1997**, 401, 279.

[4.] (a) Turi, L.;Dannenberg, J. J., J. Phys. Chem., **1993,** 97,. 7899-909; (b) Dannenberg, J. J., THEOCHEM, **1997,** 401, 279-286.

[5.] a) Turi, L.;Dannenberg, J. J., J. Am. Chem. Soc., **1994,** 116,. 8714-21; b) Turi, L.; Dannenberg, J. J., Chem. Mater, **1994,** 6,. 1313-16; c) Turi, L.;Dannenberg, J. J., J. Phys. Chem., **1996,** 100,. 9638-964.

[6.] Van Bolhuis, F.; Kiers, C. T., Acta Crystallogr. B, **1978**, 34, 1015.

[7.] Trotter, J., Acta Crystallogr., **1960**, 13, 86.

[8.] Allen, F. H.; Kennard, O., Chemical Design Automation News, **1993**, 8, 31-37.

[9] (a) S. F. Boys, and F. Bernardi, Mol. Phys., **1970,** 19, 553; (b) A. Meunier, B. Levy, and G. Berthier, Theor. Chim. Acta, **1973,** 29, 49; (c) H. B. Jansen, and P. Ross, Chem. Phys. Lett., **1969,** 3, 40.

[10.] Simon, S;.Duran, M.;Dannenberg, J. J., J. Phys. Chem. A.., **1999**, 103, 1640; Simon, S.; Duran, M.;Dannenberg, J. J., J. Chem. Phys., **1996,** 105,. 11024, and references cited therein.

[11.] McCarthy, W.; Plokhotnichenko, A. M.; Radchenko, E. D.; Smets, J.; Smith, D. M. A.; Stepanian, S. G.; Adamowicz, L., J. Phys. Chem., **1997**, 101, 7208.

[12.] Magnus, A, Z. Phys. Chem (Frankfurt), **1956**, 9, 141.

[13] (a) Dovesi, R.; Causa, M., Orlando, R., Roetti, C.; Saunders, V. R., J. Chem. Phys., **1990**, 92, 7402; (b) Gatti, C.; Saunders, V. R.; Roetti, C. J. Chem. Phys., **1994**, 101, 10686.

[14] Abramov,Y.A; Volkov, A.; Wu, G.; Coppens, P.: J. Phys. Chem. B; **2000**; 104(9); 2183.

15. Silvi, B.: Phys. Rev. Lett., **1994**, 73(6), 842.

16. Steve Maginn, MSI, private communication, 1995.

17. Mayo, S.L.; Olafson, B.D.; Goddard, W.A.: J. Phys. Chem., **1990,** 94, 8897.

18. Dewar, M. J. S.; Zoebisch, E. G.; Healy, E. F.; Stewart, J. J. P. J. Am. Chem. Soc., **1985**, 107, 3902.

19. Victor Lobanov, University of Florida, 1996;
http://www.ccl.net/cca/software/NT/mopac6

CHAPTER 4

4. MO CALCULATIONS OF UREA MONOMERS AND DIMERS

In order to check the validity of approximations necessary to simplify cluster calculations, we performed a series of calculations on urea and thiourea monomers and dimers at different levels of the theory.

Ab initio (HF, MP2 and B3W91 with basis sets up to D95++**) and semiempirical (AM1, PM3 and SAM1) molecular orbital calculations are presented in this Chapter for urea and four different general classes of urea dimeric structures that correspond to interactions between the nearest neighbor molecular pairs in the crystal structures of urea and thiourea. While the urea monomers have nonplanar minima on all *ab initio* surfaces, on the HF and MP2/6-311+G (3df,2p) surfaces they are planar after vibrational and thermal corrections. Urea chain and ribbon dimers are calculated to be planar after counterpoise and thermal corrections for all HF calculations and nonplanar for MP2 calculations (D95** and D95++**). The DFT calculations predict planar chain, but nonplanar ribbon dimers. The ribbon dimer is the most stable, as it uses both H-bond acceptors, while the chain dimer uses only one, and the herring-bone dimer has one H-bond. Stacking interaction is much less stabilizing, and does not correspond to the energy minimum. The PM3 method fails in both predicting molecular conformations and H-bonds while AM1 gives reasonable results.

4.1 Molecular conformations and transition states of urea

The results for the urea monomer are summarized in Tables 4.1-4.4. Figure 4.1

Table 4.1. Results of semiempirical and *ab initio* calculations for urea transition states and conformers. NI - number of imaginary frequencies; ΔH_0 - heat of formation (kcal/mol); E - total electronic energy (a.u.); ΔE - relative energy (kcal/mol); $\Delta\Delta H_0$ - relative energy with zero point vibration correction (kcal/mol); $\Delta\Delta H_{298}$ - relative energy corrected for thermal vibrations at 298K (kcal/mol).

Method	Symmetry	NI	ΔH_0	E	ΔE	$\Delta\Delta H_0$	$\Delta\Delta H_{298}$
AM1	C_{2v}	1	-44.08				0.87
	C_2	0	-44.95				0.00
	C_s'	1	-40.22				4.73
	C_s''	1	-36.32				8.63
SAM1	C_{2v}	1	-44.07				0.04
	C_2	0	-44.11				0.00
	C_s'	1	-37.86				6.25
	C_s''	1	-33.02				11.09
PM3	C_{2v}	2	-40.96				6.05
	C_2	0	-47.01				0.00
	C_s	0	-45.82				1.19
	C_1	1	-44.10				2.91
	C_s'	2	-42.38				4.63
	C_s''	2	-37.35				9.66
	C_1'	1	-43.55				3.46
	C_1''	1	-39.37				7.64
HF/D95**	C_{2v}	2		-224.046152	1.29	0.00	0.00
	C_2	0		-224.048215	0.00	0.14	0.37
	C_s	0		-224.046551	1.04	0.35	1.05
	C_1	1		-224.046550	1.04	0.25	0.46
	C_s'	1		-224.034185	8.80	8.38	8.50
	C_s''	2		-224.023599	15.45	14.26	13.76
	C_1''	1		-224.023616	15.44	14.50	14.28
MP2/D95**	C_{2v}	2		-224.681770	2.49	1.04	0.84
	C_2	0		-224.685742	0.00	0.00	0.00
	C_s	0		-224.683453	1.44	1.01	1.20
	C_1	1		-224.683216	1.59	0.78	0.71
	C_s'	1		-224.673522	7.67	6.86	6.82
	C_s''	2		-224.662535	14.56	13.13	12.76
	C_1''	1		-224.662733	14.44	13.45	13.30
DFT/D95**	C_{2v}	2		-225.234852	1.46	0.10	0.00
	C_2	0		-225.237182	0.00	0.00	0.15
	C_s	0		-225.235506	1.05	0.43	0.91
	C_1	1		-225.235484	1.07	0.27	0.33
	C_s'	1		-225.224584	7.91	7.33	7.31
	C_s''	1		-225.214070	14.50	13.20	13.45
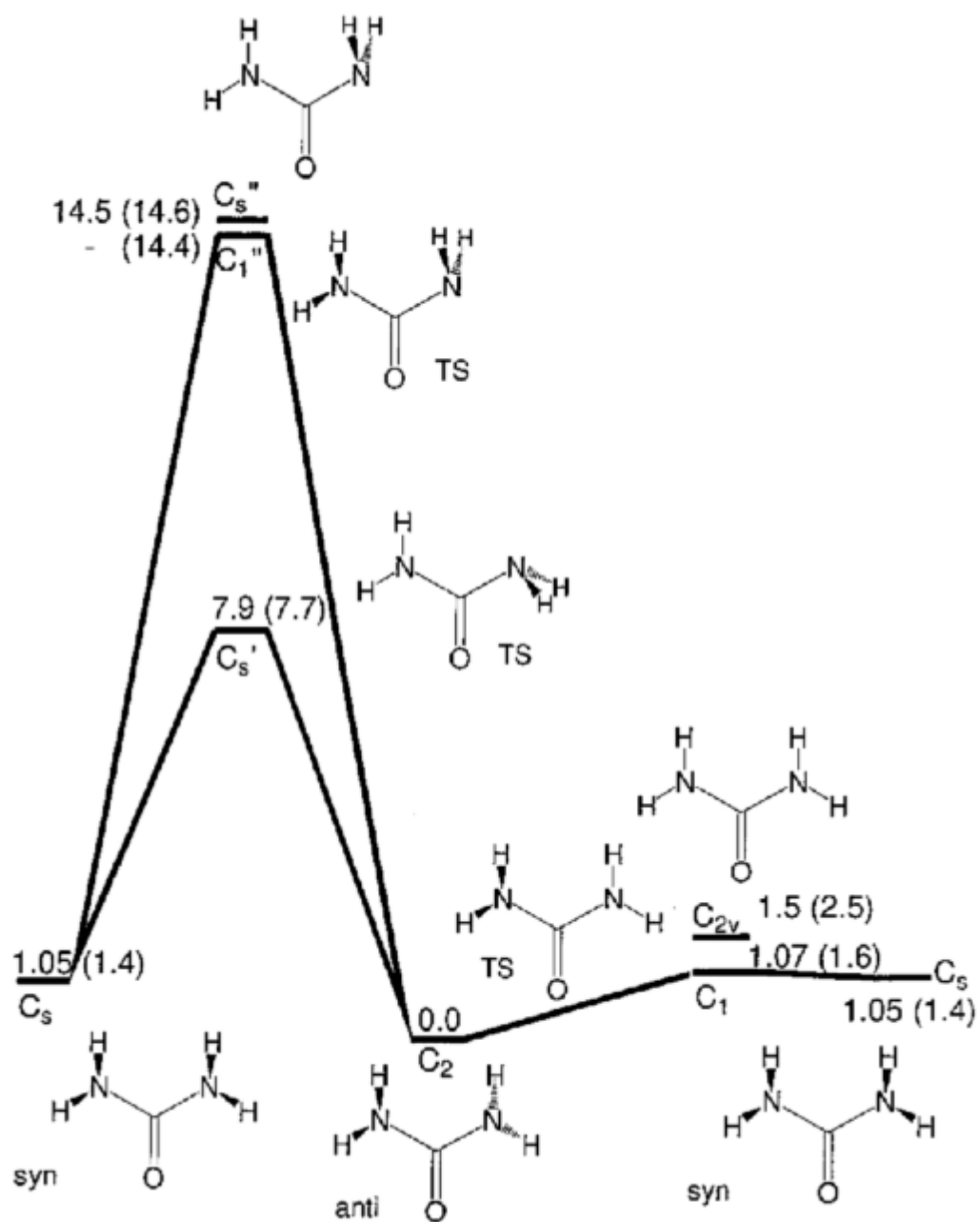
Figire 4.1. Energetic relationships between stationary points on potential surface for urea monomer.B3PW91/D95** relative energies before vibrational corrections are presented with MP2/D95** values in parentheses.

Table 4.2. Results of semiempirical and ab initio calculations for urea conformers. Total energy, au (or, in case of semiempirical methods, the heat of formation, kcal/mol) for planar conformation is given for each method. NI - number of imaginary frequencies (0 characterizes energy minimum, 1 - saddle point, op – no frequency calculations, optimization only); ΔE - relative energy of conformers, kcal/mol; $\Delta\Delta H_0$ - relative energy with zero point vibration correction, kcal/mol; $\Delta\Delta H_{298}$ - relative energy corrected for thermal vibrations at 298K, kcal/mol; m_D - dipole moment, D.

Basis set, Symmetry	IF	$\Delta\mu$	ΔE	$\Delta\Delta H_0$	$\Delta\Delta H_{298}$	IF	$\Delta\mu$	ΔE	$\Delta\Delta H_0$	$\Delta\Delta H_{298}$	IF	$\Delta\mu$	ΔE	$\Delta\Delta H_0$	$\Delta\Delta H_{298}$
Semiempirical			AM1, -44.08					SAM1, -44.07					PM3, -40.96		
C_{2v}	1	4.13			0.87	1	4.23			0.04	2	4.07			6.05
C_2	0	3.59			0.00	0	4.13			0.00	0	3.02			0.00
C_s											0	3.82			1.19
6-31G*			HF,-223.982192					MP2(full), -224.617929							
C_{2v}	2	4.60	1.57	0.08	0.00	2	4.74	2.59	1.06	0.86	0				
C_2	0	3.85	0.00	0.00	0.17	0	3.78	0.00	0.00	0.00	0				
C_s	1	4.60	1.31	0.32	0.44	0	4.73	1.70	1.12	1.38	0				
D95**			HF, -224.046152					MP2(full), -224.681770					B3PW91, -225.234852		
C_{2v}	2	4.70	1.29	0.00	0.00	2	4.85	2.49	1.04	0.84	2	4.43	1.46	0.10	0.00
C_2	0	4.01	0.00	0.14	0.37	0	3.92	0.00	0.00	0.00	0	3.74	0.00	0.00	0.15
C_s	0	4.69	1.04	0.35	1.05	0	4.82	1.44	1.01	1.20	0	4.43	1.05	0.43	0.91
D95++**			HF, -224.050373					MP2, -224.694839					B3PW91, -225.242745		
C_{2v}	2	4.73	1.32	0.00	0.00	2	4.89	3.08	1.35	1.23	2	4.51	1.32	0.00	0.00
C_2	0	4.05	0.00	0.14	0.40	0	3.96	0.00	0.00	0.00	0	3.84	0.00	0.05	0.30
C_s	0	4.68	0.96	0.48	1.03	0	4.79	1.16	0.91	1.03	0	4.46	0.87	0.41	0.93
6-311++G**			HF, -224.060855					MP2, -224.752121					B3PW91, -225.258980		
C_{2v}	2	4.69	0.73	0.00	0.00	2	4.82	2.75	1.05	0.92	2	4.47	0.69	0.00	0.00
C_2	0	4.06	0.00	0.19	0.38	0	3.95	0.00	0.00	0.00	0	3.87	0.00	0.18	0.38
C_s	1	4.65	0.61	0.18	0.34	0	4.73	1.20	0.89	1.03	0	4.43	0.55	0.22	0.72
6-311+G(3df,2p)			HF, -224.080708					MP2, -224.887657					B3PW91, -225.274381		
C_{2v}	2	4.59	0.58	0.00	0.00	op	4.72	1.19	0.00	0.00	2	4.38	0.59	0.00	0.00
C_2	0	4.06	0.00	0.26	0.47	op	3.91	0.00	0.51	0.64	0	3.86	0.00	0.21	0.43
C_s	1	4.56	0.49	0.17	0.35	op	4.68	0.86	1.06	1.33	1	4.35	0.47	0.15	0.31

depicts the various possible structures for the urea monomer and transition states between them. The energetic data of Table 4.2 show that none of the methods used found a planar minimum for the monomeric urea molecule. Most *ab initio* methods (before vibrational correction) and PM3 found two negative vibrational frequencies for planar urea, while HF/6-31G*, AM1 and SAM1 each found only one.

    Ab initio methods using medium basis sets, all MP2 and PM3 calculations predict two minima on the potential energy surface: (a) an anti-conformation of C_2

symmetry with the H's of the NH_2 groups located on opposite sides of the molecule, and (b) a less stable syn-conformation C_s, with the H's of the NH_2 groups located on the same side. The conversion between these two conformations could occur either by inversion (via transition-state C_1) or rotation (via transitions states C_s', C_1"). The HF method at TZ basis sets predicts syn-conformation to be a transition state, and the DFT result depends on the number of polarization functions used.

In order to properly compare the energies obtained from *ab initio* calculations (which give ΔE's) with those obtained from semiempirical calculations (which give ΔH's) thermal and vibrational corrections must be applied to the *ab initio* results. After application of zero-point vibrational correction all *ab initio* methods predict the planar, C_{2v}, to be only slightly less stable stable than the C_2 at smaller basis sets. As the size of the basis set increases, C_2 becomes more stable (by 0 to 0.4 kcal/mol). The inversion in stability is observed at D95** for HF, D95++** for DFT, and 6-311+G(3df,2p) for MP2. AM1 predicts the C_2 structure to be more stable than the C_{2v} by 0.9 kcal/mole, in agreement with the MP2 calculations in the medium basis sets. SAM1 favors the C_{2v} by less than 0.1 kcal/mol. PM3, on the other hand favors the C_2 structure by over 6 kcal/mol in clear disagreement with all the others. The largest energy range among the three structures among the *ab initio* results is 1.45 kcal/mol for MP2(full)/6-31G*.

While the best calculations predict planar urea in the gas phase, one should note that the calculated dipole moments of the C_2 structure are consistently in better agreement with the reported gas phase experimental value of 3.83 D[92] and the calculated dipole moments of the planar C_{2v} structure are in better agreement with solution experimental value of 4.2 D.[91] However, HF calculations generally overestimate dipole moments. MP2 calculations, while usually significantly better

than HF, still often overestimate dipoles.[1]

The internal rotations of the urea molecule were the subjects of previous theoretical studies. Rotational barriers of about 8-9 kcal/mol have been reported for the lower barrier[2] and 13.5-14.3 kcal/mol for the higher.[2c] We have calculated similar values of 8.5 and 13.7 (HF/D95**), 6.8 and 12.8 (MP2/D95**), and 7.3 and 13.4 kcal/mol (DFT/D95**) after thermal correction (Table 4.1, Figure 4.1).

The apparent planarity of the molecule after vibrational correction argues that the barrier for inversion should be zero or very close to zero. A TS with one pyramidal and one planar NH_2 group was studied for the first time. Its uncorrected energy is intermediate between C_2 and C_{2v}, lying below C_s after ZPVE and thermal correction for all *ab initio* methods. The C_{2v} structure becomes the most stable after vibrational corrections at the MP2/6-311G+(3df,2p) level. Therefore, one can effectively consider the urea molecule as planar. These results agree with the recent microwave spectroscopic investigation of the urea molecule in the gas phase.[3] The experiment shows the zero-point vibration to be above the planarization barrier. The nuclear wavefunction is symmetric, with the planar conformation as the average.

Selected geometrical information of the monomers is collected in Table 4.3. The semiempirical calculations tend to have longer C-N and shorter C=O distances than the best (MP2 and DFT) calculations, while the HF calculations tend to have shorter C-N and longer C=O distances. We compared calculated rotational constants to the experimental values from MW study.[3] The results of comparison are presented on the Table 4.4. The best agreement is found for MP2/6-311++G**, and DFT/D95** values for planar structure and DFT/6-311++G** values for nonplanar conformation. MP2 with smaller basis set and HF calculations do not agree well with experimental values.

Table 4.3. Optimized geometrical parameters for urea conformers

method	sym	R(CO)	r(CN)	r(CN')	r(NH$_a$)	OCNH$_a$	r(N'H$_a$)	OCN'H$_a$	r(NH$_s$)	OCNH$_s$	r(N'H$_s$)	OCN'H$_s$
AM1	C$_{2v}$	1.258	1.390		0.984	180.0			0.988	0.0		
	C$_2$	1.256	1.403		0.991	155.6			0.994	14.1		
	C$_s$'	1.254	1.449	1.376	0.987	180.0	1.002	59.7	0.989	0.0	1.002	300.3
	C$_s$"	1.199	1.433	1.349	0.992	180.0	1.004	126.6	0.994	0.0	1.004	233.4
SAM1	C$_{2v}$	1.279	1.391		0.988	180.0			0.989	0.0		
	C$_2$	1.278	1.393		0.989	169.3			0.099	6.6		
	C$_s$'	1.264	1.431	1.392	0.989	180.0	1.002	61.0	0.990	0.0	1.002	299.0
	C$_s$"	1.264	1.431	1.392	0.989	180.0	0.997	113.7	0.990	0.0	0.997	246.3
PM3	C$_{2v}$	1.233	1.405		0.990	180.0			0.990	0.0		
	C$_2$	1.227	1.430		0.996	146.5			0.997	17.6		
	C$_s$	1.228	1.428		0.995	147.3			0.996	16.7		
	C$_1$	1.230	1.438	1.399	0.990	182.2	0.996	139.7	0.997	12.6	0.991	358.4
	C$_s$'	1.229	1.468	1.387	0.990	180.0	0.999	59.7	0.990	0.0	0.999	300.3
	C$_s$"	1.219	1.465	1.406	0.990	180.0	0.997	119.0	0.991	0.0	0.997	241.0
	C$_1$'	1.225	1.468	1.409	0.994	159.0	0.999	53.8	0.994	22.7	0.999	294.1
	C$_1$"	1.216	1.464	1.434	0.996	145.6	0.998	123.5	0.997	14.8	0.998	245.2
HF/D95**	C$_{2v}$	1.205	1.364		0.991	180.0			0.992	0.0		
	C$_2$	1.201	1.376		0.995	151.0			0.996	12.6		
	C$_s$	1.203	1.370		0.993	163.6			0.994	12.8		
	C$_1$	1.203	1.372	1.368	0.993	160.9	0.992	192.9	0.994	13.4	0.994	348.5
	C$_s$'	1.199	1.433	1.349	0.992	180.0	1.004	56.6	0.994	0.0	1.004	303.4
	C$_s$"	1.192	1.365	1.429	0.991	180.0	1.001	119.6	0.994	0.0	1.001	240.4
	C$_1$"	1.192	1.367	1.429	0.992	170.6	1.001	118.6	0.995	7.0	1.001	239.6
HF/D95++**	C$_{2v}$	1.204	1.364		0.992	180.0			0.993	0.0		
	C$_2$	1.201	1.376		0.996	151.6			0.996	12.8		
	Cs	1.203	1.370		0.994	162.8			0.995	13.8		
MP2/D95**	C$_{2v}$	1.232	1.381		1.005	180.0			1.006	0.0		
	C$_2$	1.229	1.397		1.011	146.5			1.011	14.7		
	C$_s$	1.230	1.392		1.009	157.4			1.009	18.3		
	C$_1$	1.231	1.399	1.380	1.010	149.7	1.006	184.8	1.011	17.0	1.006	349.8
	Cs'	1.221	1.360	1.452	1.007	180.0	1.020	55.5	1.008	0.0	1.020	304.5
	C$_s$"	1.223	1.380	1.449	1.005	180.0	1.017	121.7	1.008	0.0	1.017	238.3
	C$_1$"	1.222	1.387	1.449	1.007	163.0	1.017	119.5	1.010	13.0	1.017	236.0
MP2/D95++**	C$_{2v}$	1.233	1.381		1.006	180.0			1.006	0.0		
	C$_2$	1.229	1.396		1.012	146.7			1.012	14.4		
	C$_s$	1.231	1.393		1.010	157.2			1.011	19.5		
MP2/6-311++G**	C$_{2v}$	1.215	1.393		1.009	145.9			1.009	14.6		
	C$_2$	1.218	1.391		1.010	147.4			1.010	13.8		
	C$_s$	1.219	1.388		1.008	157.7			1.009	18.3		
MP2(full)/6-31G*	C$_{2v}$	1.228	1.374		1.007	180.0			1.007	0.0		
	C$_2$	1.225	1.390		1.013	145.8			1.013	13.4		
	C$_s$	1.227	1.384		1.011	157.9			1.011	16.9		

Table 4.3. (continued)

B3PW91/D95**	C$_{2v}$	1.226	1.378		1.006	180.0			1.007	0.0		
	C$_2$	1.223	1.390		1.011	149.1			1.011	13.2		
	C$_s$	1.225	1.385		1.009	161.2			1.009	15.1		
	C$_1$	1.225	1.389	1.379	1.010	155.6	1.007	189.2	1.010	15.2	1.008	348.6
	C$_s$'	1.221	1.360	1.452	1.007	180.0	1.020	55.5	1.008	0.0	1.020	304.7
	C$_s$"	1.215	1.376	1.445	1.007	180.0	1.017	120.6	1.010	0.0	1.017	239.4
B3PW91/D95++**	C$_{2v}$	1.226	1.377		1.007	180.0			1.007	0.0		
	C$_2$	1.223	1.388		1.011	150.5			1.011	13.0		
	C$_s$	1.225	1.384		1.009	161.5			1.010	15.1		
Neutron diffraction		1.258	1.344		1.022	180.0			1.004	0.0		

Table 4.4. Comparison between experimental MW and calculated rotational constants (MHz).

	(NH$_2$)$_2$CO			(^{15}NH$_2$)$_2$CO			Rms
Exp	11233	10369	5417	11027	9828	5220	
MP2/6-311++G**, C$_{2v}$	11175	10401	5387	10973	9859	5193	
exp-MP2, C$_{2v}$	-58	32	-30	-54	31	-27	73
MP2/6-311++G**, C$_2$	11053	10375	5409	10846	9833	5211	
exp-MP2, C$_2$	-180	6	-8	-181	5	-9	180
B3PW91/6-311++G**, C$_{2v}$	11371	10437	5442				
exp-B3PW91/6-311++G**, C$_2$	52	44	38				78
B3PW91/6-311++G**, C$_2$	11285	10413	5455				
exp-B3PW91/6-311++G**, C$_{2v}$	138	68	25				156
HF/6-311++G**, C$_{2v}$	11693	10597	5559				
exp-HF/6-311++G**, C$_2$	460	228	142				533
HF/6-311++G**, C$_{2v}$	11615	10558	5568				
exp-HF/6-311++G**, C$_2$	382	189	151				452
MP2/D95**, C$_{2v}$	11036	10347	5340				
exp-MP2/D95**, C$_{2v}$	-197	-22	-77				213
MP2/D95**, C$_2$	10897	10320	5360				
exp-MP2/D95**, C$_2$	-336	-49	-57				344
B3PW91/D95**, C$_{2v}$	11167	10331	5366				
exp-B3PW91/D95**, C$_{2v}$	-66	-38	-51				92
B3PW91/D95**, C$_2$	11057	10320	5388				
exp-B3PW91/D95**, C$_2$	-176	-49	-29				185
HF/D95**, C$_{2v}$	11527	10524	5501				
exp-HF/D95**, C$_{2v}$	294	155	84				343
HF/D95**, C$_2$	11438	10484	5516				
exp-HF/D95**, C$_2$	205	115	99				255

Table 4.5. Vibrational frequencies (cm^{-1}), IR intensities (relative units), and isotope shifts (cm^{-1}) upon deuteration for urea molecule: comparison gase phase and matrix isolation experimental data with calculated at MP2/6-311++G** (MP2), B3PW91/6-311++G** (DFT1), B3PW91/D95** (DFT2), and HF/D95** (HF) level.

	Description		frequency			frequency			intensity			Isotope shift		
			gas	MP2		DFT$_1$	DFT$_2$	HF	gas	MP2		matr	MP2	
				C$_{2v}$	C$_2$	C$_2$	C$_2$	C$_2$		C$_{2v}$	C$_2$		C$_{2v}$	C$_2$
$\tau_s(NH_2)$	syn out-of-plane H atoms	A2	-	-626	386	368	372	398	-	0	113		-141	109
$\omega_a(NH_2)$	anti out-of-plane H atoms	B1	-	-552	466	433	446	475	-	507	36		-123	119
$\tau_a(NH_2)$	anti rotations of NH2 groups	A1	-	290	480	473	470	512	-	0	29		82	72
$\delta(CN)$	in-plane NCN angle bent	A1	-	482	568	524	543	584	-	2	3		90	44
$\omega_s(NH_2)$	syn rotations of NH2 groups	B1	-	542	602	532	576	619	-	13	68		138	103
$\delta(CO)$	in-plane O atom moves	B2	572	563	658	578	587	624	vw	12	291	61	57	144
$\omega(CO)$	out-of-plane C atom moves	B1	775	735	793	782	780	683	w	0	111		20	35
$\nu_s(CN)$	in-plane C-N bonds stretch, symm	A1	1023	977	960	961	961	1029	m	16	11	115	116	98
$\rho_a(NH_2)$	in-pane HNC angles bent, asymm	B2	1157	992	1066	1038	1048	1151	m	15	30		190	201
$\rho_s(NH_2)$	in-pane HNC angles bent, symm	A1	1157	1149	1198	1172	1176	1278	m	0.1	4		163	202
$\nu_a(CN)$	in-plane C-N bonds stretch, asymm	B2	1394	1427	1419	1415	1427	1538	s	260	220	-14	-38	-9
$\delta_s(NH_2)$	in-plane HNH angles bent, symm	A1	1604	1638	1637	1624	1627	1776	s	285	187	371	373	389
$\delta_a(NH_2)$	in-plane HNH angles bent, asymm	B2	1749	1636	1647	1625	1632	1785	s	0.1	0.4		484	475
$\nu(CO)$	C=O bond stretch	A1	1776	1807	1820	1804	1835	1978	s	566	445	11	17	20
$\nu_s(NH_2)$	inphase N-H bonds stretch, asymm	B2	3434	3805	3729	3596	3616	3831	vs	45	31	900	985	972
$\nu_s(NH_2)$	inphase N-H bonds stretch, symm	A1	3460	3808	3729	3601	3620	3835	vs	80	49	900	984	971
$\nu_a(NH_2)$	antiphase N-H bonds stretch, asymm	B2	3533	3662	3607	3715	3744	3960	vs	88	56	935	1019	1001
$\nu_a(NH_2)$	antiphase N-H bonds stretch, symm	A1	3559	3670	3611	3716	3744	3960	vs	11	5	935	1018	1000

4.2 Vibrational frequencies calculations for the urea molecule

The vibrational frequency calculations were performed on C_2 and C_{2v} conformations of the monomer. Although it is common practice to apply a scaling factor of 0.85-0.97 depending on the level of theory used[4] to *ab initio* frequencies in order to better reproduce experimental values, we avoid such scaling. The non-scaled results for the highest level MP2/6-311++G** are presented in Table 4.5 together with experimental gas-phase spectra. The frequencies at DFT and HF level are also shown for comparison. One can see that HF significantly overestimates frequencies, while DFT gives values closer to the experimental ones than MP2 does. Basis set effects are relatively small. The R^2 deviation from experimental values is insignificantly better for the C_{2v} (0.990), than for the C_2 (0.989) conformer. We also calculated vibrational frequencies for the deuterated urea. Unfortunately, experimental gas-phase data are incomplete (only C=O and N-H stretching frequencies were reported), and we compare calculated isotope shifts with experimental matrix-isolation data (Table 4.4). This time preference toward planar conformation is more pronounced (R^2 is 0.999 for C_{2v} and 0.996 for C_2). We can therefore conclude that comparison of calculated and experimental IR spectra present weak evidence in favor of planar conformation of urea in the gas phase.

4.3 Planarization barrier in the thiourea molecule

Conformational behavior of the thiourea molecule is very similar to that of urea. The results for the thiourea monomer are summarized in Table 4.6. At the HF/D95** level, the planar conformation is the only critical point on the surface.

Table 4.6. Energetic results of ab initio calculation on thiourea monomer. Total energies in hartree, others in kcal/mol.

Method	Symmetry	Total Energy, au	ΔE, kcal/mol	ΔH_0, kcal/mol	ΔH_{298}, kcal/mol
HF/D95**	C_{2v}	-546.652508	0.00	0.00	0.00
DFT/D95**	C_{2v}	-548.143869	0.73	0.00	0.00
DFT/D95**	C_2	-548.145032	0.00	0.49	0.82
DFT/D95**	C_s	-548.143977	0.66	0.30	0.58
MP2/D95**	C_{2v}	-547.238024	1.50	0.15	0.00
MP2/D95**	C_2	-547.240409	0.00	0.00	0.10
MP2/D95**	C_s	-547.238691	1.08	0.52	0.91

Using DFT and/or MP2 with the same basis set resulted in minima representing anti- and syn- conformers, as in the case of urea. However, the planar barrier for thiourea is about half that of urea. Like urea, the thiourea becomes planar after zero-point corrections are applied.

4.4 Conformations of the dimers

The results of the calculations on the dimers are collected in Tables 4.7-4.9. The geometric analysis for the dimers becomes somewhat complex due to: (a) the possible combinations of monomer conformations that can statistically occur in the dimer, (b) the different possibilities of intermolecular interactions. We located four general classes of dimeric interactions: chain dimers, **C**, ribbon dimers, **R**, herringbone dimers, **H**, and stacked dimers, **S** (Figure 4.2). The first three of these structure types
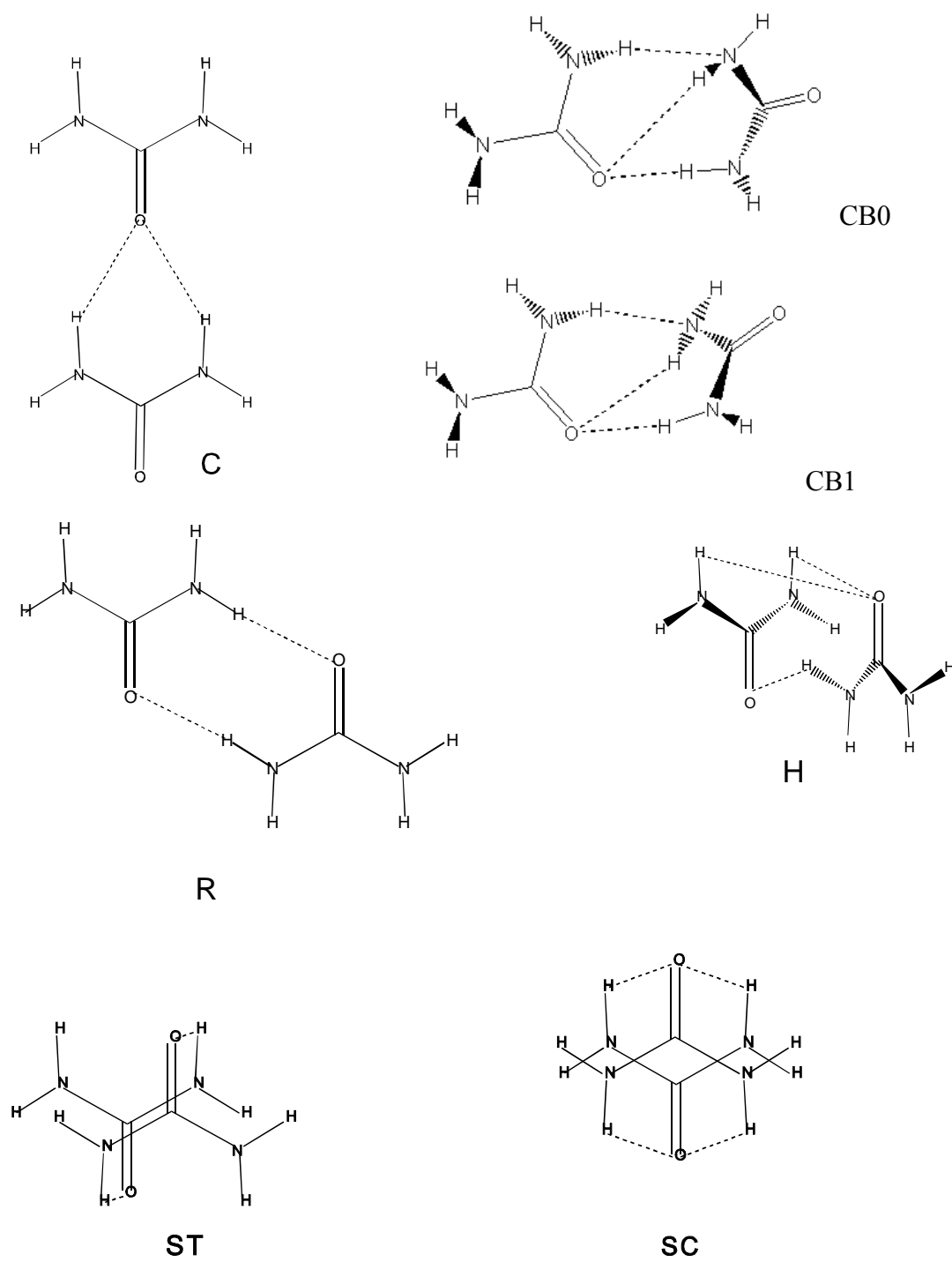
Figure 4.2. Conformations and notations for urea dimers

(**C**, **R**, and **H**) correspond to minima on the potential surface, while stacked dimers correspond to saddle points between **C** and **R** dimers. All four of these kinds of interactions play important roles in the crystal structures of urea and thiourea. The **C** interactions are similar to those in the linear chains found in urea crystals while the T-shaped interactions **H** are representative of the inter-chain interactions in these crystals. The **R** interactions form the 'ribbon'-like structure of the thiourea crystals, while the **C** interactions link the ribbons together. **S** interactions are typical for many crystals with planar molecules and were found[5] to be the most stable configuration for the dimers of acetone molecules with molecular shape similar to urea. The fragments of urea and thiourea crystal structures are shown in Figure 3.4-3.5.

In order to better compare the MO optimized geometries with experimental crystal structures, we imposed geometrical constraints in some calculations. For the chains, we optimized the geometries with (a) both molecules constrained to be planar and geometrically equivalent, **CE**; (b) planar but geometrically different (flat chain), **CF**; (c) collinear C=O bonds, but not planar (linear chain), **CL**; and (d) no constraints (bent chain), **CB**. The **CE** structure mimics the translational symmetry of the urea crystal. In the **CB** structure, one urea molecule is turned to form an additional H-bond between the H_s atom of one monomer and one of N atoms of the other. For the ribbons, we (a) enforced both a twofold axis and a plane of symmetry for each molecule (equivalent ribbon), **RE**; (b) enforced only a plane of symmetry (flat ribbon), **RF**; (c) no constraints, centrosymmetric dimer with heavy atoms in parallel planes (parallel ribbon), **RP**; and (d) no constraints, C_2 dimer (twisted ribbon), **RT**. The **RE** mimics idealized crystal structure with planar ribbons, **RP** mimics mutual orientation of the molecules found in high-temperature phase, and **RT** in low-temperature phase, reported for the orthogonal thiourea. Inclusion compounds also contain dimers of **RT**

Table 4.7. *Ab initio* and semiempirical results for urea dimers: I.F. - number of imaginary frequencies; approximate symmetry marked *; $\Delta\Delta H_{298}$ (interaction enthalpy, kcal/mol) is defined as the difference between ΔH_{298} for the dimer and monomers in C_2 conformation. Interaction energy with the reference to the planar (non-equilibrium) monomers shown in brackets. X…Y denotes symmetrically-independent intermolecular distances (A) between the atom X of the first monomer and the atom Y of the second monomer.

	type	Sym	IF	Monomer sym.		$\Delta\Delta H_{298}$	H...O	H...O	O...H	N...H	N...H	C...O	O...C
MP2/D95++**	CF	C_{2v}	op	C_{2v}	C_{2v}	-3.78(-4.57)	2.116	2.116					
MP2/D95**	CF	C_{2v}	op	C_{2v}	C_{2v}	-4.73(-5.05)	2.104	2.104					
DFT/D95**	CF	C_{2v}	5	C_{2v}	C_{2v}	-6.17(-5.87)	2.122	2.122					
HF/D95++**	CF	C_{2v}	5	C_{2v}	C_{2v}	-7.23(-6.43)	2.242	2.242					
HF/D95**	CF	C_{2v}	5	C_{2v}	C_{2v}	-7.26(-6.52)	2.222	2.222					
AM1	CF	C_{2v}	4	C_{2v}	C_{2v}	-4.41(-6.15)	2.209	2.209					
PM3	CF	C_{2v}	4	C_{2v}	C_{2v}	8.99(-3.11)	2.596	2.596					
PM3	CF1	C_{2v}	4	C_{2v}	C_{2v}	10.59(-1.49)	1.929	1.929					
SAM1	CF	C_{2v}	2	C_{2v}	C_{2v}	-3.92(-4.00)	1.989	1.989					
MP2/D95++**	CL	C_2	op	C_2	C_2	-6.12	2.163	2.163					6.12
MP2/D95**	CL	C_2	op	C_2	C_2	-5.41	2.145	2.145					5.41
DFT/D95**	CL	C_2	1	C_2	C_2	-4.03	2.155	2.155					4.03
HF/D95++**	CL	C_2	1	C_2	C_2	-5.50	2.272	2.272					5.50
HF/D95**	CL	C_2	1	C_2	C_2	-5.30	2.275	2.275					5.30
AM1	CL	C_2	1	C_2	C_2	-5.62	2.221	2.221					5.62
PM3	CL	C_2	1	C_2	C_2	-1.83	2.682	2.682					1.83
SAM1	CL	C_2	1	C_{2v}	C_{2v}*	-4.05	1.991	1.991					4.05
MP2/D95++**	CB1	C_1	0	C_2*	C_2*	-6.75	1.971	2.773	2.103				6.75
MP2/D95**	CB1	C_1	0	C_2*	C_2*	-6.73	1.962	2.712	2.084				6.73
DFT/D95**	CB0	C_1	0	C_2*	C_2*	-7.05	1.908	2.933	2.070				7.05
DFT/D95**	CB1	C_1	0	C_2*	C_2*	-6.94	1.911	2.863	2.070				6.94
HF/D95++**	CB1	C_1	0	C_2*	C_2*	-5.80	2.158	2.591	2.436				5.80
HF/D95**	CB0	C_1	0	C_2*	C_2*	-5.98	2.120	2.656	2.391				5.98
HF/D95**	CB1	C_1	0	C_2*	C_2*	-6.17	2.131	2.613	2.411				6.17
AM1	CB0	C_1	0	C_2*	C_2*	-6.55	2.205	2.239	2.645				6.55
AM1	CB1	C_1	0	C_2*	C_2*	-6.57	2.177	2.260	2.617				6.57
AM1	CB2	C_1	0	C_s*	C_2*	-6.68	2.176	2.182		2.724	2.752		6.68
SAM1	CB2	C_s*	0	C_s*	C_{2v}*	-4.19	1.995	1.995		3.844	3.856		4.19
SAM1	CB3	C_1	0	C_{2v}*	C_{2v}*	-4.42	1.871	3.103		3.448	3.878		4.42
PM3	CB0	C_1	0	C_2*	C_2*	-2.59	1.840	3.707	2.696				2.59
PM3	CB1	C_1	0	C_2*	C_2*	-2.52	1.838	3.544	2.833				2.52
PM3	CB2	C_1	0	C_2*	C_s*	-1.62	1.840	1.840	2.692				1.62

Table 4.7. *Ab initio* and semiempirical results for urea dimers (continued)

Method												
PM3	CB3	C_1	0	$C_s{*}$	$C_2{*}$	-2.26	1.835	3.007	3.269	3.878	2.26	
PM3	CB4	C_1	0	$C_s{*}$	$C_s{*}$	-1.31	1.832	3.027	3.244	3.746	1.31	
PM3	CB5	C_1	0	$C_s{*}$	$C_s{*}$	-1.29	1.835	2.898	3.201	4.632	1.29	
PM3	CB6	C_1	0	$C_2{*}$	$C_2{*}$	-2.29	1.835	3.608	3.326	4.594	2.29	
PM3	CB7	C_1	0	$C_2{*}$	$C_2{*}$	-2.25	1.835	3.512	3.275	5.154	2.25	
PM3	CB8	C_1	0	$C_s{*}$	$C_2{*}$	-2.34	1.836	2.915	3.275	5.154	2.34	
PM3	CB9	C_1	1	$C_.{*}$	$C_.{*}$	-1.16	2.715	2.699	4.539	5.240	1.16	
MP2/D95++**	RF	C_{2h}	op	$C_{2v}{*}$	$C_{2v}{*}$	-6.18(-8.88)						
MP2/D95**	RF	C_{2h}	op	$C_{2v}{*}$	$C_{2v}{*}$	-7.38(-9.47)						
DFT/D95**	RF	C_{2h}	5	$C_{2v}{*}$	$C_{2v}{*}$	-11.82(-11.52)						
HF/D95++**	RF	C_{2h}	5	$C_{2v}{*}$	$C_{2v}{*}$	-10.07(-9.27)						
HF/D95**	RF	C_{2h}	5	$C_{2v}{*}$	$C_{2v}{*}$	-10.13(-8.03)						
AM1	RF	C_{2h}	3	$C_{2v}{*}$	$C_{2v}{*}$	-6.90(-8.64)	2.036	2.036				
PM3	RF	C_{2h}	4	$C_{2v}{*}$	$C_{2v}{*}$	4.07(-8.03)	1.792	1.792				
PM3	RF	C_{2h}	4	$C_{2v}{*}$	$C_{2v}{*}$	7.99(-4.09)	2.410	2.410				
SAM1	RF	C_{2h}	0	$C_{2v}{*}$	$C_{2v}{*}$	-8.34(-8.42)	1.801	1.801				
MP2/D95++**	RP	C_i	0	$C_2{*}$	$C_2{*}$	-8.56	1.874	1.874			8.56	
MP2/D95**	RP	C_i	0	$C_2{*}$	$C_2{*}$	-8.46	1.870	1.870			8.46	
DFT/D95**	RP	C_i	0	$C_2{*}$	$C_2{*}$	-10.22	1.803	1.803			10.22	
HF/D95++**	RP	C_i	0	$C_2{*}$	$C_2{*}$	-8.30	2.006	2.006			8.30	
HF/D95**	RP	C_i	0	$C_2{*}$	$C_2{*}$	-8.41	1.992	1.992			8.41	
AM1	RP	C_i	0	$C_2{*}$	$C_2{*}$	-8.56	2.071	2.071			8.56	
PM3	RP	C_i	0	$C_2{*}$	$C_2{*}$	-5.75	1.813	1.813			5.75	
PM3	RP2	C_i	0	$C_2{*}$	$C_2{*}$	-4.15	1.811	1.811			4.15	
PM3	RP3	C_1	0	$C_2{*}$	$C_2{*}$	-4.91	1.811	1.813			4.91	
MP2/D95++**	RT	C_2	0	$C_2{*}$	$C_2{*}$	-8.55	1.874	1.874			8.55	
MP2/D95**	RT	C_2	0	$C_2{*}$	$C_2{*}$	-8.47	1.870	1.870			8.47	
DF/D95**	RT	C_2	0	$C_2{*}$	$C_2{*}$	-10.24	1.804	1.804			10.24	
HF/D95++**	RT	C_2	0	$C_2{*}$	$C_2{*}$	-8.31	1.993	1.993			8.31	
HF/D95**	RT	C_2	0	$C_2{*}$	$C_2{*}$	-8.41	1.993	1.993			8.41	
AM1	RT	C_2	0	$C_2{*}$	$C_2{*}$	-8.86	2.088	2.088			8.86	
PM3	RT	C_2	0	$C_2{*}$	$C_2{*}$	-4.66	1.847	1.847			4.66	
PM3	RT2	C_2	0	$C_s{*}$	$C_s{*}$	-3.93	1.814	1.814			3.93	
PM3	RT3	C_2	0	$C_s{*}$	$C_s{*}$	-2.44	2.603	2.603			2.44	3.559
PM3	RT4	C_1	0	$C_2{*}$	$C_s{*}$	-3.30	2.551	2.652			3.30	3.524
PM3	RT5	C_2	0	$C_2{*}$	$C_2{*}$	-4.01	2.548	2.548			4.01	3.774
PM3	RT6	C_1	0	$C_2{*}$	$C_2{*}$	-4.66	1.825	2.500			4.66	3.718
PM3	RT7	C_1	0	$C_2{*}$	$C_s{*}$	-3.98	1.824	2.586			3.98	3.542
PM3	RT8	C_1	0	$C_s{*}$	$C_s{*}$	-3.04	1.823	2.601			3.04	3.507
PM3	RT9	C_1	0	$C_s{*}$	$C_2{*}$	-3.78	1.825	2.513			3.78	3.678

Table 4.7. Dimers of urea (continued)

Method	Type	PG	N	Sym1	Sym2	ΔH	d_1	d_2	d_3	[ ]	extra
PM3	RTA	C_1	0	C_s*	C_s*	-2.87		1.823	2.542	2.87	3.609
PM3	RTB	C_1	0	C_2*	C_s*	-3.76		1.823	2.557	3.76	3.579
PM3	RTC	C_1	0	C_2*	C_2*	-2.37		1.825	2.518	2.37	3.718
DFT/D95**	HB	C_1	0	C_s*	C_2*	-3.34	2.962	3.468	1.925	3.34	
HF/D95**	HB	C_1	0	C_s*	C_2*	-3.77	3.221	3.306	2.090	3.77	
AM1	HB	C_1	0	C_s*	C_2*	-6.71	2.582	2.618	2.139	6.71	
SAM1	HB	C_1	0	C_s*	C_2*	-3.67	2.932	2.946	1.858	3.67	
PM3	HB	C_1	1	C_s*	C_2*	-3.06	3.253	3.268	2.543	3.06	
PM3	HB1	C_1	1	C_s*	C_s*	-2.07	3.096	3.993	2.543	2.07	
PM3	HB2	C_1	1	C_s*	C_s*	-2.24	3.162	3.752	2.550	2.24	
PM3	HB3	C_1	1	C_s*	C_s*	-2.08	3.100	3.940	2.544	2.08	
DFT/D95**	ST0	C_{2h}	2	C_s	C_s	-1.75				1.75	
DFT/D95**	ST1	C_i	1	C_2*	C_2*	-3.32				3.32	
HF/D95**	ST0	C_{2h}	2	C_s	C_s	-1.88				1.88	
HF/D95**	ST1	C_i	1	C_2*	C_2*	-3.36				3.36	
AM1	ST0	C_{2h}	2	C_s	C_s	-1.98				1.98	
SAM1	ST0	C_{2h}	3	C_s	C_s	-1.60	4.014	4.014	4.014	1.60	4.245
PM3	ST0	C_{2h}	2	C_s	C_s	-1.67	3.722	3.722	3.722	1.67	3.221

type. For herringbone dimers, we (a) used no constraints, **HB;** (b) enforced a plane of symmetry (flat herringbone), **HF**, and (c) constrained molecules to be geometrically equivalent, have antiparallel C=O bonds, and be planar with molecular planes perpendicular to each other (equivalent herringbone), **HE**. For the stacking dimers we imposed C_{2h} (**ST**) or centrosymmetric (**SC**) structures. Without these constraints, the optimizations of the stacked dimers converged to the chain or ribbon dimers. The energetic data for the dimers are presented in Tables 4.7-4.8. For the PM3 calculations, the planarization energy more than canceled the stabilization due to H-bond formation, resulting in net repulsion. For this reason we list pure H-bonding stabilization (the difference between ΔH_f's for planar dimers and monomers) in brackets.

Only **CB, RP, RT** and **HB** are true minima on the potential surface as only

they have no imaginary vibrational frequencies. The *ab initio* and AM1 calculations (Table 4.7) agree reasonably well both for geometries and interaction enthalpies. Since the **CE, RE** and **HE** dimers are not stationary points on the potential surface, we approximated the zero-point vibrational and thermal corrections using the corresponding results for **CF** and **RF**. Due to computational limitations, frequency calculations were not possible at the MP2/D95++** level. We used the MP2/D95** calculations to estimate the vibrational corrections. Despite the fact that the planar dimers can have as many as five imaginary frequencies, all thermally corrected HF calculations predict the relaxed planar dimers (**CF** and **RF**) to be the most stable of each type (chain or ribbon). The corresponding thermally corrected MP2 structures remain pyramidal about the nitrogens. However, the enthalpies required to planarize the dimers are much less than required to planarize two monomers (except for the **CB** type structures which have an additional H-bond not possible in the crystal). Together with our earlier conclusion that the monomer is effectively planar (see above), this suggests that a growing aggregate would likewise tend to be planar, in accord with the crystal structure. The corrected DFT calculations predict planar dimers (once again except for **CB** dimers). However, the enthalpy required for planarization of the **CB** dimers is quite small (0.9 kcal/mol). All *ab initio* methods predict the uncorrected planarization energies of the **CL**, **RP**, and **RT** dimers to be similar to that of the monomer. Thus, the H-bond overcomes the planarization barrier of the second molecule. To illustrate this point, we optimized the transition state for NH_2 group inversion in a ribbon dimer, **RTP** (a saddle point between **RP** and **RT** conformers). The uncorrected inversion barrier is significantly lower than that of the monomer (0.7 vs. 1.0 kcal/mol in both HF/D95** and DFT/D95**).

Among the semiempirical methods, AM1 produces the closest agreement to

Table 4.8. Ab initio results for urea dimers: IF - number of imaginary frequencies; approximate symmetry marked *; E_{rel} - relative energy, kcal/mol; ΔE - interaction energy of molecules in dimer (relative to C_2 conformation); cp - counterpoise basis set superposition error correction, kcal; $\Delta\Delta H_0$, $\Delta\Delta H_{298}$ - interaction enthalpy, kcal/mol;

Method	type	sym	IF	Monomer		$\Delta\mu$	E_{rel}	ΔE	ΔE cp	$\Delta\Delta H_0$	$\Delta\Delta H_0$ cp	$\Delta\Delta H_{298}$	$\Delta\Delta H_{298}$ cp
HF/D95**	CE	C_{2v}	op	C_{2v}	C_{2v}	10.85	5.55	-6.06	-5.37	-7.86	-7.17	-7.83	-7.14
HF/D95**	CF	C_{2v}	5	C_{2v}	C_{2v}	10.89	5.41	-6.19	-5.49	-7.99	-7.29	-7.96	-7.26
HF/D95**	CL	C_2	1	C_2	C_2	10.11	4.27	-7.33	-6.48	-7.09	-6.24	-6.15	-5.30
HF/D95**	CB1	C_1	0	C_2*	C_2*	6.78	2.64	-8.96	-8.35	-7.82	-7.21	-6.78	-6.17
HF/D95**	CB0	C_1	0	C_2*	C_2*	6.72	2.57	-9.03	-8.17	-7.87	-7.01	-6.84	-5.98
HF/D95**	RE	C_{2h}	op	C_{2v}	C_{2v}	0.00	1.75	-9.85	-8.90	-10.79	-9.84	-10.85	-9.90
HF/D95**	RF	C_{2h}	4	C_{2v}*	C_{2v}*	0.00	1.44	-10.16	-9.13	-11.10	-10.07	-11.16	-10.13
HF/D95**	RP	C_i	0	C_2*	C_2*	0.00	0.01	-11.59	-10.57	-10.36	-9.34	-9.43	-8.41
HF/D95**	RT	C_2	0	C_2*	C_2*	0.17	0.00	-11.60	-10.58	-10.37	-9.35	-9.43	-8.41
HF/D95**	RTP	C_1	1	C_2*	C_1	0.70	0.70	-10.90	-9.87	-10.55	-9.52	-9.67	-8.64
HF/D95**	ST	C_{2h}	2	C_s*	C_s*	0.00	9.38	-2.22	-1.44	-2.55	-1.77	-1.88	-1.10
HF/D95**	SC	C_i	1	C_2*	C_2*	0.00	6.72	-4.88	-4.20	-4.02	-3.34	-3.36	-2.68
HF/D95**	HE	C_s	op	C_{2v}	C_{2v}	0.65	8.52	-3.08	-2.51	-5.04	-4.46	-4.43	-3.86
HF/D95**	HF	C_s	2	C_{2v}*	C_s*	0.50	8.34	-3.26	-2.63	-5.22	-4.59	-4.61	-3.98
HF/D95**	HB	C_1	0	C_2*	C_2*	3.86	5.01	-6.59	-5.77	-5.85	-5.03	-4.59	-3.77
HF/D95++**	CE	C_{2v}	op	C_{2v}	C_{2v}	10.87	5.35	-5.56	-5.24	-7.48	-7.16	-7.46	-7.14
HF/D95++**	CF	C_{2v}	5	C_{2v}	C_{2v}	10.91	5.24	-5.68	-5.33	-7.60	-7.60	-7.58	-7.23
HF/D95++**	CL	C_2	1	C_2	C_2	10.10	3.88	-7.03	-6.64	-6.73	-6.34	-5.88	-5.50
HF/D95++**	CB	C_1	0	C_2*	C_2*	6.84	2.43	-8.48	-7.93	-7.32	-6.77	-6.35	-5.80
HF/D95++**	RE	C_{2h}	op	C_{2v}	C_{2v}	0.00	1.85	-9.06	-8.58	-10.29	-9.81	-10.28	-9.80
HF/D95++**	RF	C_{2h}	4	C_{2v}*	C_{2v}*	0.00	1.56	-9.35	-8.86	-10.58	-10.09	-10.56	-10.07
HF/D95++**	RP	C_i	0	C_2*	C_2*	0.00	0.02	-10.89	-10.37	-9.72	-9.20	-8.82	-8.30
HF/D95++**	RT	C_2	0	C_2*	C_2*	0.14	0.00	-10.91	-10.39	-9.73	-9.21	-8.83	-8.31

Table 4.8. Ab initio results for the dimers of urea (continued)

DFT/D95**	CE	C_{2v}	op	C_{2v}	C_{2v}	10.63	8.13	-5.58	-4.31	-7.20	-5.93	-7.27	-5.99
DFT/D95**	CF	C_{2v}	5	C_{2v}	C_{2v}	10.63	7.90	-5.81	-4.49	-7.43	-6.11	-7.49	-6.17
DFT/D95**	CL	C_2	1	C_2	C_2	10.63	6.75	-6.96	-5.84	-6.55	-5.43	-5.15	-4.03
DFT/D95**	CB1	C_1	0	C_2*	C_2*	5.77	3.24	-10.47	-9.04	-9.13	-7.70	-8.37	-6.94
DFT/D95**	CB0	C_1	0	C_2*	C_2*	5.71	3.19	-10.52	-9.13	-9.20	-7.81	-8.44	-7.05
DFT/D95**	RE	C_{2h}	op	C_{2v}	C_{2v}	0.00	2.25	-11.46	-9.91	-12.44	-10.89	-12.70	-11.15
DFT/D95**	RF	C_{2h}	4	C_{2v}*	C_{2v}*	0.00	1.59	-12.12	-10.58	-13.10	-11.56	-13.36	-11.82
DFT/D95**	RP	C_i	0	C_2*	C_2*	0.00	0.01	-13.71	-12.12	-12.54	-10.95	-11.80	-10.22
DFT/D95**	RT	C_2	0	C_2*	C_2*	0.27	0.00	-13.71	-12.13	-12.55	-10.97	-11.82	-10.24
DFT/D95**	RTP	C_2	1	C_2*	C_1	0.67	0.75	-12.96	-11.35	-12.60	-10.99	-11.94	-10.33
DFT/D95**	ST	C_{2h}	2	C_s*	C_s*	0.00	12.18	-1.53	-0.29	-1.73	-0.49	-1.75	-0.51
DFT/D95**	SC	C_i	1	C_2*	C_2*	0.00	8.88	-4.83	-3.75	-3.85	-2.77	-3.32	-2.24
DFT/D95**	HE	C_s	op	C_{2v}	C_{2v}	0.92	11.00	-2.71	-1.89	-4.68	-3.86	-4.67	-3.85
DFT/D95**	HF	C_s	4	C_{2v}*	C_s*	0.78	10.82	-2.89	-2.02	-4.86	-3.99	-4.85	-3.98
DFT/D95**	HB	C_1	0	C_2*	C_2*	3.17	7.25	-6.46	-5.22	-5.85	-4.61	-4.57	-3.34
MP2/D95**	CE	C_{2v}	op	C_{2v}	C_{2v}	11.35	9.14	-5.42	-2.83	-7.24	-4.65	-7.17	-4.57
MP2/D95**	CF	C_{2v}	5	C_{2v}	C_{2v}	11.40	8.94	-5.62	-2.96	-7.44	-4.78	-7.37	-4.71
MP2/D95**	CL	C_2	1	C_2	C_2	10.16	6.38	-8.19	-6.59	-7.58	-5.98	-6.87	-5.26
MP2/D95**	CB	C_1	0	C_2*	C_2*	6.12	1.88	-12.68	-8.91	-11.25	-7.48	-10.48	-6.71
MP2/D95**	RE	C_{2h}	op	C_{2v}	C_{2v}	0.00	3.69	-10.88	-7.01	-12.15	-8.28	-12.09	-8.22
MP2/D95**	RF	C_{2h}	4	C_{2v}*	C_{2v}*	0.00	3.22	-11.35	-7.38	-12.61	-8.65	-12.56	-8.60
MP2/D95**	RP	C_i	0	C_2*	C_2*	0.00	0.02	-14.55	-10.63	-13.14	-9.22	-12.38	-8.46
MP2/D95**	RT	C_2	0	C_2*	C_2*	0.20	0.00	-14.57	-10.64	-13.15	-9.22	-12.39	-8.46
MP2/D95**	HF	C_s	2	C_{2v}*	C_s*	1.36	0.00	-2.90	-0.02	-6.13	-3.25	-2.16	0.72
MP2/D95++**	CE	C_{2v}	op	C_{2v}	C_{2v}	11.38	10.35	-3.74	-1.76	-5.56	-3.58	-5.29	-3.31
MP2/D95++**	CF	C_{2v}	op	C_{2v}	C_{2v}	11.43	10.17	-3.91	-1.87	-5.73	-3.69	-5.46	-3.43
MP2/D95++**	CL	C_2	op	C_2	C_2	10.11	5.95	-8.14	-5.96	-7.53	-5.36	-6.62	-4.44
MP2/D95++**	CB	C_1	op	C_2*	C_2*	6.03	1.59	-12.49	-8.88	-11.06	-7.45	-10.10	-6.48
MP2/D95++**	RE	C_{2h}	op	C_{2v}	C_{2v}	0.00	5.04	-9.04	-5.82	-10.31	-7.09	-10.06	-6.84
MP2/D95++**	RF	C_{2h}	op	C_{2v}*	C_{2v}*	0.00	4.59	-9.49	-6.18	-10.76	-7.44	-10.51	-7.19
MP2/D95++**	RP	C_i	op	C_2*	C_2*	0.00	0.00	-14.09	-10.63	-12.67	-9.22	-11.72	-8.27
MP2/D95++**	RT	C_2	op	C_2*	C_2*	0.16	0.00	-14.08	-10.63	-12.66	-9.21	-11.71	-8.25

the *ab initio* calculations. SAM1 does reasonably well. However, it finds neither **RP**

nor **RT** minima and has another inconsistency with *ab initio* results. When optimized

with no symmetry constraints, **CF** dimer is distorted at SAM1 level with one part of

the forked H-bond shorter than the other one. PM3 appears to be erratic both for energies and geometries, as it was previously noted.[6] For example, PM3 predicts unreasonably large enthalpies for planarization of the NH_2 groups in both monomers and dimers. Another peculiarity of PM3 results is the abundance of dimeric conformations (Table 4.7). In part, this is the result of strong molecular nonplanarity: all the different combinations of NH_2 groups pyramidal conformations are present. For the comparison, at the AM1 level (where syn-conformation does not exist for an isolated molecule) optimization of some conformers leads to spontaneous inversion, and other dimers stablize syn-conformation for one of the molecules. However, the other kind of isomer observed at PM3 level, is bond-length isomers. For example, PM3 gives 3 minima for **RF** dimer: in one both H-bonds are 1.8Å, in another they are both 2.4Å, and in the third one is shorter than another. This is clearly a pitfall of PM3 calculation, which was attributed[7] to oscillating functional form for the core-core repulsion, implemented in PM3. We see that AM1 predicts multiple minima in only one case (**CB**). Two minima (denoted **CB0** and **CB1** in Table 4.5a) differ in the relative orientation of the molecules (see Figure 4.2). HF and DFT methods also predict these minima (we did not attempt to find them using MP2). The third minimum (**CB2**) contains one syn-urea, which is unstable as an isolated molecule using this method. Only SAM1 found a similar minimum.

Geometrical information on the dimers is collected in Table 4.9. All methods predict C=O bond lengthening upon dimerization by about 0.004 Å for the H-bond donor and 0.008 Å for the H-bond acceptor in the chain dimer, and 0.014 Å for the ribbon dimer. This correlates with shortening of the H-bond. The N-H bond involved in H-bonding formation elongates by 0.005 Å (**CF**) or 0.025 Å (**RF**), other N-H bonds change insignificantly. The C-N bonds shorten (by 0.01 Å for **CF** and 0.02 Å for **RF**)

Table 4.9. Bond lengths and H-bonds for planar urea monomers and dimers (Å). For chain dimers d and a refer to the H-donor and H-acceptor, respectively

Method		C=O	C-N	C-N'	N-H	N-H"	N'-H"	N'-H"'	H...O	H"...O
AM1	Monomer	1.258	1.390		0.984	0.988				
	CF dimer, d	1.262	1.388		0.988	0.986			2.206	
	CF dimer, a	1.262	1.387		0.985	0.988				
	RF dimer	1.268	1.382	1.391	0.988	0.996	0.985	0.987		1.988
PM3	monomer	1.232	1.405		0.990	0.990				
	CF dimer, d	1.236	1.402		0.991	0.990			2.597	
	CF dimer, a	1.236	1.402		0.990	0.990				
	RF dimer	1.245	1.391	1.403	0.989	1.011	0.990	0.990		1.792
HF/6-31G*	monomer	1.202	1.360		0.990	0.991				
HF/D95**	monomer	1.205	1.364		0.991	0.992				
	CF dimer, d	1.210	1.362		0.994	0.991			2.222	
	CF dimer, a	1.213	1.357		0.992	0.993				
	RF dimer	1.217	1.349	1.363	0.991	1.004	0.991	0.992		1.966
HF/D95++**	monomer	1.204	1.364		0.992	0.993				
	CF dimer, d	1.209	1.361		0.994	0.992			2.242	
	CF dimer, a	1.213	1.357		0.992	0.993				
	RF dimer	1.217	1.349	1.363	0.992	1.004	0.992	0.993		1.980
HF/6-311G**	monomer	1.196	1.361		0.990	0.991				
MP2/6-31G*	monomer	1.228	1.374		1.007	1.007				
MP2/D95**	monomer	1.232	1.381		1.005	1.005				
	CF dimer, d	1.237	1.379		1.009	1.005			2.104	
	CF dimer, a	1.240	1.372		1.005	1.006				
	RF dimer	1.247	1.362	1.379	1.006	1.024	1.005	1.005		1.836
MP2/D95++**	monomer	1.233	1.381		1.006	1.006				
	CF dimer, d	1.237	1.378		1.010	1.006			2.121	
	CF dimer, a	1.241	1.372		1.006	1.007				
	RF dimer	1.247	1.362	1.379	1.006	1.024	1.006	1.006		1.841
MP2/6-311G**	monomer	1.221	1.377		1.004	1.005				
MP2/6-311G(3df,2p)	monomer	1.219	1.370		1.002	1.002				
B3PW91/D95**	monomer	1.226	1.378		1.006	1.006				
	CF dimer, d	1.231	1.376		1.011	1.005			2.122	
	CF dimer, a	1.234	1.370		1.007	1.007				
	RF dimer	1.243	1.357	1.376	1.007	1.032	1.006	1.006		1.779
B3PW91/D95++**	monomer	1.226	1.377		1.007	1.007				
	CF dimer, d	1.231	1.374		1.011	1.006			2.153	
	CF dimer, a	1.234	1.369		1.007	1.007				
	RF dimer	1.242	1.356	1.375	1.007	1.031	1.007	1.007		1.795
Neutron diffraction	crystal	1.261	1.345		1.005	1.009			2.058	

for the NH_2 groups involved in the H-bonds. The effects are larger for the **RF** than the **CF** dimers. Effects similar to those observed for **RF** were reported for acetic acid dimers[8] (which have a similar cyclic H-bonding structure), in agreement with experimental[9] observations. No similar experimental reports exist for urea dimers in the gas phase. These trends are consistent with reinforced polarization (opposite charge developing on alternate atoms) in O=C-N-H...O in the ribbon dimer. They are also consistent with the resonance-assisted H-bonds proposed by Gilli.[10]

4.5 Simulation of H-bonding effects with a uniform electric field .

From the above discussion, one sees that HF calculations favor planar monomers and dimers while MP2 favors nonplanarity. The DFT calculations tend to favor planar structures except for the **R** dimers. If one considers the interaction energies between planar monomers to form planar dimers, all the *ab initio* methods agree reasonably well, as does AM1. However, the interaction energy between optimized monomers and dimers includes a destabilizing contribution from the energy of planarization. One might reasonably expect the monomers to planarize upon polarization.

To test this hypothesis, we optimized the urea monomers in uniform electric fields up to 0.06 atomic units (electron/bohr) using the HF and MP2/D95** models. The field strength in the crystal was estimated using HF/D95** calculations for the cluster of 6 molecules (Figure 3.4) with the central molecule removed. The values obtained for the field strength in the positions of the atoms of the central molecule are from 0.017 to 0.023 au. Therefore, the molecule in the crystal is subject to external field of about 0.02 au.

The results for the monomer optimization in the external field are presented in Table 4.10. At HF level urea molecule planarizes at a field of 0.02 au and remains planar at higher fields. At MP2 level urea molecule becomes almost planar at 0.04 au (the planarization energy is < 0.1 kcal/mol). However, increase in the field strength to 0.06 au drive H atoms in syn positions to O atom, which form N-H bonds orthogonal to the field direction, out of the molecular plane (planarization energy is 0.24 kcal/mol). Apparently, more sophisticated configurations of the electric field are necessary to simulate H-bonds in different directions.

To further investigate the possibility of simulating H-bonding effects with an electric field we performed geometry optimization of CH...O-bonded complexes H2O...HCN, H2O...HCCH, and H2O...HCH3, and compared the changes in C-H bond length with those in uniform electric field. GAMESS-UK was used, the numerical force constant matrix was calculated on each optimization step. The results are presented in Table 4.11. One can see, that C-H bonds in HCN and HCCH become longer upon H-bond formation, whereas in methane C-H bond involved in H-bonding becomes longer. This trend is well reproduced by a uniform electric field. Increasing field strength from 0 to 0.02 a.u. makes C-H bond in methane shorter, but a further increase elongates the bond again. Also, the electric field in the H-C direction stabilizes CH_4 molecule stronger, then in the C-H direction. The possible reason for this unusual behavior could be found in the polarity of C-H bond. In methane this bond has polarity C^+H^-, opposite to the one it has in acetylene C^-H^+, so that H-bonding (or weak external electric field) decrease its polarity, and the bond becomes more covalent. Unfortunately, the Mulliken charge does not capture this subtle effect: charges on H atoms in HCN, HCCH, and HCH_3 are: 0.22, 0.19, 0.14. However, integration of the electron density over the atomic

Table 4.10. Urea planarization in uniform electric field: F - field strength, a.u.; ΔE_{pl} - planarization energy, kcal/mol; μ_D - molecular dipole moment, D; OCNH, OCNH' - dihedrals,^{o}; ΔE - stabilisation energy in the field (the difference in total energy with and without the field), kcal; classical value $m_D F$ is given for comparison, kcal/mol

Method	F	ΔE_{pl}	OCNH	OCNH'	$\mu_D(C_2)$	$\mu_D(C_{2v})$	ΔE	$\Delta_D F$
HF/D95**	0.00	1.29	12.6	151.0	4.01	4.70	0.00	-0.00
HF/D95**	0.01	0.21	12.0	164.3	5.39	5.61	-12.73	-13.86
HF/D95**	0.02	0.00	0.0	180.0	6.52	6.52	-27.70	-32.22
HF/D95**	0.04	0.00	0.0	180.0	8.35	8.35	-64.41	-82.54
HF/D95**	0.06	0.00	0.0	180.0	10.24	10.24	-110.27	-151.72
MP2/D95**	0.00	2.50	14.7	146.5	3.46	4.38	0.00	-0.00
MP2/D95**	0.01	0.87	17.1	158.4	4.44	5.37	-12.03	-13.26
MP2/D95**	0.02	0.24	16.8	169.1	6.24	6.36	-26.50	-31.43
MP2/D95**	0.04	0.07	15.9	178.3	8.39	8.38	-62.87	-82.80
MP2/D95**	0.06	0.24	22.4	178.3	10.54	10.47	-109.37	-155.27

basin (following Bader[11]) yields 0.21, 0.14, and -0.06. Based on C-H bond length, H_2O creates the field of 0.018, 0.015, and 0.007 a.u. in the vicinity of H atoms in complexes with HCN, HCCH, and HCH_3 respectively. Values for the induced dipole moment and stabilization energy of the molecule in the external field of this strength are reasonably close to those obtained for H-bonded complexes (see Table 4.11). The decrease in the field strength is consistent with the increase of O...H distances from 2.08, to 2.24, to 2.90Å in these complexes.

Table 4.11. HF/D95** results on C-H bond lengths (Å) in H-bonded complex and a uniform electric field: F (a.u.): Mulliken charge on H atom, dipole moment (D), and stabilization energy (kcal/mol). For H-bonded complexes: molecular dipole moments μ are obtained by subtraction of μ(H_2O) form the total dipole moment, interaction energies ΔE are CP-corrected.

F	H-C	q(H)	μ	ΔE
H_2O...HCN	1.0691	0.24	3.86*	-5.14
-0.0400	1.0544	0.06	1.07	21.22
-0.0100	1.0585	0.18	2.68	7.26
0.0000	1.0614	0.21	3.21	0.00
0.0100	1.0652	0.25	3.74	-8.57
0.0200	1.0699	0.28	4.27	-18.41
0.0500	1.0907	0.38	5.90	-56.02
H_2O...HCCH	1.0643	0.16	0.56*	-1.20
-0.0500	1.0579	-0.03	-3.86	-23.60
-0.0400	1.0566	0.01	-3.07	-15.05
-0.0300	1.0561	0.05	-2.29	-8.44
-0.0200	1.0564	0.09	-1.52	-3.75
-0.0100	1.0576	0.13	-0.76	-0.94
-0.0050	1.0585	0.15	-0.38	-0.23
0.0000	1.0597	0.17	0.00	0.00
0.0050	1.0610	0.19	0.38	-0.23
0.0100	1.0626	0.20	0.76	-0.94
0.0200	1.0665	0.24	1.52	-3.75
0.0300	1.0715	0.27	2.29	-8.44
0.0400	1.0776	0.31	3.07	-15.05
0.0500	1.0852	0.34	3.86	-23.60
H_2O...HCH_3	1.0832	0.160	0.20*	-0.12
-0.0500	1.1160	-0.157	-1.79	-10.71
-0.0400	1.1057	-0.096	-1.40	-6.76
-0.0300	1.0977	-0.037	-1.03	-3.76
-0.0200	1.0916	0.019	-0.67	-1.66
-0.0150	1.0891	0.046	-0.50	-0.93
-0.0100	1.0871	0.073	-0.33	-0.41
-0.0075	1.0862	0.087	-0.24	-0.23
-0.0050	1.0854	0.100	-0.16	-0.10
-0.0025	1.0847	0.113	-0.08	-0.03
0.0000	1.0840	0.127	0.00	0.00
0.0025	1.0835	0.140	0.08	-0.03
0.0050	1.0830	0.153	0.16	-0.10
0.0075	1.0826	0.166	0.24	-0.23
0.0100	1.0822	0.179	0.32	-0.40
0.0200	1.0818	0.230	0.65	-1.61
0.0300	1.0824	0.281	0.97	-3.61
0.0400	1.0850	0.319	1.31	-6.47
0.0500	1.0875	0.383	1.61	-10.00

4.6 Heat of sublimation estimated from enthalpy of dimerization

The relative stabilities of the dimers are calculated to be the same: **R>C>HB>SC>ST** by all *ab initio* methods used. If one compares enthalpy of the H-bond relative to the planar monomer, the results of different methods also agree (Table 4.8). One can try to estimate enthalpy of sublimation for urea crystal by adding *ab initio* values for enthalpy of dimerization for all the H-bonding dimers in the crystal. For tetragonal structure (Figure 3.4) at HF level one **CF** dimer (7.2 kcal/mol) and two **HF** dimers (4.0 kcal/mol) yield 15.2 kcal/mol, and at DFT level we get 6.2+2x4.0=14.2 kcal/mol. For orthogonal structure (Figure 3.5) at HF level one **RF** dimer (10.1 kcal/mol) and one **CF** dimer (7.2 kcal/mol) yield 17.3 kcal/mol and at DFT level we get 11.2+6.2=17.4 kcal/mol. As a result, the orthogonal structure turns out to be 2-3 kcal/mol more stable than the experimental tetragonal structure. Thus, the dimeric interactions are insufficient to explain the observed crystal structures. Rather, the crystal structure must be dictated by cooperative interactions involving several molecules, as it will be shown in Chapters 5 and 7.

4.7 Conclusions

The present calculations confirm the previous reports that the minima on the urea potential surface correspond to a nonplanar structure. However, increasing size of the basis set decrease the planarization energy so that after ZPVE the monomer is more stable in the planar conformation at HF/D95**, B3PW91/D95++**, MP2/6-311+G(3df,2p) and higher levels.

MP2/D95** calculations predict the transition state between the C_2 and C_s structures to be below the zero point vibration, which means that neither of them can be observed in the experiment.

The multiple minima found for the urea monomer complicate the calculations of urea dimers. HF and DFT calculations suggest that the dimers are planar or planarize with little distortion. The MP2 calculations predict the dimers to be nonplanar. However, the planarization energies for the dimers are similar to that of one monomer (not two). These results justify the use of planar geometry for ribbons and chains, considered in the next chapter.

References for Chapter 4

[1] (a) Palmer, M. H., <u>J. Mol. Str.</u>, **1997,** <u>405</u>, 179; (b) Martinezmerino, V.; Garcia, J. I.; Mayoral, J. A.; Gil, M. J.; Zabalza, J. M.; Fayet, J. P.; Vertut, M.C.; Carpy, A.; Gonzalez, A., <u>Tetrahedron</u>, **1996,** <u>52</u>, 8947.

[2] (a) Kontoyianni, M.; Bowen, P. <u>J. Comput. Chem</u>. **1992**, <u>13</u>, 657; (b) Gobbi, A.; Frenking, G. <u>J. Am. Chem. Soc.</u> **1993**, <u>115</u>, 2362; Dixon, D. A.; (c) Matsuzawa, N. <u>J. Phys. Chem.</u> **1994**, *98*, 3967.

[3] Godfrey, P. D.; Brown, R. R.; Hunter, A. N. <u>J. Mol. Struct.</u> **1997**, <u>413</u>, 405.

[4] Scott, A.P.; Radom, L.: <u>J. Phys. Chem.</u>, **1996,** <u>100</u> (41), 16502.

[5] Turi, L.: <u>Chem. Phys. Lett.</u> **1997**, <u>275</u>(1,2), 35.

[6] (a) Dannenberg, J. J., <u>Theochem.</u>, **1997**, <u>401</u>, 279; (b) Turi, L.; Dannenberg, J. J., <u>J. Phys. Chem.</u>, **1995**, <u>99</u>, 639; (c) Turi, L.; Dannenberg, J. J., <u>J. Phys. Chem.</u>, **1993**, <u>97</u>, 7899; (d) Jurema, M. W.; Shields, G. C., <u>J. Comput. Chem'</u>, **1992**, <u>14</u>, 89; (e) Messinger, J.; Heuser, N., <u>QCPE Bulletin</u>, **1991**, <u>11(1)</u>.

[7] Csonka, G.I.; Angyan, G.: Proc. 9th Int. Congr. Of Quantum Chem., Atlanta, **1997**, P064.

[8] Turi, L.; Dannenberg, J. J.: <u>J. Phys. Chem</u>. **1993**, <u>97</u>, 12197.

[9] Derisson, J. L., <u>Mol. Struct.</u>, **1971**, <u>7</u>, 67.

[10] Bertolasi, V.; Gilli, P.; Ferretti, V.; Gilli, G., <u>Chemistry - A European Journal</u>, **1996**, <u>2</u>, 925.

[11] Bader, R. F. W. Atoms in Molecules - A Quantum Theory; Oxford University Press: Oxford, U.K., **1990**.

CHAPTER 5

5. ONE-DIMENSIONAL CLUSTERS OF UREA AND THIOUREA

This chapter describes *ab initio* and semiempirical molecular orbital calculations on one-dimensional hydrogen-bonding aggregates of urea and thiourea corresponding to the two patterns: chains and ribbons. We will also consider transverse chains, obtained from ribbons by 90° rotation of every other molecule about the C=O bond. All of these aggregates are found in the crystal structures of these molecules. Ribbons are primary agglomerates in orthogonal structure (**CAB** on Figure 3.5), while chains are primary agglomerates in tetragonal structure (**CAB** on Figure 3.4). Transverse chains are orthogonal to the chains in tetragonal crystal structure (**DAE** on Figure 3.4) and are related to ribbons by rotation of all odd molecules perpendicular to the ribbon plane. As we described in Chapter 4, ribbons are formed by cyclic dimers, the most stable for urea. Chains are formed by head-to-tail dimers, the next stable type. Transverse chains are formed by herringbone dimers, the least stable for urea.

In the previous chapter we have shown that equilibrium geometry of the urea molecule is not planar at all levels of theory. The barrier to planarization is systematically lowered by increasing size of the basis set, H-bond formation and application of external electric fields. Moreover, zero-point vibrational energy corrections make the planar structure of the isolated molecule preferable at the Hartree-Fock, Møller-Plesset and density functional theory levels using the large 6-311+G(3df,2p) basis set. Based on these results, we considered the urea molecule to be planar for all aggregates considered. The thiourea molecule, which is even more

easily planarized, was also held planar in the aggregates calculated.

5.1 Method

Theoretical calculations were performed using the GAUSSIAN 94/98 programs for both *ab initio* and semiempirical molecular orbital (MO) methods. Unless otherwise noted, all geometries were optimized with the following constraints: (a) all molecules are assumed to have C_{2v} symmetry; (b) inter- and intramolecular geometrical parameters were kept equivalent for molecules within a given aggregate. These constraints are meant to simulate translational symmetry within the crystal. Full optimization was performed in some cases for comparison.

Periodic HF calculations on infinite chains and ribbons were performed using the CRYSTAL 92/95 programs. We used single-point energy calculations on the optimized geometry of the decamer.

Since the result of partial optimization is not a stationary point, vibrational frequencies were calculated for fully optimized oligomers only. These were used to estimate ZPVE corrections for other oligomers. We performed HF, DFT and MP2(frozen core) calculations using the D95** basis set, as well as AM1 semiempirical calculations. For the DFT calculations, we used the hybrid B3PW91.

5.2 Energy of the last H-bond and errors due to constraints and finite cluster size

We have considered the primary one-dimensional agglomerates in tetragonal and orthogonal crystal structures: planar chains and ribbons (Figure 5.1). The energies
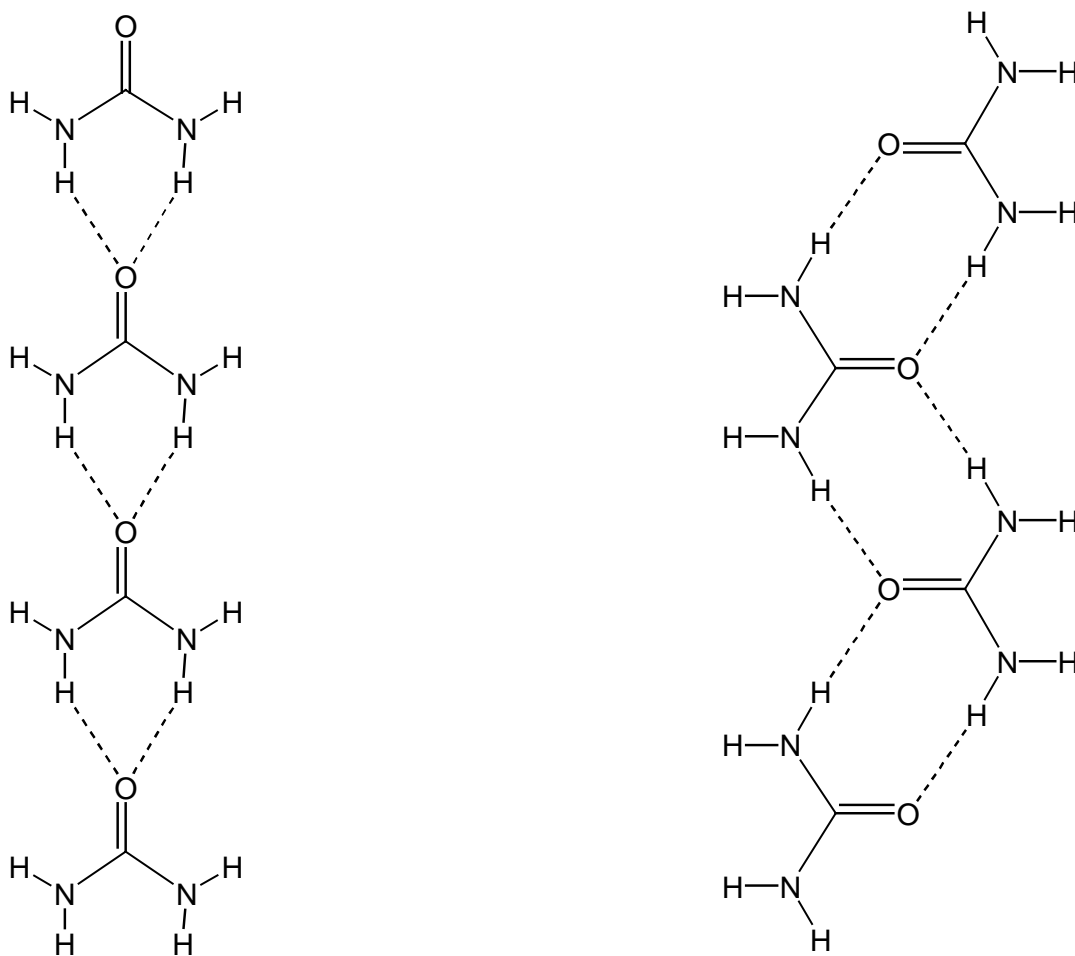
Figure 5.1. Hydrogen-bonding patterns in chains (left) and ribbons (right) of urea. The structures for thiourea are analogous.

obtained for these oligomers at the HF/D95** level are presented in Table 5.1. The geometrical parameters are summarized in Table 5.2. As one can see from Table 5.1, the net stabilization energy, ΔE, is greater for ribbons than for chains when the oligomers are small. The difference is most significant for the dimers, decreasing as the oligomer grows. For the decamer (the largest oligomer considered) the order of stability reverses. Extrapolating this trend, we can expect the infinite chain to be more

Table 5.1. HF/D95** results for urea ribbons and chains. All values are given in kcal/mol. Total stabilization energy ΔE is uncorrected, last H-bond energy $\Delta E_n=\Delta E(n)-\Delta E(n-1)$ is given before and after counterpoise (CP) and zero-point vibrational (ZPVE) correction is applied. Values in parenthesis correspond to completely optimized oligomers, ZPVE correction values for n=5-10 are estimated, asymptotic values obtained by extrapolation using formula $E_n=E_2+a\cdot(exp(b\cdot(2-n))-1)$.

n	ΔE	ΔE_n	CP	ZPVE	ΔE_n,CP	ΔE_n,ZPVE	ΔE_n,CP+ZPVE
				ribbons			
2	-12.44	-12.44 (-12.75)	0.95	(1.92)	-11.49	-10.52	-9.57
3	-23.62	-11.18 (-11.37)	2.03	(3.63)	-10.10	-9.48	-8.40
4	-35.18	-11.56 (-11.65)	3.02	(5.37)	-10.57	-9.82	-8.38
5	-46.67	-11.49	4.04	7.08	-10.46	-9.78	-8.75
6	-58.23	-11.56	5.06	8.85	-10.54	-9.79	-8.77
7	-69.76	-11.54	6.08	10.62	-10.52	-9.77	-8.75
8	-81.32	-11.56	7.10	12.39	-10.54	-9.79	-8.77
9	-92.88	-11.55	8.13	14.16	-10.53	-9.78	-8.76
10	-104.44	-11.56	9.14	15.93	-10.55	-9.79	-8.78
∞		-11.58			-10.65	-9.81	-8.91
1D					-10.62		-8.88
				chains			
2	-8.64	-8.64 (-8.78)	0.69	(1.06)	-7.96	-7.58	-6.90
3	-19.54	-10.89 (-11.01)	1.45	(2.08)	-10.13	-9.74	-8.97
4	-31.23	-11.69 (-11.79)	2.15	(3.36)	-11.00	-10.41	-9.71
5	-43.27	-12.04	3.06	4.80	-11.13	-10.60	-9.69
6	-55.49	-12.22	3.88	6.00	-11.41	-11.02	-10.21
7	-67.82	-12.33	4.69	7.20	-11.52	-11.13	-10.32
8	-80.22	-12.40	5.52	8.40	-11.57	-11.20	-10.37
9	-92.66	-12.44	6.34	9.60	-11.62	-11.24	-10.42
10	-105.14	-12.47	7.17	10.80	-11.65	-11.27	-10.45
∞		-12.49			-11.77	-11.38	-10.70
1D					-11.65		-10.58

stable than the infinite ribbon.

To analyze individual H-bonds, we used the last H-bond energy, ΔE_n, defined as the difference between stabilization for oligomers with *n* and *(n-1)* molecules. This value converges to the same asymptotic limit as the average H-bond energy. However, the convergence is faster, and thus, easier to extrapolate. After the pentamer the last H-bonding energy is stable within 0.1 kcal/mol for both chains and ribbons. This is in contrast with literature data for formamide, discussed previously in Section 2.4.

Table 5.1 indicates the last H-bond to be stronger for chains than for ribbons

starting with tetramer. Application of CP and especially ZPVE corrections favors

the chains, moving the crossover point to the trimers. For the chains the increase in the

magnitude of ΔE_n, is monotonic with the growth of the cluster. This behavior is

consistent with the chain structure which has only one repeating unit (Figure 5.1).

However, the magnitude of ΔE_n, oscillates for ribbons: decreasing with n for odd

oligomers, and almost constant for even oligomers. Ribbons have a repeating unit that

contains two molecules (Figure 5.1) where 1-3 interactions should be destabilizing

(see below). Thus, aggregation is progressively stabilizing H-bonding for chains, but

not for ribbons. We extrapolated the last H-bond energy (for ribbons, only even

oligomers were used) applying the same relationship:

$$\Delta E_n = \Delta E_2 + a \cdot (exp(b \cdot (2-n))-1)$$

The asymptotic value of ΔE_n, for chains is about 1 kcal/mol more stable than the

corresponding value for ribbons, which is comparable to H-bonding energy for the

ribbon dimer (see Figure 5.2). CP and ZPVE corrections increase the energetic

preference for the chain.
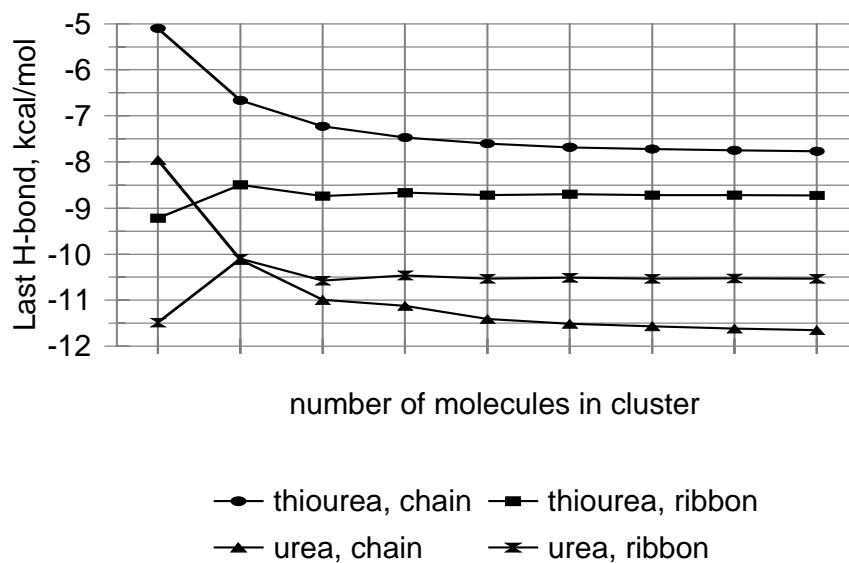
Figure 5.2. Comparison of last H-bond interaction energies, ΔE_n, urea and thiourea chain and ribbon aggregates

Table 5.2. HF/D95** results on dipole moments μ(D), bond lengths (Å), and monomer deformation energies E_{def} (kcal/mol) for planar ribbons and chains of urea. Crystallographic values from neutron diffraction shown for comparison.

				Ribbon				
1	C=O	C-N	N-Hs	N-Ha	O...H	μ		E_{def}
2	1.2047	1.3644	0.9911	0.9923		4.70		0.29
3	1.2164	1.3563	0.9997	0.9912	1.9856	0.00		0.48
4	1.2199	1.3543	0.9989	0.9912	1.9948	4.78		0.61
5	1.2218	1.3531	0.9998	0.9912	1.9943	0.00		0.69
6	1.2230	1.3525	1.0003	0.9912	1.9960	4.81		0.75
7	1.2238	1.3520	1.0007	0.9912	1.9958	0.00		0.80
8	1.2243	1.3517	1.0009	0.9912	1.9956	4.82		0.83
9	1.2248	1.3514	1.0011	0.9912	1.9954	0.00		0.86
10	1.2251	1.3512	1.0013	0.9912	1.9951	4.83		0.88
∞	1.2254	1.3511	1.0014	0.9912	1.9951	0.00		
	1.2259	1.3507	1.0018	0.9912	1.9919			
				Chain				
1	C=O	C-N	N-Hs	N-Ha	O...H	μ/n	$μ_n$	E_{def}
2	1.2047	1.3644	0.9911	0.9923		4.70	4.70	0.12
3	1.2110	1.3595	0.9927	0.9919	2.2405	5.42	6.14	0.26
4	1.2146	1.3568	0.9938	0.9917	2.1894	5.82	6.62	0.38
5	1.2169	1.3551	0.9946	0.9915	2.1614	6.06	6.78	0.47
6	1.2184	1.3541	0.9952	0.9914	2.1440	6.22	6.86	0.54
7	1.2195	1.3533	0.9956	0.9914	2.1323	6.33	6.88	0.59
8	1.2204	1.3527	0.9959	0.9913	2.1239	6.41	6.88	0.64
9	1.2210	1.3523	0.9961	0.9914	2.1174	6.48	6.93	0.67
10	1.2215	1.3519	0.9963	0.9913	2.1126	6.53	6.93	0.70
∞	1.2220	1.3516	0.9964	0.9912	2.1087	6.57	6.93	
cryst	1.2233	1.3507	0.9967	0.9911	2.1002			
	1.2580	1.3440	1.0220	1.0040	2.001			

To evaluate the error in cluster calculations due to pseudoperiodical constraints we should compare constrained ΔE_n values from Table 5.1 with the totally optimized results (in parentheses). One can see, that the difference decreases from 0.3 kcal/mol in the ribbon dimer to 0.1 kcal/mol in both tetramers. Another possible cause for the errors in extrapolation of the cluster results to infinite systems is finite size of the system. The last H-bond energy values allow us to compare periodical and cluster calculation on chain and ribbon decamers. One can see, that difference between decamer and infinite structure (of the same molecular geometry) is small (0.07 kcal/mol) for ribbons and is absent for chains. The latter could be attributed to the

absence of geometric relaxation. Comparison with extrapolated value let us conclude that the presented scheme for extraction of intermolecular interaction from cluster calculations practically eliminates the errors due to finite cluster size. One can also note that chain termination error is significantly smaller than the geometry relaxation effect. This suggests the importance of geometry optimization for periodical calculations.

5.3 Comparison with previously published data

The results on interaction energies agree reasonably well with the results on dimers and trimers reported previously. Single-point HF calculations by Perez and Dupuis[1] in the custom basis set of DZ quality gave interaction energy of 12.4 kcal/mol and 27.8 kcal/mol for chain dimer and trimer (not accounted for the monomer relaxation and BSSE). Our values are lower: 8.6 and 19.5 kcal/mol (Table 5.1). For the interactions in the transverse trimer their value of 15.4 kcal/mol also exceeds 10.2 kcal/mol obtained in the present study.

A HF/6-31++G** value of 6.9 kcal/mol reported by Belosludov, Li, and Kawazoe[2] for the chain dimer (including molecular relaxation to nonplanar structure, but not CP correction), is in better agreement with our result of 6.2 kcal/mol (Table 4.8). Their value of interaction energy for the herringbone dimer is almost the same, compared to our value of 5.7 kcal/mol. For **CB** dimer they reported 9.0 kcal/mol, excellent agreement with the value of 9.0 in the present study (see Table 4.8). For the ribbon dimer and trimer their values (after CP correction) are 11.5, and 21.1 kcal/mol. If we subtract the planarization energy of 0.9 and 0 kcal/mol accordingly, the values (10.6 and 21.1 kcal/mol) are again in a good agreement with our values of 11.5 and

21.6 kcal/mol.

Our results disagree with conclusions by Belosludov, Li, and Kawazoe[2] about planarity of the ribbon trimer, based on frequency calculations at HF/6-31++G** level. Our full optimizations and frequency calculations on chain and ribbon clusters up to tetramers at HF/D95** level resulted in multiple imaginary frequencies (6 and 8 for ribbon trimer and tetramer, 8 and 9 for chain trimer and tetramer), proving the planar structure to be unstable. The biggest absolute values of imaginary frequencies correspond to piramidalization of NH_2 groups not involved in H-bonding and their values are close to those of the monomer. As we noticed in Chapter 4 for the urea monomer, increasing the size of the basis set tends to reduce the planarization barrier. However, planarization energies obtained by Belosludov, Li, and Kawazoe[2] for the monomer and the ribbon dimer (0.9 kcal/mol for both) exactly match our values.

We performed frequency calculations for the ribbon trimer at HF/6-31++G** level for fully optimized planar urea ribbon trimer. It yielded 4 imaginary frequencies. Therefore, planar conformation is not a minimum at this level of theory, and results reported by Belosludov, Li, and Kawazoe[2] are not confirmed.

5.4 Cooperative effects in chains and ribbons and pairwise decomposition

For chains the extrapolated value of ΔE_n is 46% greater than that of the chain dimer. For ribbons the extrapolated value of ΔE_n is 8% less than that of the dimer but very similar to ΔE_n, for the trimer and higher aggregates. The apparent anti-cooperative behavior of the ribbon is due to the repulsive nature of the 1-3 interactions

Table 5.3. Pairwise analysis HF/D95** results for urea chains and ribbons. All values are given in kcal/mol. Total stabilization energy: E_{DEF} molecular deformation in the cluster; Σpair - sum of pairwise interactions 12, 13, 14, and 15 taken m, l, k and j times accordingly to the number of the pairs in the cluster; ΔE_{NA} - difference between total stabilization for the cluster and Σpair.

n	E_{DEF}	m	ΔE_{12}	l	ΔE_{13}	k	ΔE_{14}	j	ΔE_{15}	Σpair	ΔE_{NA}
Chains											
2	0.11	1	-8.19							-7.96	-0.00
3	0.26	2	-8.35	1	-0.88					-16.80	-1.29
4	0.38	3	-8.42	2	-0.91	1	-0.25			-25.82	-3.26
5	0.47	4	-8.46	3	-0.93	2	-0.25	1	-0.10	-33.90	-6.31
Ribbons											
2	0.26	1	-12.01							-11.49	0.00
3	0.48	2	-12.32	1	1.37					-21.83	0.24
4	0.61	3	-12.51	2	1.37	1	-0.26			-32.50	0.34
5	0.69	4	-12.61	3	1.37	2	-0.26	1	0.12	-43.42	0.79

that do not exist in the dimer. To illustrate this point we calculated the pairwise components of the stabilization energies of the oligomers (Table 5.3). To this end, we performed single point CP-corrected calculations for all possible molecular pairs within the structure of the cluster. Interaction components for single molecules and molecular pairs are listed in the Table 5.2 along with the number of those components present in the total sum. The interaction for 1-2 pair is attractive (-12.3 to -12.6 kcal/mol), and for the 1-3 pair is repulsive (1.37 kcal/mol). The ratio of 1-2 to 1-3 interactions decreases from 2 (for the trimer) to 1 (for an infinite chain) as the aggregate grows. This is the primary reason for non-monotonic behavior of the last H-bond in the ribbons. All dimeric interactions within the chain are attractive, which is why the stabilization is monotonic with the cluster size.

As one can see from the Table 5.3, the total interaction energy is not the sum of 1- and 2-body interactions (i.e. monomer deformation and pairwise stabilization). This is because in the dimeric pairs molecular polarization differs from that in a cluster. We can see that a non-additive component is negative for the chains, and

slightly positive for the ribbons. In the ribbon dimer **AB** molecule **B** polarizes the
molecule **A** in the direction AB. In the trimer **CAB** molecule **C** polarizes the molecule
A in the opposite direction. As a result, interaction between **A** and **B** is not as
attractive, as in the dimer. This results in destabilization of the trimer relative to the
sum of dimeric interactions.

The dipole moment of the aggregates is also non-additive (is not equal to the
vector sum of the monomers). The average dipole moment/molecule is increasing as a
function of size (Table 5.3). For the urea chain, the dipole moment/molecule increases
from the monomeric value of 4.70 D to 6.57 D in the decamer, an increase of 40%.
Thus, the molecules become increasingly polarized as the chain grows. For the ribbon,
the situation is quite different. All aggregates that contain even number of monomers
have zero dipole moments because they are centrosymmetric. The dipole moments of
the aggregates that contain odd quantities of monomers increase only modestly from
4.70 D in the monomer to 4.83 D in the nonamer. This behavior is consistent with a
negligible level of non-additive component for the ribbons stabilization energy.

The results of the MP2, DFT and semiempirical calculations are qualitatively
similar to the HF calculations discussed above. Table 5.4 indicates that the chain

Table 5.4. MP2/D95** results for urea ribbons and chains. See Table 5.1 for
explanations. HF/D95** values were used for ZPVE corrections.

n	Ribbons					
	ΔE	ΔE_n	CP	ΔE_n, CP	ΔE_n, ZPVE	ΔE_n, CP+ZPVE
2	-15.86	-15.86	3.87	-12.00	-14.23	-10.36
3	-30.95	-15.08	7.62	-11.33	-13.64	-9.89
4	-46.41	-15.46	11.44	-11.64	-13.99	-10.16
5	-61.85	-15.44	15.28	-11.60	-13.99	-10.15
ext		-15.48		-11.66	-13.99	-10.17
	chains					
2	-10.41	-10.41	2.59	-7.81	-9.32	-6.73
3	-23.41	-13.00	5.31	-10.28	-11.95	-9.24
4	-37.36	-13.95	8.14	-11.12	-12.64	-9.81
5	-51.75	-14.39	11.04	-11.50	-12.92	-10.03
ext		-14.50		-11.55	-13.00	-10.05

dimer is 4% less stable, while the ribbon dimer is 4% more stable at the

MP2/D95** level than at HF/D95** level (after all corrections). Consequently, ΔE_n,

for the chain tetramer does not exceed that for the ribbon tetramer (as it did for HF).

However, the extrapolated values suggest that ΔE_n, for the chain will exceed that for

the ribbons at some later point in the growth of the aggregates. The DFT results

reported in Table 5.5 are very similar to MP2. Although the stabilization energies and

CP-corrected ΔE_n for the ribbons are more negative than those for the chains even for

the decamer, this is not true after ZPVE correction. This result must be qualified since

ZPVE correction is extrapolated from the HF results for the tetramers. The AM1 and

SAM1 semiempirical calculation results are presented in Table 5.6. These are close to

the DFT results prior to ZPVE correction, which predict ribbons to be more stable.

Table 5.5. B3PW91/D95** results for urea ribbons and chains.

n	μ	ΔE	ΔE_n	ΔE_n, CP	ΔE_n, ZPVE	ΔE_n, CP+ZPVE
			Ribbons			
1	4.43					
2	0.00	-14.38	-14.38	-12.83	-12.46	-10.91
3	4.53	-27.60	-13.22	-11.64	-11.52	-9.94
4	0.00	-41.24	-13.64	-12.03	-11.90	-10.29
5	4.56	-54.85	-13.60	-11.99	-11.89	-10.28
6	0.00	-68.53	-13.69	-12.08	-11.92	-10.31
7	4.58	-82.21	-13.68	-12.06	-11.91	-10.29
8	0.00	-95.92	-13.71	-12.09	-11.94	-10.32
9	4.59	-109.63	-13.71	-12.09	-11.94	-10.32
10	0.00	-123.35	-13.72	-12.10	-11.95	-10.33
ext	4.61		-13.73	-12.11	-11.96	-10.34
			chains			
1	4.43					
2	5.31	-8.51	-8.51	-7.23	-7.59	-6.31
3	5.83	-19.69	-11.18	-9.74	-10.03	-8.59
4	6.15	-31.90	-12.21	-10.71	-10.93	-9.43
5	6.37	-44.59	-12.69	-11.16	-11.25	-9.72
6	6.54	-57.53	-12.94	-11.39	-11.74	-10.19
7	6.66	-70.63	-13.10	-11.53	-11.90	-10.33
8	6.76	-83.82	-13.19	-11.63	-11.99	-10.43
9	6.84	-97.08	-13.26	-11.67	-12.06	-10.47
10	6.89	-110.38	-13.30	-11.75	-12.10	-10.55
ext	7.07		-13.34	-11.77	-12.12	-10.57

Table 5.6. Semiempirical results for urea ribbons and chains. Energies are in kcal/mol, dipole moments in D.

	ribbons				chains		
n	μ	ΔE	ΔE_n		μ/n	ΔE	ΔE_n
	AM1					AM1	
1	4.14				4.14		
2	0.00	-8.80	-8.80		4.60	-6.13	-6.13
3	4.13	-17.02	-8.22		4.85	-13.54	-7.40
4	0.00	-25.41	-8.39		4.99	-21.38	-7.84
5	4.14	-33.75	-8.34		5.08	-29.40	-8.03
6	0.00	-42.13	-8.38		5.15	-37.53	-8.12
7	4.14	-50.49	-8.36		5.20	-45.70	-8.18
8	0.00	-58.87	-8.38		5.24	-53.91	-8.21
9	4.15	-67.24	-8.37		5.27	-62.15	-8.23
10	0.00	-75.61	-8.37		5.29	-70.39	-8.25
∞	4.15		-8.37		5.35		-8.27
	SAM1					SAM1	
1	4.23				4.23		
2	0.00	-8.04	-8.04		4.79	-3.85	-3.85
3	4.25	-15.41	-7.37		5.10	-9.33	-5.48
4	0.00	-23.10	-7.69		5.28	-15.40	-6.06
5	4.27	-30.72	-7.62		5.40	-21.72	-6.33
6	0.00	-38.40	-7.68		5.49	-28.18	-6.46
7	4.28	-46.07	-7.66		5.56	-34.72	-6.54
8	0.00	-53.76	-7.69		5.61	-41.31	-6.59
9	4.29	-61.43	-7.68		5.65	-47.93	-6.62
10	0.00	-69.11	-7.68		5.68	-54.57	-6.64
∞	4.32		-7.68		5.71		-6.67

5.5 Cooperative effects in transverse chains

Let us consider now transverse chains (Table 5.7). In the dimer (**AD** on Figure 3.4) one molecule **A** is H-donor, and molecule **D** is H-acceptor. Since permanent dipole moments of the molecules are antiparallel, the dipole moment of the dimer is due to the H-bond. Components of the dipole moment in the chain direction X and in the direction Z parallel to C=O bond are presented in Table 5.7. There are 2 types of transverse trimers: **EAD** and **GAF** on Figure 3.4. In **EAD** the central molecule is a donor of two H-bonds, and in **GAF** it accepts two H-bonds. Accordingly, the Z-

Table 5.7. HF/D95** results urea transverse chains. Energies are in kcal/mol, dipole moments are in D. See text for explanations.

n	ΔE	ΔE_n	ΔE_n,cp	ΔE_n,zpve	ΔE_n,cp+zpve	μ_x	μ_z	μ_z/mol	μ_{Hb}	μ_{nHb}
1							4.430	4.430		
2	-5.67	-5.67	-5.09	-4.77	-4.19	0.485	0.435		0.485	0.485
3	-10.18	-4.50	-4.00	-3.66	-3.16		5.496	4.705	0.791	0.306
3	-10.55	-4.88	-4.68	-4.04	-3.84		3.915			
4	-15.34	-5.16	-4.59	-4.32	-3.75	0.502	1.171		1.171	0.380
5	-20.00	-4.67	-4.15	-3.82	-3.31		6.250	4.711	1.539	0.369
5	-20.43	-5.10	-4.52	-4.25	-3.68		3.171			
6	-25.15	-5.15	-4.57	-4.30	-3.73	0.506	1.914		1.914	0.375
7	-29.84	-4.69	-4.17	-3.84	-3.33		7.000	4.715	2.285	0.371
7	-30.28	-5.13	-4.55	-4.29	-3.71		2.431			
8	-34.98	-5.15	-4.57	-4.30	-3.72	0.508	2.659		2.659	0.374
9	-39.67	-4.69	-4.19	-3.85	-3.34		7.745	4.717	3.028	0.368
9	-40.12	-5.14	-4.57	-4.30	-3.73		1.689			
10	-44.82	-5.15	-4.56	-4.30	-3.72	0.508	3.402		3.402	0.374

components of the dipole moments due to these H-bonds are parallel and antiparallel to the total dipole moment of the trimer, and X-componets cancel each other. Similar sinpolar and antipolar isomers exist for all the clusters with an odd number of molecules. The value for the dipole moment averaged over these isomers (μ_z/mol) corresponds to the dipole moment of one monomer, since Z-components of the dipole moment due to H-bonds cancel each other. This value shows a 6% increase from the monomeric dipole moment and does not significantly change with the cluster size. We can define the dipole moment due to one H-bond (μ_{Hb}) as the difference between μ_z/mol and the actual dipole moment. In the even cluster the whole value of Z-component of the dipole moment is due to one H-bond, as molecular dipole moments cancel each other.

The increment of μ_{Hb} after addition of one new H-bond (μ_{nHb}) is also listed in Table 5.7. It is decreasing for even clusters (from 0.49 D for the dimer) and increasing for odd clusters (from 0.31 D for the timer) to the same asymptotic value of 0.37 D). The energy of the last H-bond displays similar behavior. Like in the ribbons, H-bond

is the strongest for the dimer (4.2 kcal/mol after CP and ZPVE corrections), and

the weakest for the trimer (3.2 kcal/mol). As the cluster grows, the value decreases for

even clusters, and increases for odd clusters, converging around 3.7 kcal/mol. Both

possible conformers of odd clusters have weaker H-bonds then even clusters.

5.6 Chains and ribbons of the thiourea

The results of similar calculations of ribbons and chains formed by thiourea are

presented in Tables 5.8. Ribbons are predicted to be more stable than chains for all

aggregates (independent of size) at both HF and DFT levels. No MP2 calculations

were performed for the thiourea aggregates due to the limitations of our computational

resources. The interaction energies between thiourea molecules are significantly less

than between urea molecules. Furthermore, the ratio of the interaction energies in the

chain vs. ribbon dimers is 0.55 for the thiourea compared to 0.72 for the urea

(HF/D95**). While the cooperative effect upon the extrapolated value of the thiourea

chain for the infinite chain is comparable to that for urea, 53% vs. 55% (HF/D95**), it

is insufficient to overcome the more favorable interaction energy of the chain

compared to the ribbon dimer. Figure 5.2 presents a comparison of urea and thiourea

CP-corrected ΔE_n's in chains and ribbons.

The dipole moments of the thiourea chain increase from the monomeric value

of 5.95 to 7.96 D in the decamer, an increase of 36% (similar to the 40% increase for

urea). For the ribbon, the nonamer has a dipole moment of 6.13 D, only slightly more

than the monomeric value of 5.96 D.

Table 5.8. Ab initio results for thiourea ribbons and chains. Energies are in kcal/mol, dipole moments in D.

	Ribbons					chains			
N	μ	ΔE	ΔE_n	ΔE_n, CP		μ/n	ΔE	ΔE_n	ΔE_n, CP
					HF/D95**				
1	5.95					5.95			
2	0.00	-10.67	-10.67	-9.22		6.73	-5.42	-5.42	-5.10
3	6.08	-20.59	-9.92	-8.50		7.15	-12.45	-7.03	-6.66
4	0.00	-30.76	-10.17	-8.74		7.41	-20.05	-7.61	-7.23
5	6.11	-40.87	-10.11	-8.67		7.58	-27.92	-7.86	-7.47
6	0.00	-51.04	-10.16	-8.72		7.70	-35.91	-8.00	-7.60
7	6.12	-61.18	-10.15	-8.70		7.79	-43.99	-8.07	-7.68
8	0.00	-71.35	-10.17	-8.72		7.86	-52.11	-8.12	-7.72
9	6.13	-81.51	-10.16	-8.72		7.92	-60.26	-8.15	-7.75
10	0.00	-91.67	-10.17	-8.73		7.96	-68.43	-8.17	-7.77
∞	6.14		-10.17	-8.73		8.11		-8.19	-7.79
					B3PW91/D95**				
1	5.43					5.43			
2	0.00	-11.91	-11.91	-10.38		6.38	-5.19	-5.19	-4.78
3	5.60	-23.08	-11.17	-9.66		6.92	-12.25	-7.06	-6.59
4	0.00	-34.53	-11.45	-9.91		7.27	-20.05	-7.79	-7.28
5	5.63	-45.94	-11.41	-9.87		7.50	-28.17	-8.13	-7.61
6	0.00	-57.42	-11.48	-9.95		7.68	-36.48	-8.30	-7.76
7	5.64	-68.86	-11.44	-9.89		7.80	-44.74	-8.26	-7.71
8	0.00	-80.34	-11.48	-9.93		7.90	-53.36	-8.62	-8.07
9	5.65	-91.81	-11.47	-9.92		7.98	-61.87	-8.51	-7.96
10	0.00	-103.29	-11.48	-9.93		8.04	-70.42	-8.54	-7.99
∞	5.64		-11.48	-9.93		8.10		-8.57	-8.02

5.7 Simulations of intermolecular interactions using a uniform electric field

In the chain cluster considered in this chapter all molecular dipole moments are aligned in parallel. Therefore, an external field exerted upon one of the central molecules of the cluster by its neighbors is expected to be rather uniform. This opens up an opportunity to compare the effect of purely electrostatic interactions with the total effect of intermolecular interaction on atomic and electronic structure of the molecule. To perform this comparison we completed geometry optimization on planar

Table 5.9. HF/D95** results for urea monomer and chain dimer in a uniform electric field F (a.u.): dipole moment μ (D), stabilization energy ΔE (kcal/mol), classical stabilization energy μF (kcal/mol), and bond lengths (Å). Available values for the chain decamer, and experimental values are shown for comparison.

F	μ/mol	ΔE	μ F	H...O	C=O	C-N	N-Ha						
		chain monomer											
0.00	4.70	0.00	0.00		1.205	1.364	0.991						
0.01	5.61	-12.74	-13.86		1.216	1.357	0.993						
0.02	6.52	-27.72	-32.21		1.229	1.351	0.996						
0.03	7.44	-44.95	-55.08		1.243	1.345	1.000						
0.04	8.36	-64.45	-82.52		1.259	1.339	1.004						
0.05	9.29	-86.23	-114.65		1.276	1.334	1.009						
		chain dimer			Average			H-donor monomer			H-acceptor monomer		
0.00	5.45	-8.84	0.00	2.222	1.211	1.359	0.993	1.210	1.361	0.994	1.212	1.357	0.991
0.01	6.29	-12.37	-15.53	2.118	1.225	1.351	0.997	1.223	1.354	0.999	1.228	1.348	0.994
0.02	7.11	-18.33	-35.13	2.020	1.241	1.344	1.002	1.238	1.347	1.007	1.245	1.340	0.998
0.03	7.93	-24.95	-58.74	1.924	1.260	1.337	1.009	1.255	1.341	1.017	1.265	1.333	1.002
0.04	8.75	-33.25	-86.37	1.825	1.281	1.330	1.020	1.275	1.335	1.033	1.288	1.325	1.007
0.05	9.56	-43.81	-118.06	1.710	1.307	1.324	1.036	1.298	1.330	1.059	1.316	1.318	1.014
MW	3.83	0.00			1.221	1.378	0.998						
crystal	4.66	-21.00		2.062	1.265	1.349	1.008						
decamer	6.93	-11.65		2.109	1.222	1.352	0.996						

urea monomers and chain dimers in a uniform electric field of different strength. The results are reported in Table 5.9 and Figure 5.3.

One can see that classical electrostatic stabilization of the dipole in a field is close to HF stabilization energy of the molecule in the field. The values of the dipole moment, stabilization energy and C-N, C=O and N-H covalent bond lengths in the monomer change to their respective values in the decamer (marked by horizontal lines on Figure 5.3) in rather narrow range of an external field 0.015-0.022 a.u. The stabilization that corresponds to an infinite chain of H-bonding urea molecules occurs at an applied field of 0.016 a.u., dipole moment and C=O bond length attains the infinite chain value at the same value of an applied field, whereas C-N and N-H bonds attain the infinite chain value at 0.018 and 0.021 a.u., respectively. For the monomer a weaker field (about 0.01 a.u.) is necessary to achieve these values. This is expected, since a second monomer creates an additional field. H-bond length in the dimer also
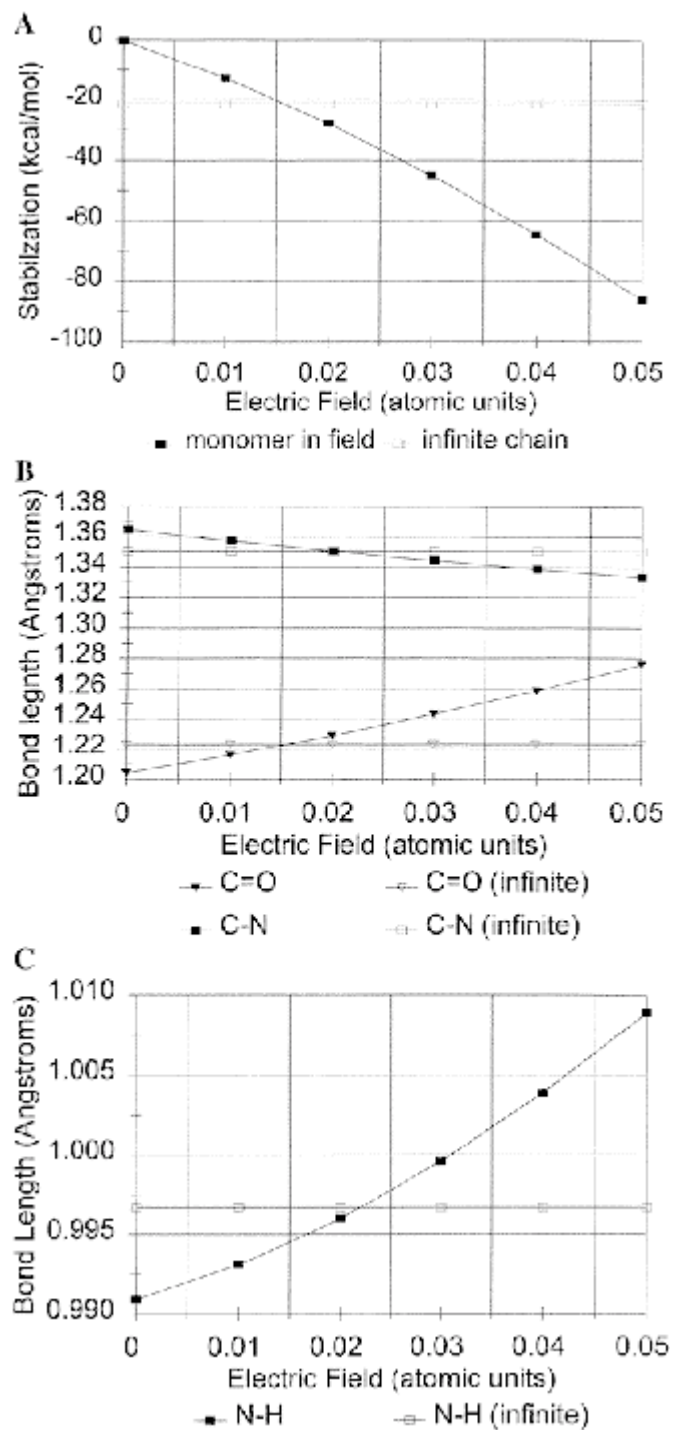
Figure 5.3. Urea in an electric field: (A) Stabilization energy; (B) C=O and C-N bond lengths; (C) N-H bond length. The unfilled markers that form the horizontal lines indicate extrapolated values for infinite H-bonding chains at the HF/D95** level.

follows this trend.

To apply a similar approach to another system, we compared HF/D95** results on an H-bonded chain of 1,3-pentenedione molecules (Figure 5.4) to the monomer in the uniform field (Table 5.10, and Figure 5.5). This system is simulating crystalline 1,3-cyclohexanedione, (Figure 5.4) studied previously.[3]

This time one can see the striking difference. An applied field of about 0.012 au corresponds to the stabilization of an infinite chain. The C=C and C=O bond lengths reach the infinite chain values at applied fields of 0.008 and 0.007 a.u., respectively, whereas the C-C and C-O bonds reach the corresponding values at applied fields of 0.020 and 0.021 au, respectively. The value of the applied electric field which reproduces the stabilization of an individual molecule as calculated in an infinite hydrogen-bonding chain (0.008 au) is very different from that needed to reproduce the changes of the dipole (0.018 au), and most of the geometric parameters (C-C and C-O bond lengths). Fields of 0.007 to 0.021 au are needed to reproduce all of the infinite chain data for 1,3-propanedione. This range of fields is almost three times that calculated for urea. Thus, the hydrogen bonds in the infinite chains of urea and 1,3-propanedione seem to fall into distinctly different categories.
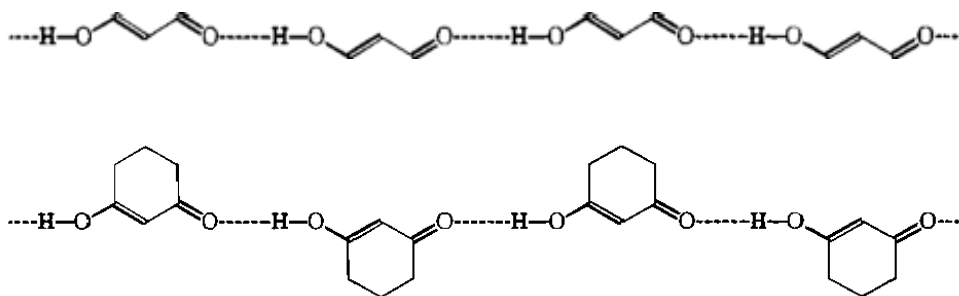
Figure 5.4. H-bonded chain of 1,3-propanedione molecules (top) simulating the chain in crystal structure of 1,3-cyclohexanedione (bottom)
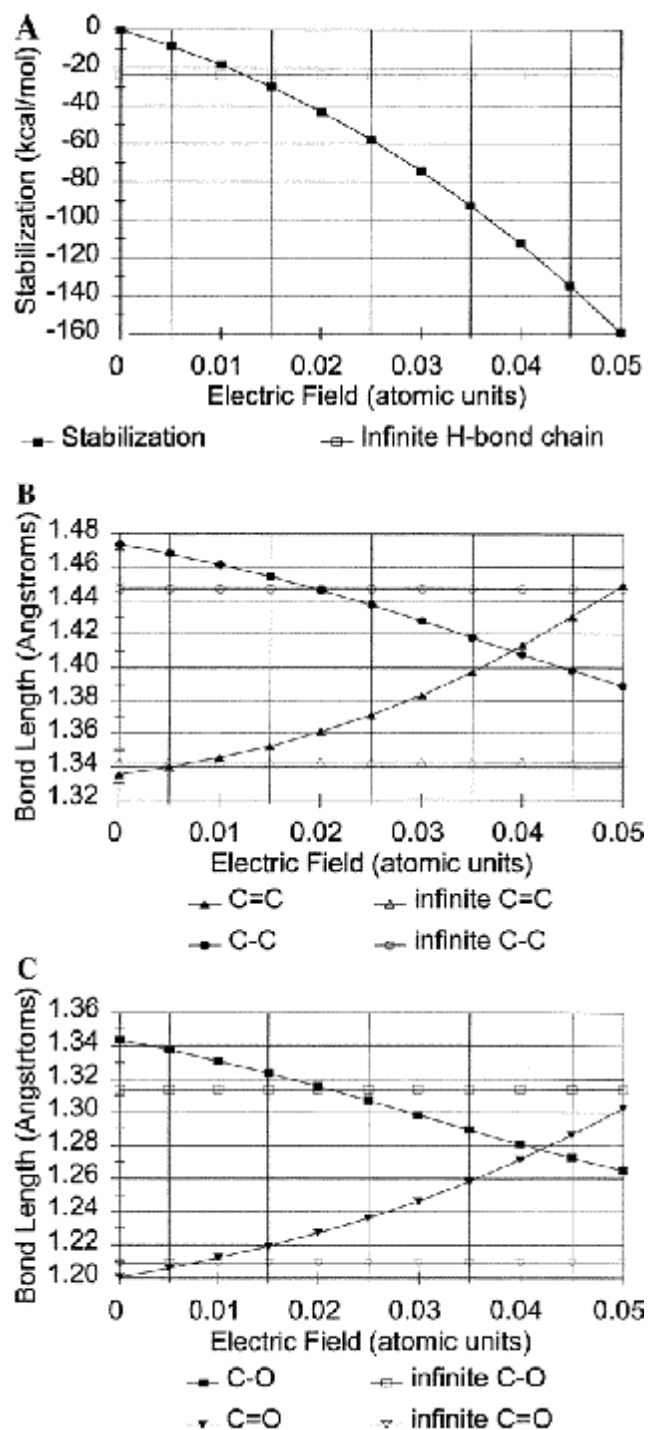
Figure 5.5. Enol of 1,3-propanedione in an electric field. (A) Stabilization energy (equivalent to H-bonds at each end); (B) C-C and C=C bond lengths; (C) C-C and C=C bond lengths. The unfilled markers indicate extrapolated values for infinite H-bonding chains at the HF/D95** level.

Table 5.10. HF/D95** results for monomer and dimer of 1,3-pentenedione in a uniform electric field F (a.u.), compared to chains up to octamer: dipole moment μ (D), stabilization energy ΔE (kcal/mol), and bond lengths (Å).

N	O...O	C=O	C-C	C=C	C-O	O-H	ΔE_n	ΔE_n,cp	ΔE_n,cp+zpve	μ_n	μ
1	-	1.195	1.469	1.330	1.338	0.943				5.62	5.62
2	2.812	1.201	1.461	1.335	1.328	0.948	-9.90	-9.32	-8.02	7.60	13.22
3	2.775	1.204	1.456	1.338	1.323	0.951	-11.86	-11.19	-9.89	8.72	21.94
4	2.754	1.205	1.453	1.339	1.320	0.952	-12.51	-11.81	-10.51	8.86	30.80
5	2.741	1.207	1.451	1.341	1.318	0.954	-12.80	-12.09	-10.79	9.00	39.80
6	2.734	1.208	1.450	1.341	1.316	0.954	-12.94	-12.24	-10.94	9.03	48.83
7	2.727	1.208	1.449	1.342	1.315	0.955	-13.04	-12.37	-11.07	9.09	57.92
8	2.722	1.209	1.448	1.343	1.314	0.956	-13.09	-12.42	-11.12	9.11	67.03
∞	2.694	1.209	1.447	1.343	1.314	0.956		-13.11	-11.81		
F	dimer						monomer				
0.000	2.811	1.195	1.469	1.330	1.338		0.00			5.62	
0.005	2.731	1.201	1.463	1.335	1.329		-7.52			6.58	
0.010	2.640	1.206	1.455	1.341	1.321		-16.26			7.58	
0.015	2.539	1.213	1.447	1.348	1.311		-26.26			8.64	
0.020	2.449	1.221	1.438	1.357	1.302		-37.61			9.77	
0.025		1.230	1.429	1.368	1.292		-50.40			10.97	
0.030		1.241	1.419	1.381	1.282		-64.73			12.27	
0.035		1.253	1.408	1.396	1.272		-80.71			13.64	
0.040		1.267	1.398	1.414	1.262		-98.44			15.09	
0.045		1.283	1.389	1.433	1.253		-117.99			16.60	
0.050		1.300	1.381	1.455	1.245		-139.43			18.13	

We can intrpret this difference as being due to the increased covalent character of H-bonding in 1,3-propanedione than in urea. H-bonds in the former are symmetric in the sense that concerted hydrogen transfer from the donor to the acceptor in the infinite chain results in the identical state of the system.

The dimer calculations show that an external field is necessary to bring the H-bond length to that of the infinite chain is 0.008 au. At the strength of the filed of 0.018 au the hydrogen is transferred from the donor to the acceptor molecule. Increase in the field strength over 0.019 a.u. breaks the H-bond and pulls the ionic pair apart (Figure 5.6). Similar results on external electric field initiating proton transfer,[4] and other chemical reactions[5] were reported previously. The trend toward equilization of the bond lengths in an external field also reported for H-bonded complexes,[6] as well as

for conjugated molecules.[7]
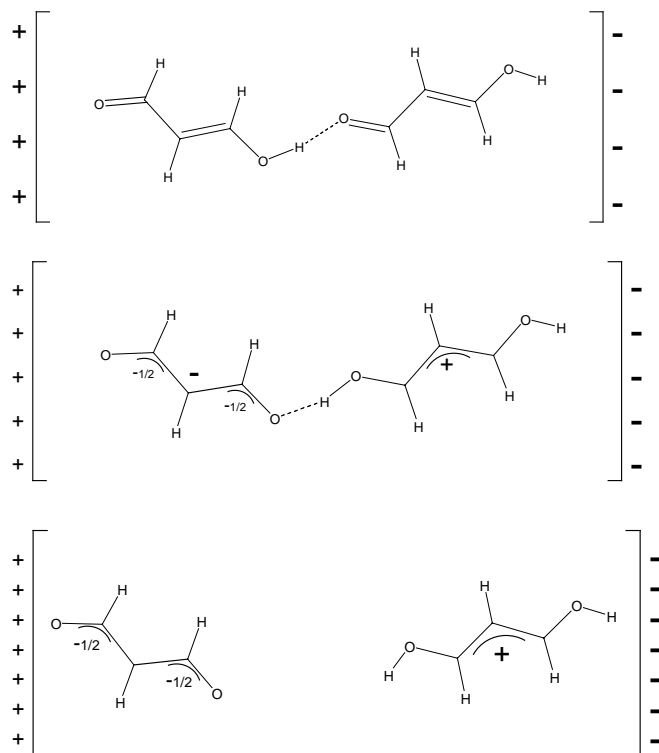
Figure 5.6. The dimer of 1,3-propanedione in an electric field of 0.018 a.u. (top), 0.019 a.u. (middle), and 0.020 a.u. (bottom)

5.8 Conclusions

The observed differences in the hydrogen-bonding patterns within the crystal structures of the urea (which forms chains) and the thiourea (which forms ribbons) is primarily due to the relative quantitative strengths of the H-bonds in the relevant dimers. For both urea and thiourea, the ribbon dimer (which contains two H-bonds with each O or S acting as an acceptor) is more stable than the chain dimer (where one O or S is the acceptor for both H-bonds). The comparable interactions are weaker in the thiourea than in urea. Furthermore, the relative strength of the ribbon vs. the chain

is greater in the thiourea. The cooperative interactions for the urea and thiourea chains are similar. The cooperative interactions for both ribbons are negligible. The result is that, as the chains grow, the cooperative interaction of the urea chain (but not the thiourea chain) becomes sufficient to overcome the disparity between the H-bonding energies of the chain and ribbon dimers. Whereas relative cooperative stabilization for urea is even less than for the thiourea, the chain dimer for urea is only 44% less stable than the ribbon dimer, and chain dimer for thiourea is 81% less stable than the ribbon dimer. That inequality allows urea chains to become the most stable aggregate for larger clusters.

References for Chapter 5.

[1.] Perez, J.; Dupuis, M.: <u>J. Phys. Chem.</u>, **1991**, <u>95</u>, 6526.

[2.] Belosludov, R.V.; Li, Z.Q.; Kawazoe, Y. <u>Molecular Engineering</u> **1999**, <u>8,</u> 105.

[3] Turi, L.; Dannenberg, J. J.: <u>J. Phys. Chem.</u> **1992**, <u>96</u>, 5819.

[4] Ramos, M.; Alkorta, I.; Elguero, J.; Golubev, N.S.; Denisov, G.S.; Benedict, H.; Limbach, H.H.: <u>J.Phys. Chem. A</u>, **1997,** <u>101</u>(50), 9791; Yin, J.; Green, M.E.: <u>J. Phys. Chem. A</u>, **1998,** <u>102</u>(36), 7181.

[5] Lobanov, V.V.; Bogillo, V.I.: <u>Langmuir</u>, **1996,** <u>12</u>(21), 5171.

[6] Kairys, V.; Head, J.D.: <u>J. Phys. Chem. A</u>, **1998,** <u>102</u>(8), 1365.

[7] Albert, I.D.L.; Marks, T.J.; Ratner, M.A.: <u>J. Phys. Chem.</u>, **1996,** <u>100</u>(23), 9714.

CHAPTER 6

6. CLASSICAL MODELS FOR INTERMOLECULAR INTERACTIONS

One of the important applications of MO calculations at the high level of theory is to build simpler yet accurate models for intermolecular interactions. In this chapter we will describe our efforts to construct classical models of intermolecular interactions based on *ab initio* calculations. According to the Hellman-Feynman theorem, forces on nuclei in the molecular system can be calculated classically from the charge density of the molecule. Therefore, when building a classical model one has to make sure that (a) wavefunction complies with the Hellman-Feynman theorem, and (b) electron density is reproduced by classical charge distribution to a good approximation. Classical charge distribution schemes in the form of different partial atomic charge separation methods are considered in the first Section. We found that the *ab initio* values on interaction energy in the urea chain dimer are best reproduced by Mulliken charges. These values are used in Section 6.2 to describe polarization effects in larger chain clusters. The modification of the wavefunction to satisfy the Hellman-Feynman theorem by optimizing centroid positions of each basis function is described in Section 6.3. The resulting charge distribution is significantly improved, so that the residual electric field on the nuclei in the optimized molecule vanishes.

Since the existing codes are not well suited to handle floating basis sets, these calculations present a computational challenge. Reducing the number of the basis functions N to the minimum ($N = N_\sigma/2 + N_\pi$, where N_σ and N_π are the number of σ- and π-electrons, respectively) greatly reduces computational costs while maintaining built-

in polarization flexibility of the basis set. This possibility is considered in Section 6.4. A semiempirical approach to optimizing parameters of this minimal floating basis set is also suggested. The ability of the wavefunctions in the form of minimal floating basis set to be exactly represented by N^2 point charges opens the possibility of building classical and combined models based on these wavefunctions.

Finally, alternatives to the electrostatic approach in description of the H-bonds are considered in Section 6.5. Linear correlations between H-bonding energy and monomer properties were found for the number of H-bonded systems. These are interpreted in Section 6.5 in terms of the donor-acceptor nature of H-bonds.

6.1 Applicability of various definitions for atomic point charges

Atomic charge is not a quantum-mechanical observable and therefore does not have a unique definition. Methods of defining atomic charge can be classified in four groups: (I) empirical fit, including electronegativity schemes; (II) population analysis; (III) fitting to electrostatic potential; (IV) systematic corrections of population atomic charges to fit experimental dipole moments.[1,2] Here we will consider only class II and III definitions.

The first and most widely used definition of atomic charge, based on the wave function, was suggested by Mulliken.[3] The arbitrary aspect of this definition (equal splitting of the overlap populations) was subject to criticism and gave rise to several improved schemes, including that of Löwdin[4] and natural population analysis (NPA) by Weinhold,[5] in which the basis set is orthogonalized and the overlap population vanishes. Another approach is to divide charge density in real, rather then in Hilbert space. Such schemes were suggested by Hiershfeld[6] (based on electron density for

spherical atoms), and Bader[7] (based on topological analysis of the total electron density). There are also charge partition schemes especially designed to reproduce intermolecular interaction energies. This group is called potential derived charges,[8] and they are optimized to give the best fit to the distribution of *ab initio* electrostatic potential around the molecule. Another approach is to calculate the partial atomic charge from *ab initio* force acting on the nucleus in the external electric field, perpendicular to the molecular plane. These charges are called force derived charges and were reported to accurately reproduce intermolecular interaction energy.[9] Unfortunately, they are difficult to define for non-planar molecules. The projection of all multipole momenta from all overlap densities on the nearest expansion point (an atom, a bond centroid, etc.) defines distributed charges (and multipoles) as suggested by Stone.[10] Finally, the gradient of molecular dipole moment with respect to the coordinates of a given atom is a definition of the charge according to Cioslovski[11] (one of the properties of this definition is that calculated IR intensities are equal to *ab initio* predicted values).

We applied the charge definitions named above to describe a chain dimer of urea. Lowdin and Stone charges were calculated using GAMESS-UK; the other charges were obtained with GAUSSIAN 94 using options of the keyword Pop (Regular for Mulliken, NPA for Weinhold, ChelpG and MK for potential-derived charges). Force derived charges were calculated from forces exerted on nuclei in a finite electric field, orthogonal to the molecular plane. The results are shown in Table 6.1. Presumably, if the charge scheme is correct, replacement of one molecule in the cluster with a set of point charges does not change polarization of the other molecules.

Examination of the differences between the charges in the dimer and in the

Table 6.1. Comparison between different atomic charge partition schemes for the chain dimer of urea, all results are at HF/D95** level, charges are in a.u., interaction energy is in kcal/mol.

	Mulliken	Lowdin	NPA	Stone	ChelpG	MK	Force-derived
			Atomic PC in the monomer				
O1	-0.50	-0.42	-0.82	-0.90	-0.78	-0.74	-0.54
C1	0.48	0.24	1.06	1.17	1.30	1.21	0.54
N1	-0.60	-0.32	-0.95	-0.57	-1.23	-1.19	-0.75
H1	0.31	0.20	0.42	0.23	0.54	0.51	0.35
H1'	0.29	0.20	0.41	0.21	0.45	0.45	0.36
			difference between charges in dimer vs. monomer				
O1	-0.018	-0.017	-0.019	-0.025	-0.039	-0.040	-0.008
C1	-0.020	-0.001	0.001	0.011	0.089	0.077	-0.026
N1	-0.012	-0.004	-0.007	-0.008	-0.089	-0.051	0.017
H1	0.038	0.007	0.024	0.038	0.081	0.054	-0.022
H1'	-0.020	-0.010	-0.013	-0.016	-0.008	-0.010	-0.012
O2	-0.029	-0.019	-0.042	-0.045	-0.134	-0.091	0.031
C2	0.025	0.017	0.019	0.010	0.145	0.103	0.012
N2	0.003	0.010	0.008	-0.000	-0.055	-0.022	0.018
H2	0.010	0.005	0.007	0.009	0.019	0.014	-0.001
H2'	0.002	0.001	0.001	0.002	0.022	0.015	-0.005
			% error of polarization by PC vs. polarization in dimer				
O1	72	292	107	37	86		
C1	34	604	110	48	47		
N1	151	-17	133	70	42		
H1	110	693	135	32	58		
H1'	68	214	109	26	180		
O2	139	111	20	462	61		
C2	71	33	1096	1262	48		
N2	121	46	-2730	-20426	29		
H2	74	52	999	-1120	64		
H2'	25	31	3912	3528	45		
mean	88	192	403	-2123	67		
			Molecular HF stabilization in the presence of PC				
$\Delta E(12)$	-8.29	-31.57	-13.12	-14.25	-13.04		-7.88
$\Delta E(21)$	-7.86	-5.55	-10.75	-8.72	-12.94		-7.15
$\Delta E(av)$	-8.07	-18.56	-11.93	-11.48	-12.99		-7.51

monomers shows a very similar picture of molecular polarization. The only exception is the decrease of the force related charge on an O2 atom accepting an H-bond. This is counterintuitive and allows us to eliminate this charge scheme. The next block reports error of the PC model in representing polarization in the dimer. Here we compare the

deformation of the charges on one monomer exerted by a PC set representing
another monomer with deformation of *ab initio* charge in the dimer. We can see that
the Stone and NPA schemes overestimate the charge deformations on the second
monomer (H-bond acceptor) by an order of magnitude. By contrast, the Löwdin
scheme overestimates the charge changes on the first monomer. The Pop=MK option
is not available in GAUSSIAN in the presence of external point charges, but seems to
give the results similar to Pop=ChelpG option in the absence of point charges.

Thus, we are left with Mulliken and with potential derived charge ChelpG.
Both pass the last test, monomer stabilization energy in the presence of point charges
representing another monomer. Both are reasonably symmetrical and close to HF
interaction energy (slightly greater, probably due to sterical repulsion in the HF
dimer). In the following Section we will use Mulliken charges.

6.2 Variation of atomic point charges upon molecular polarization simulates cooperative effects

As discussed in Chapter 2, polarizability can be introduced into the force field
by assigning an induced dipole to the molecular center or to each atom or bond. We
examined the possibility of obtaining the same result by a much simpler approach. In
this approach each atomic charge q in the molecule varies quadratically upon the
external electric field F at the position of this atom:

$$q(F) = q_0 + a^{.}F + b^{.}F^2$$

Parameters a and b are different for each of x, y, and z components of the field. The set
of parameters and the charge q_0 in the absence of the external field are individual
characteristics of atoms in molecules. We fit these parameters to HF/D95** Mulliken

charges in external dipolar field of ±0.01 au. We used quadratic rather then linear dependence to describe symmetric molecules. For example, an external field perpendicular to the planar molecule will induce the same atomic charges, as the field in the opposite direction. Therefore, the linear component of the charge dependence a is zero for this configuration, and the charge deformation is described by quadratic component b.

We applied the model of variable atomic charges to the urea chain clusters considered in Chapter 5. Intramolecular geometry was fixed to that of a monomer and H-bonding distance to that of the dimer. Since the external field experienced by the atom in a cluster is created by charges from the other monomers, it is no longer uniform. As a result, the sum of modified atomic charges deviates from zero. In the spirit of Mulliken analysis, we divided this deviation equally among all atoms so that the molecules remain neutral.

The results are shown in Table 6.2. As one can see, ΔE_n for the hexamer is increased by 40%, compared to a 15% increase for the constant charge model and a 50% increase for the HF results. The dipole moments and total stabilization energies are underestimated (up to 25% for higher clusters), as often happens when Mulliken charges are used. We can conclude that polarization as described by this model

Table 6.2. Dipole moments μ (D), and interaction energies for chain clusters of urea using HF/D95**, constant point charges (PC) and variable point charges (VPC) methods.

N	μ, HF	μ, PC	μ, VPC	ΔE_n, HF	Δ, %	ΔE_n-ΔE_{def}	Δ, %	ΔE_n,PC	Δ, %	ΔE_n,VPC	Δ, %
1	4.8	4.0	4.0								
2	10.9	7.9	9.0	-7.96	100	-8.19	100	-5.07	100	-6.84	100
3	17.5	11.9	14.0	-10.12	127	-10.67	130	-5.58	110	-8.71	127
4	24.2	15.8	19.1	-11.00	138	-11.73	143	-5.73	113	-9.22	135
5	31.1	19.8	24.2	-11.13	140	-11.96	146	-5.79	114	-9.42	138
6	38.0	23.8	29.4	-11.41	143	-12.29	150	-5.82	115	-9.51	139

accounts for a large part of the cooperative effect in H-bonding. Further improvements of the variable charges model may be necessary before it can be incorporated in the empirical force fields.

6.3 Improving calculated molecular electric properties with floating gaussian basis sets

There is a theoretical possibility of reducing intermolecular interactions to Coulomb forces in accordance with the Hellman-Feynman theorem. However, this requires high quality monomer wavefunction, properly deformed by intermolecular interactions. The medium size atom centered basis sets widely used in MO calculations produce wavefunctions that are not compliant with the Hellman-Feynman theorem. To improve the wavefunction, a larger number of basis functions with high angular momenta is necessary. The alternative is optimization of the center coordinates for all basis functions rather than keeping them fixed to nuclear positions (so-called floating gaussian basis set). It was shown that wavefunctions built with floating gaussian (FG) basis sets satisfy the Hellman-Feynman theorem.[12] For this reason the Coulomb interaction energy of charges obtained in FG basis (even within Mulliken approximations) is much close to the total HF interaction energy, as was shown by Dannenberg, Simon and Duran.[13]

Any model that reduces continuous electron density distribution to point charges, suffers a penetration problem. The interaction energy between a charged particle and a charge distribution is determined by the charge in the inner area of this distribution, as the outer area has no effect. So the interaction becomes weaker and vanishes when the particle reaches the center of the charge distribution. This effect is

neglected by the point charge model, unless explicit corrections are made (e.g., in the form of damping factors). To reduce the error, Dannenberg, Simon and Duran used point charges to represent one part of the system, and *ab initio* electron density to represent another part.

As compared to conventional double-ζ basis sets, FGs do not significantly improve the total energy. However, the bonds, angles, dipole moments and polarizabilities of small molecules (2-4 atoms) are shown to be much closer to HF limits in FG basis sets.[14]

When standard MO programs are used, the FG centroid positions are treated together with atomic coordinates and determined according to the variational principle. Unfortunately, the existing algorithms for molecular geometry optimization are not well suited for FG specifics, such as large energy change at small coordinate displacements. Optimization problems drastically increase with the size of the molecule. Despite many insistent attempts, we were not able to obtain the wavefunction for the urea ribbon dimer in floating D95** basis set. The results for the urea chain dimer are presented in Table 6.4.

In calculations of the urea chain dimer in standard D95** basis set positions for all atoms and basis functions were optimized separately (sets of 3 p-functions and 6 d-functions moved together respectively). One can see that optimization of the positions for basis functions decreases the dipole moment for monomer and dimer (bringing it closer to experimental value), as well as intermolecular interaction (by about 1 kcal/mol). To access the quality of the point-charge representation for FG basis function, we performed calculations on 3 levels: PC-PC interaction, PC-electric field created by charge density of the monomer, and PC-electric field created by the charge density of the monomer polarized in a dimer. To measure the values of the

latter, we performed the SCF procedure for the dimer, then modified the geometry

so that the second monomer was removed to infinity (actually, 900Å), and read in the

density matrix from the checkpoint file without repeating the SCF procedure

(keywords Density=Checkpoint, Guess=Only). Reading in the wavefunction instead of

the density matrix with modified geometry (keywords Guess=(Read,Only)) did not

give any meaningful results. The interaction energies in all the models are reported in

Table 6.3. Since molecules 1 and 2 in the dimer are represented differently, we report

the results in both ways, as well as the average values.

Comparing PC-PC interaction energy to the last column of Table 6.4

(dimerization energy of rigid monomers) we can conclude that conventional Mulliken

charges significantly underestimate the interaction energy, even if molecular

polarization is taken into consideration. FG-based monomer charges perform better,

but only (polarized) dimer charges give interaction energy obtained at HF level.

Surprisingly, the most accurate approximation (floating PCs for the dimer in the field

of the polarized monomer) significantly overestimates the interaction. This is probably

due to steric repulsions, which are not taken into account by the PC model. All the

other models give results reasonably consistent with *ab initio* interaction energy.

Table 6.3. Interaction energy for the chain dimer of urea calculated in Mulliken PC
model (conventional and fully floating D95** basis set parametrization).

	conventional			Floating		
	E(12)	E(21)	E(av)	E(12)	E(21)	E(av)
Monomer PC:						
PC-PC	-5.13	-5.13	-5.13	-5.42	-5.42	-5.42
PC-monomer field	-6.45	-7.63	-7.04	-7.51	-7.39	-7.45
PC-dimer field	-6.39	-8.46	-7.42	-8.34	-9.35	-8.85
dimer PC:						
PC-PC	-6.20	-6.20	-6.20	-8.34	-8.34	-8.34
PC-monomer field	-7.60	-7.82	-7.71	-9.84	-8.68	-9.26
PC-dimer field	-7.55	-8.69	-8.12	-10.93	-11.00	-10.96

The difference between 1-2 and 2-1 interactions can be considered a measure of systematic error for the model. The lowest difference (except for the PC-PC model, where it is 0 by design) is observed for our best approximation (FG-based dimer PCs in the dimer field), as well as for FG-based monomer PCs in the monomer field. This is a result of uniform representation for both parts of the dimer. The next lowest difference is observed in the conventional dimer PC in the monomer field model, and is most likely an interplay between underestimated polarizability and overestimated polarity, typical for the conventional HF method.

We can conclude that the use of Mulliken point charges obtained in the FG basis set for the dimer is advantageous compared to those of the conventional basis set. It is also worth noting, that the polarization mechanism described by the FG basis set is well suited for classical implementation. In fact describing polarizability using the charges harmonically oscillating around the centers of heavy atoms had been suggested.[15] In this model the displacement of the charge from its equilibrium position at the atomic center increases the total molecular energy but creates an atomic dipole, stabilizing the molecule in the external field. The value of the charge and the force constant describing its displacement are obtained by fitting to *ab initio* electrostatic potential distribution in the presence of electric field. Results were found encouraging, but needed adjustments in Van der Waals parameters. Also, the anisotropy of polarizability was not accounted for in this model.

In our opinion, fitting the oscillator parameters to the experimentally obtained partial atomic polarizabilities[16] would yield a more transferable model. However, using the positions and populations of FG functions directly to describe the oscillating charge would eliminate the necessity of any fitting.

6.4 Construction of minimal floating spherical gaussian basis set wavefunction, and its exact point charge model

A simplified version of the FG basis set, in which only s-functions are used (floating spherical gaussian orbitals, FSGO) and both their positions and exponent parameters are optimized, has been suggested[16] and implemented.[17] It was shown that electric properties as well as energies are drastically improved in this approach for the whole range of interatomic distances from equilibrium to the dissociation limit.[18] More accurate multiconfigurational correlation treatment is also possible. As the orbitals are explicitly localized in FSGO basis set, we should expect to enjoy all the benefits reported for use of natural localized orbitals for this purpose.[19]

Spherical functions allow for analytical description of nonbonding intermolecular interactions without resorting to empirical parameter fitting. It was shown that orbital-orbital dispersion coefficients and three- and four-body non-additive corrections to the dispersion interaction energy are easily obtainable for these FSGO wavefunction using second and higher order perturbation energy.[20] Damping functions and exchange repulsion energy formulas were obtained using the surface integral method.[21]

Since the product of two gaussian s-functions

$$\chi_i(\mathbf{r}) = (\alpha_i/\pi)^{3/2} \exp(-\alpha_i (\mathbf{r}-\mathbf{r}_i)^2); \quad \chi_j(\mathbf{r}) = (\alpha_j/\pi)^{3/2} \exp(-\alpha_j (\mathbf{r}-\mathbf{r}_j)^2)$$

is an s-function itself,

$$\chi_{ij}(\mathbf{r}) = \chi_i(\mathbf{r}) \chi_j(\mathbf{r}) = (\alpha_{ij}/\pi)^{3/2}\exp(-\alpha_{ij} (\mathbf{r}-\mathbf{r}_{ij})^2); \quad \alpha_{ij} = (\alpha_i+\alpha_j)/2; \quad \mathbf{r}_{ij} = (\alpha_i \mathbf{r}_i+\alpha_j \mathbf{r}_j)/(\alpha_i+\alpha_j).$$

The electron density of the FSGO wavefunction is a sum of N spherical gaussians, and can be exactly represented by the sum of (N^2-N) point charges.[22] To account for penetration in close proximity to the molecule, dumping factors must be used. The

FSGO model was modified to describe *p*-electrons using a tetrahedral arrangement of FSGO around the core[23] or lobe functions, i.e., pairs of s-orbitals at a fixed distance to simulate *p*-orbital.[24] The latter were found successful in reproducing geometries and energies of hydrides HX and Van der Waals dimers, including Ar...HCl.[25] The former yielded fairly small errors in bond length (within 2%) and conformational barriers (but not the total energies) for series of hydrocarbons, and allows one to establish trends in positions and exponents of FSGO, depending on local environment.[26] Simple geometric rules were found to predict the size and approximate location of the FSGO centers based on closest packing principle:[27] each orbital is assigned a radius based on its exponent factor, so that these spheres are touching each other in the molecule but do not penetrate. Once the rules for the molecules of a certain class are established, these parameters may be treated as constants to allow HF as well as post-HF calculations on large molecules and clusters.[28]

As one can see, HF/FSGO is a powerful yet computationally light *ab initio* method, capable of quantitative treatment of intermolecular interactions. The numerical optimization of exponent parameters is clearly a disadvantage, and has

Table 6.4. Comparison between chain dimer of urea optimized with at HF level with conventional and fully floating basis set: dipole moments μ (D), total energy E (a.u.), interaction energy, CP correction, CP-corrected interaction energy, and CP-corrected interaction energy less monomer relaxation (kcal/mol).

method	monomer μ	dimer μ	E	ΔE	ΔEcp	$\Delta E'cp$
HF/6-311+G(3df,2p)	4.59	10.61	-448.173633	-7.67	-7.50	-8.08
conventional HF/D95**	4.70	10.84	-448.106299	-8.78	-8.08	-8.44
floating HF/D95**	4.61	10.70	-448.121097	-8.02	-7.01	-8.16
HF/FSGO, model 1	5.59	11.65	-381.296431	-9.62	-6.66	-7.89
HF/FSGO, model 2	6.05	13.06	-393.211024	-11.81	-9.45	-10.84
HF/FSGO, model 3	2.98	6.84	-385.459652	-4.62	-2.05	
HF/FSGO, model 4	4.80	10.69	-381.776555	-8.98	-6.04	

prevented this method from being widely used.

We are mostly interested in the FSGO model as an inexpensive way to obtain a wavefunction with accurate electric properties. Hence, it would be logical to select exponent parameters of FSGO functions, which reproduce electrostatic potentials obtained at HF or correlated limits, rather than from the variational principle. This could be achieved by a semiempirical adjustment of the optimal exponent factors for small molecules or functional groups. The values obtained could be then tabulated similarly to conventional basis sets and used for complete HF/FSGO optimizations of large clusters and macromolecules. Since FSGO wavefunctions can be exactly represented by classical force fields (PC model with steric and dispersion terms), total optimization can be carried out on a fragment-by-fragment basis, allowing a high degree of parallelization. This has the advantage of a built-in mixed QM/MM technique, where *ab initio* fragments can be as small as an isolated bond or a lone pair.

As a first step toward this goal, we carried out preliminary FSGO calculation on the urea chain dimer. First, the parameters of the basis set were obtained in atomic calculations on low-spin states of C and O atoms. In these calculations one atom-centered spherical function described the core and the octahedron of six spherical functions (three lobe functions) around it described the valence shell. The distance from the lobe functions to the atomic center (separation distance) was varied to fit the quadrupole moments, while all exponents were optimized using GAMESS-US. The calculations yielded separation distances of 0.20 and 0.55Å, with exponent factors of 0.561 and 0.571 for O and C, respectively. Other atoms were nearly spherical and gave a good fit at a large interval of the parameter. For F and N we chose separation distances of 0.12 and 0.30Å, which corresponded to the optimal exponent factor of 0.56 (to keep basis set uniform). The exponent factors for the central core function

were almost independent of separation distance and were found to be 10.58, 13.45, and 18.23 for C, N, and O atoms.

In molecular and dimer calculations, core functions were placed on C, N, and O atoms, one or two lobe functions were retained on atoms O or N respectively, and single spherical functions were used to describe σ-lone pair on O atom, NH, CN, and CO bonds. The exponent values were fixed at value 0.56, obtained in atomic calculations for all valent SGOs (model 1). All geometrical parameters (atomic and electronic, except lobe separations) were optimized using GAUSSIAN 98. Unfortunately, optimization with the exact Hessian does not work for floating basis sets. That is why the options for the keyword OPT were set to Tight, Z-Matrix, NRScale, EstmFC and Iop(3/15=0) for scaled gradient optimization using small steps. The bond lengths and angles, listed on Table 6.5, were fairly close to conventional HF results. Interaction energies and dipole moments for the dimers and monomers are listed in Table 6.4. One can see that H-bond energy after CP correction closely matches high-level HF results, even though the dipoles are clearly overestimated.

BSSE in model 1 was found to be rather large (about 3 kcal/mol). In an attempt to reduce this error, we used a more realistic description of the core orbitals in the form of six contracted gaussians, taken from D95 basis set (model 2). This decreased the total energy by 12 Hartree, but CP correction decreased only by 20%. Due to high gradients, we were not able to optimize the positions of the core functions, and fixed

Table 6.5. Bond lengths and angles for urea monomer and H-bond in the chain dimer

	C=O	C-N	N-Hs	N-Ha	OCN	CNHs	CNHa	H...O
HF/6-311+G(3df,2p)	1.196	1.358	0.988	0.989	122.3	117.4	123.4	2.26
FSGO, model 1	1.292	1.396	1.001	1.001	126.8	120.4	123.2	1.98
FSGO, model 2	1.238	1.456	1.050	1.045	128.2	119.1	121.9	2.19
FSGO, model 3	1.331	1.375	1.001	1.001	126.8	120.4	123.2	2.01
FSGO, model 4	1.218	1.354	0.957	0.956	127.3	121.1	121.6	1.92

them on the nuclei. This further increased dipole moments and H-bonding interaction, and did not improve molecular geometry.

Next, the exponent factors for all SGO in the monomer were individually optimized using G98OPT utility. The resulting model (model 3) stabilizes the total energy by 2 Hartree, but strongly underestimates dipole moments (Table 6.4) and, as a result, intermolecular interaction. This supports our idea to choose exponents which well reproduce electrostatic properties, rather than minimize the total energies. To illustrate this, we fixed exponents of lobe functions at atomic values and varied exponents of in-plane lone pairs on O atoms, as they were found to have the greatest impact on the dipole moment. The dipole moment, which is reasonably close to the high-level HF calculation, was obtained with the exponent factor value of 0.60 (model 4). This significantly improved bond lengths (they are within 0.03Å of high-level HF values). Uncorrected interaction energies decreased by 0.7 kcal, and CP correction did not change.

We can conclude that the FSGO model is precise enough to describe intermolecular interactions and, upon standardization of the technique and algorithm improvements, may well compete in accuracy with conventional HF calculations. On the other hand, low computational cost and the possibility of exact classical representation of FSGO wave function argue for its use in the development of presumably more precise hybrid quantum mechanics/molecular mechanics (QM/MM) methods and "on the fly" molecular dynamics simulations.

6.5. Non-electrostatic models for intermolecular interactions

The earlier attempts to interpret mutual orientation of the molecules in crystals

and gas phase dimers were based on the classical Lewis structure (formulated by Bent[29] as the electron pair close packing principle) and were reasonably successful. Later developments went in two directions: orbital models, based on localization procedures of various flavors, and reducible down to maximum overlap considerations;[30] electrostatic approach,[31] based on general domination of the electrostatic term in the total interaction energy.[32] As follows from the Hellman-Feynman theorem, orbital and electrostatic approaches should be equivalent. In fact, a model in which the point charges are placed at the centroids of localized orbitals was suggested by Kollman[33] to predict the geometry of molecular complexes.

Choosing the "best" approach should be a matter of convenience and simplicity. One way is to choose the approach offering more predictability at lower cost, rather than the one, which is better justified theoretically. In this respect the FSGO model, localized by design, is intuitively clear, and yet can easily be quantified from both the orbital and the electrostatic viewpoints.

There are a few examples in the literature of non-electrostatic qualitative description of intermolecular interactions in the literature. One is a linear correlation between the acidity/basicity of the hydrogen bond donor and acceptor.[34] In the case of small O-containing compounds, H-bonding with water varied despite the similarity of the charge on the O atom, whereas for substituted amines the charge significantly differed, and H-bonding strength remained almost the same.[35] The authors noticed that H-bonding energy correlates more strongly with the acidity or basicity of the participating groups than with their partial charges. An opposite conclusion was made in the case of H-bonded complexes between substituted acetylides and methanol, R-$C{\equiv}C^-$...$HOCH_3$ (R=H, *tret*-Bu, Ph, *para*-PhCH$_3$), based on experiments in the gas phase.[36] These authors found the same H-bond strength (21.5 kcal/mol) for all four

complexes, despite different basicity of acetylides (in 8 kcal/mol range). Based on potential derived charges obtained at MP2/6-311++G** level, they argued that electron distribution in $C\equiv C^-$ fragment (as well as in $C\equiv C-H$ fragment[37]) is independent on the substituent.

We looked at this relationship quantitatively on the example of *para*-substituted phenylacetylenes (Table 6.6). Enthalpies of deprotonation (DPE) and H-bond formation (HBE) were calculated with AM1 Hamiltonian. We found an excellent correlation (R^2=0.997) for the enthalpy (Figure 6.1):

$$HBE = -16.27(\pm0.05) \text{ kcal/mol} + 0.0375(\pm0.0007) \text{ x DPE}$$

and less pronounced correlation (R^2=0.970) for the H-bonding distance:

$$r(H...O) = 1.865(\pm0.004) \text{ Å} + 8.9(\pm0.5) \text{ Å mol/kcal x } 10^{-4} \text{ DPE}$$

Table 6.6. AM1 results for *para*-substituted phenylacetylenes X-Ph-$C\equiv C$-H (A): enthalpy of formation ΔH_f for the monomers, their anions, and complexes with water; enthalpies of deprotonation and H-bonding (kcal/mol), bond lengths (Å), and H-boning angles (^{o}).

X=	ΔH_f(AH)	ΔH_f(A$^-$)	ΔH_f(AH...OH$_2$)	$\Delta\Delta H$(deprot)	$\Delta\Delta H$(H-bond)	C-H	H...O	CH...O
NMe$_2$	85.05	104.90	24.09	385.53	-1.72	1.065	2.2079	166.1
NH$_2$	74.50	94.04	13.51	385.22	-1.75	1.065	2.2149	168.0
H	76.49	94.34	15.36	383.53	-1.89	1.065	2.2017	166.3
OH	32.07	49.50	-29.06	383.15	-1.88	1.065	2.2047	169.6
F	31.27	45.27	-30.01	379.68	-2.04	1.065	2.2082	180.
Cl	69.43	82.68	8.12	378.93	-2.07	1.065	2.2072	180.
CN	108.19	116.23	46.67	373.72	-2.28	1.065	2.2006	180.
NO$_2$	80.35	81.24	18.53	366.57	-2.58	1.065	2.1894	180.
NH$_3^+$	231.22	173.59	167.30	308.05	-4.68	1.065	2.1407	180.
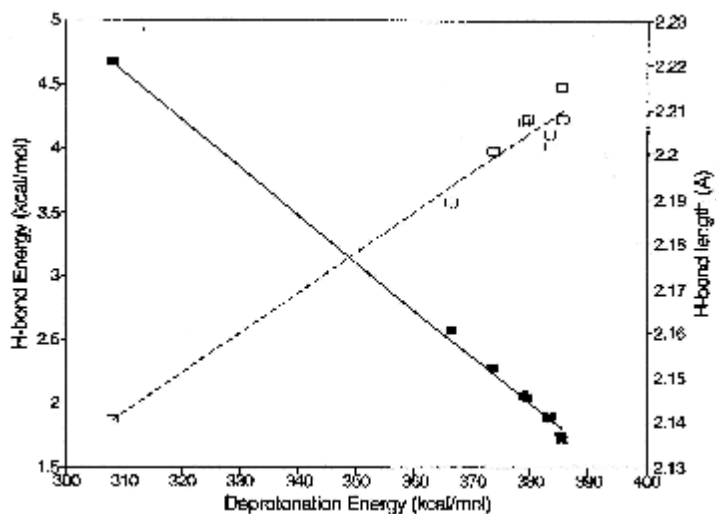
Figure 6.1. Linear correlations for complexes of substituted *para*-phenylacetylenes with water.

It is interesting to note that in the weakest complexes (X=NH$_2$, OH, H) the fragment H$_2$O...H are not planar. This feature is not easy to rationalize based on the electrostatic model. Here we suggest an explanation based on MO description of H-bond. Let us consider the interaction between electron acceptor orbital a localized on C-H fragment with electron donor orbitals n_σ, n_π, representing lone pairs of an O atom. According to second-order perturbation theory, the interaction between two orbitals is inversely proportional to the difference in their energy levels ϵ and proportional to the square of the Hamiltonian integral. Habitual replacement of the Hamiltonian with the overlap integral yields interaction energy

$$\Delta E = - k <a|n_\sigma>^2/(\epsilon(a)-\epsilon(n_\sigma)) - k <a|n_\pi>^2/(\epsilon(a)-\epsilon(n_\pi))$$

where k is proportionality constant, the first and second terms represents a-n_σ, and a-n_π interaction. Keeping the H...O distance constant, we will look at the dependence of ΔE on the angle α between the Z axis (C$_2$ axis of water molecule) and H...O direction. Assuming the lone pairs of the O atom to be sp$_z^n$ and p$_x$-AOs, we can express the angular dependence of the overlap integral as:

$<a|n_\sigma> = 1/\sqrt{(n+1)}<a|s> + \sqrt{n}/\sqrt{(n+1)}<a|p_z>=$

$\sqrt{(n+1)}<a|s>+\sqrt{n}/\sqrt{(n+1)}<a|p>cos\ \alpha$

$<a|n_\pi> = <a|p_x> = <a|p>\ sin\ \alpha$

In the case of pure s-character of the lone pair, $n=0$ and the angular dependence becomes constant. For the angular dependence of interaction energy, we now have:

$\Delta E(\alpha) = - k\ (1/(n+1)\ <a|s>^2 + n/(n+1)\ <a|p>^2cos^2\alpha +$

$\qquad 2\sqrt{n}/(n+1)\ <a|p>\ <a|s>\ cos\ \alpha)/(\epsilon(a)-\epsilon(n_\sigma)) - k\ <a|p>^2\ (1-\ cos^2\alpha)/(\epsilon(a)-\epsilon(n_\pi))$

Taking the derivative of the interaction energy with respect to $cos\ \alpha$ allows us to search for extremum:

$\delta\ \Delta E/\delta(cos\ \alpha) = - k\ (2n/(n+1)<a|p>^2cos\ \alpha + 2\sqrt{n}/(n+1)\ <a|p>\ <a|s>)/(\epsilon(a)-\epsilon(n_\sigma)) +$

$\qquad\qquad\qquad\qquad 2k\ <a|p>^2\ cos\ \alpha/(\epsilon(a)-\epsilon(n_\pi)) = 0$

which yields:

$(n/(n+1)\ <a|p>\ cos\ \alpha +\sqrt{n}/(n+1)\ <a|s>)/(\epsilon(a)-\epsilon(n_\sigma)) = <a|p>\ cos\ \alpha/(\epsilon(a)-\epsilon(n_\pi))$

or

$cos\ \alpha = \sqrt{n}/(n+1)\ <a|s>\ /\ <a|p>\ /\ (\ (\epsilon(a)-\epsilon(n_\sigma))/(\epsilon(a)-\epsilon(n_\pi))\ -\ n/(n+1)\ )$

We can substitute values obtained at HF/D95** level. The ratio of overlap integrals is $<1sH|2sO>/<1sH|2pO> = 0.08/0.15 = 0.56$ at internuclear distance of 2Å, and $0.011/0.027=0.40$ at 3Å. Lone pair energies for H_2O $\epsilon(n_\sigma)=-0.57$ au, $\epsilon(n_\pi)=-0.50$ au, and antibonding energies for HF and HCN molecules are ϵ(H-C)=0.41 and ϵ(H-F)=0.22 au. Assuming n=1, $cos\ \alpha = $ ½ 0.40/ (1.08-1/2) =0.12 for HCN, and ½ 0.56/ (1.10-1/2) = 0.34 for HF. This yields α=29° and 33° for HCN and HF respectively (compare to HF/D95** optimized values of 0° and 50°). So the angular dependence on overlap and energy is not very strong. The angle, however, strongly depends on the change in the hybridization state of the lone pair. As hybridization of σ-lone pair changes from sp^1 to sp$^{1.41}$, the angle between the C_{2v} axis of the H_2O molecule and the

direction of the O...H bond decreases from 29° to 1°. Upon a further increase in p-character smooth minimum in the angular dependence becomes a singularity extremum at 0°. The hybridization state of the lone pair can be estimated, for instance, in NBO analysis. We found it to be 1.05 for weak H-bonded complexes and free water molecules and 0.88 for the complex with HF. This brings the optimal angle values to 27° and 37°, accordingly. The hybridization state is, of course, model-dependent, but the trends should be similar regardless of the model used.

Another correlation for H-bond energy was found in a recent HF/6-31+G** study of XCHO...HF and XCN...HF complexes.[38] A common linear relationship was found between H-bonding energy and electrostatic potential at the position of H-acceptor atom O or N in the isolated molecule (rather than in the region of the H-bond). In the same study, no satisfactory correlation was found between H-bonding energy and Mulliken or potential derived charges on an O atom.

Electrostatic potentials on nuclei are not often considered. Among the few examples of their use, we could name the analysis of intramolecular interactions[39] and as a basis to derive a set of atomic charges.[40] The experimental information about electrostatic potential on the nuclei in principle can be extracted from X-Ray photoelectron spectroscopy.[41] Additional information on electric field gradient on the nuclei is available using microwave spectra,[42] NMR relaxation data,[43] and nuclear quadrupole resonance.[44] Effects of H-bonding on quadrupole tensor were studied recently on the examples of urea and HCN.[45]

We compared potential-HBE correlation with DPE-HBE correlation on the example of X-C≡C-H...N≡C-Y complexes (Figure 6.2). Mulliken charge and potential on atoms forming H-bonds, enthalpy of deprotonation, and H-bonding were again calculated at AM1 level (Table 6.7). All geometric parameters were optimized for
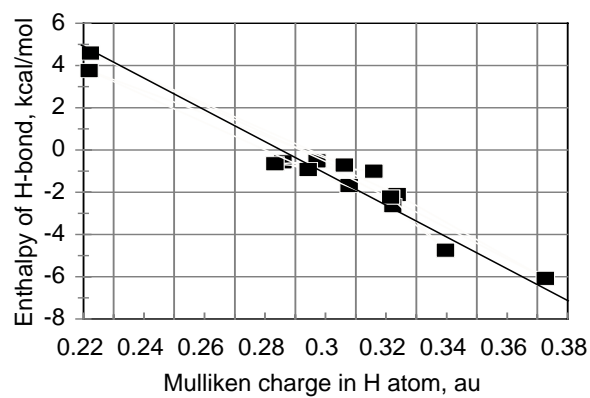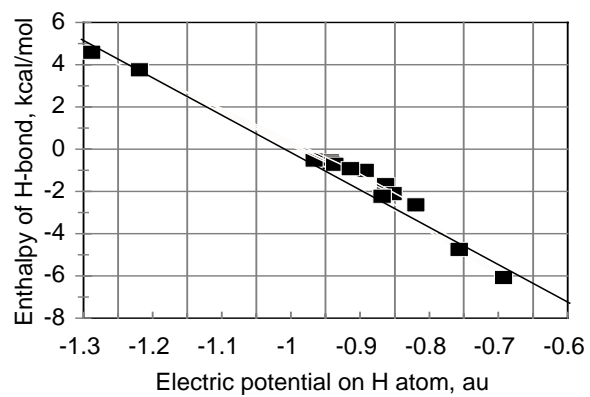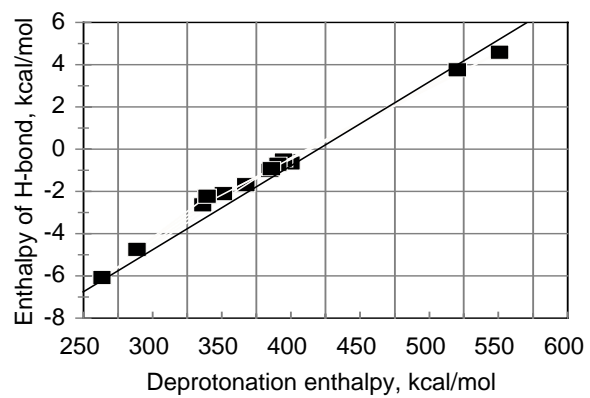
Figure 6.2. Linear correlations for complexes of substituted acetylenes with HCN.

Table 6.7. Complexes of substituted acetylene with substituted cyanide (AM1 results): H-bonding enthalpy HBE, protonation and deprotonation enthalpies PE, DPE, kcal/mol, electrostatic potential at the nucleus position in the monomer, and Mulliken charge on H-bonding atoms in the monomer.

	R-C≡N...H-C≡C-NO2				H-C≡N...H-C≡C-R			
R =	HBE	PE	φ(N)	q(N)	HBE	DPE	φ(H)	q(H)
O⁻	-16.50	-336.51	-5.361	-0.534	4.59	551.04	-1.288	0.222
S⁻	-12.86	-332.11	-5.233	-0.390	3.75	520.39	-1.219	0.222
NH$_2$	-2.39	-189.80	-4.882	-0.100	-0.52	394.80	-0.966	0.297
CH$_3$	-2.36	-189.07	-4.841	-0.095	-0.57	397.40	-0.943	0.286
H	-2.12	-182.08	-4.832	-0.105	-0.66	400.20	-0.942	0.283
OH	-1.97	-177.04	-4.837	-0.079	-0.72	390.93	-0.936	0.306
SH	-1.86	-182.90	-4.798	-0.037	-0.92	386.05	-0.914	0.294
F	-1.51	-165.78	-4.764	-0.047	-1.00	384.96	-0.892	0.316
CF$_3$	-0.90	-165.17	-4.713	0.036	-1.68	367.54	-0.863	0.308
NO$_2$	-0.44	-160.28	-4.705	0.068	-2.12	351.41	-0.852	0.324
C(NO$_2$)$_3$	-0.35	-159.26	-4.708	0.098	-2.24	339.60	-0.868	0.322
SO$_2$F	-0.04	-158.77	-4.660	0.137	-2.65	336.48	-0.819	0.322
CH$_2$NH$_3^+$	2.97	-88.51	-4.594	0.111	-4.75	289.01	-0.756	0.340
NH$_3^+$	4.22	-54.47	-4.490	0.228	-6.09	263.62	-0.692	0.373

most dimers. However, anionic acetylenes (X=O⁻, S⁻) and cationic cyanides (Y=NH$_3^+$, CH$_2$NH$_3^+$) were found unbound, and the N...H distance in these cases was fixed at 2.8 Å, a value obtained for the weakest H-bonds.

For Y=H and different substituents X in the donor molecule (Figure 6.3), the best correlation (R^2=0.991) was again with the basicity:

$$HBE = -15.0(\pm 0.3) \text{ kcal/mol} + 0.036(\pm 0.001) \text{ x DPE}$$

Electric potential (ESP$_H$) on an H atom is also correlated (R^2=0.970) with H-bonding enthalpy:

$$HBE = 17.0(\pm 0.5) \text{ kcal/mol} - 17.2(\pm 0.9) \text{ kcal/mol/au x ESP}_H$$

and Mulliken charge (Q$_H$) on H atom is correlated poorly (R^2=0.954):

$$HBE = 9.0(\pm 0.6) \text{ kcal/mol} - 67.(\pm 4.) \text{ kcal/mol/au x Q}_H$$

For X=NO$_2$ and different substituents at H-bond acceptor we found rather poor correlation (R^2=0.953) with protonation energy PE of the cyanide:
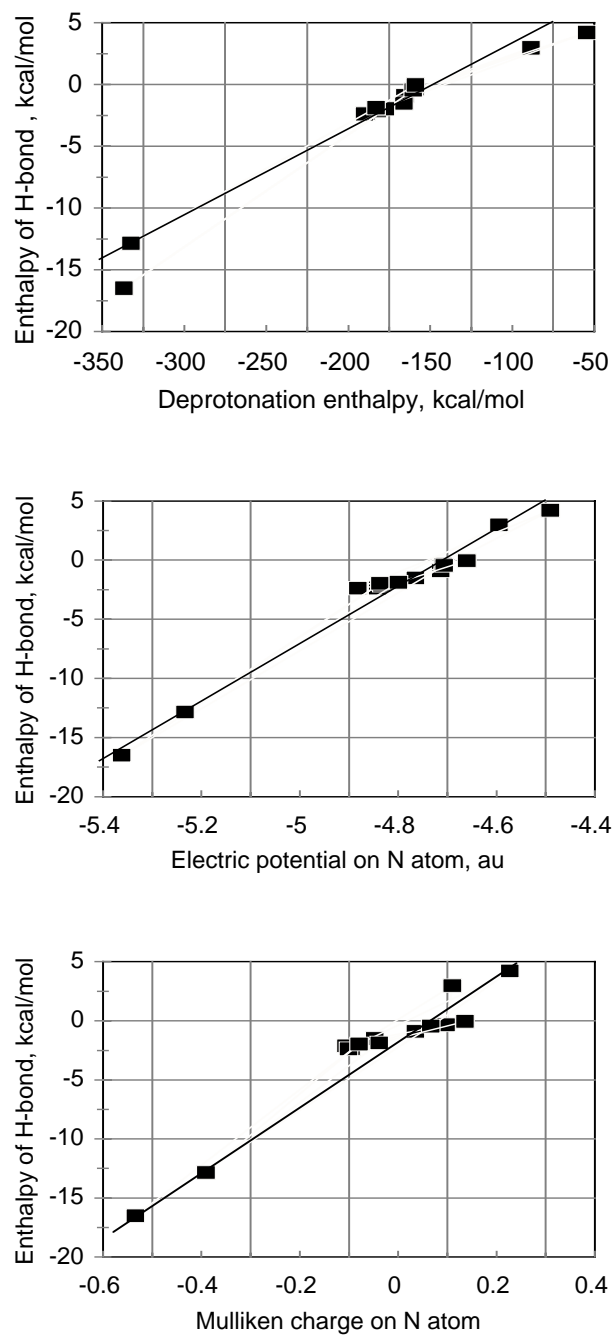
Figure 6.3. Linear correlations for complexes of substituted cyanides with nitroacetylene.

$$\text{HBE} = 10.(\pm1.) \text{ kcal/mol} + 0.07(\pm0.005) \times \text{PE},$$

whereas the correlation with electric potential on N atom was the best ($R^2=0.974$):

$$\text{HBE} = 111.(\pm1.) \text{ kcal/mol} + 23.(\pm1.) \text{ Kcal/mol/au} \times \text{ESP}_N$$

and the Mulliken charge on the N atom was poorly correlated again ($R^2=0.953$):

$$\text{HBE} = -1.(\pm1.) \text{ kcal/mol} + 26.(\pm2.) \text{ kcal/mol/au} \times Q_N$$

As ESP was the only quality to correlate with H-bonding strength for both donor and acceptor atoms, we can combine this property of donor and acceptor in a double correlation:

$$\text{HBE} = 94.5 \text{ kcal/mol} + 23. \text{ kcal/mol/au} \times \text{ESP}_N - 17. \text{ kcal/mol/au} \times \text{ESP}_H$$

The relationship can be used to predict H-bonding enthalpies for the complexes not included in the training set. For example, H-bond in H-C≡C-H...N≡C-H complex is predicted to be -0.62 kcal/mol, while AM1 calculation gives -0.66 kcal/mol.

A possible explanation for the linear dependence between H-bonding energy and electric potential on the nucleus could be found in a localized orbital picture of H-bonding. The energy of the lone pair on the H-acceptor atom, as well as the energy of the C-H antibonding orbital (which is mostly 1s orbital on H atom) are directly proportional to the electric potential on these atomic centers. In second order perturbation treatment the interaction energy between two orbitals is inversely proportional to the difference in their energy (assuming orbital overlap does not change). Fourier series expansion of the inverse proportionality gives the linear dependence in the second term. It would be interesting to build a potential function of the H-bond based on this relationship.

We can conclude that, at least for the complexes considered, electrostatic potential on atomic position in an isolated molecule can be used to evaluate its ability to serve as an H-bonding donor or acceptor.

References of Chapter 6

[1] Storer, J.W.; Geiesen, D.J.; Cramer, C.J.; Truhlar, D.J.: J. Comput.-Aided Mol. Design, **1995**, 9, 85.

[2] Li, J.; Zhu, T.; Cramer, C.J.; Truhlar, D.G.: J. Phys. Chem.A., **1998**, 102(10), 1820.

[3] Mulliken, R. S.: J. Chem. Phys. **1955**, 23, 1833.

[4] Lowdin, P.-O.: Phys. Rev. **1954**, 97(6), 1474.

[5] Reed, A.E.; Weinstock, R.B.; Weinhold, F.: J. Chem. Phys. **1985**, 83(2), 735.

[6] Hirshfeld F.L.: Theor. Chim. Acta, **1977**, 44, 129.

[7] Bader, R.F.W. Atoms in Molecules: A Quantum Theory, **1990,** Oxford Univ. Press: Oxford.

[8] Besler, B.H.; Merz, K.M.Jr.; Kollman, P.A.: J. Comp. Chem. **1990,** 11, 431.

[9] Dinur, U.: J. Comp. Chem. **1991**, 12, 469.

[10] Stone, A.J.; Chem. Phys. Lett., **1981**, 83, 233.

[11] Cioslovski, J.: J. Am. Chem. Soc., **1989**, 111, 8333.

[12] Hurley, A.C., Proc. R. Soc. London, Ser. A, **1954,** 226, 170, 179, 193.

[13] Dannenberg, J. J., Simon, S., Duran, M., J. Phys. Chem A; **1997**; 101(8); 1549.

[14] Helgaker, T., Almlöf, J., J. Chem. Phys.**, 1988,** 89, 4889.

[15] Lamoureux, G.; Allouche, D.; Souaille, M.; Roux B.: Biophisical Journal, **2000**, 78 (1, part 2), 330A.

[16] Boys, S.F.; Proc. Roy. Soc., **1950**, A200, 542.

[17] (a) Frost, A.A. J. Chem. Phys., **1967**, 47, 3707; (b) Frost, A.A.; Rouse, R.A. J. Am. Chem. Soc., **1968**, 90, 1968.

[18] Tachikawa, M.; Taneda, K.; Mori, K.: Int. J. Quant. Chem. **1999**, 75, 497.

[19] Nemukhin, A. V.; Weinhold, F.: J. Chem. Phys. **1992**, 97(2), 1095.

[20] (a) Amos, A.T.; Yoffe, J.A. Theoret. Chim. Acta, **1976**, 42, 247; (b) Amos, A.T.;

Yoffe, J.A. Chem. Phys. Lett., **1976**, 39, 53.

[21] Kleinekathofer, U.; Tang, K.T.; Toennies, J.P.; Yiu, C.L.: J. Chem. Phys., **1997**, 107(22), 9502.

[22] Hall, G.G. Chem. Phys. Lett., **1973**, 20, 501.

[23] Chu, S.Y.; Frost, A.A. J. Chem. Phys., **1971**, 54, 760.

[24] Shih, S.; Buenker, R.O.; Peyerimhoff, S.D.; Wirsam, B.: Theoret. Chim. Acta, **1970**, 18, 277.

[25] Blustin, P.H.: Theoret. Chim. Acta, **1978**, 47, 249.

[26] Blustin, P.H.; Linnett, J.W.: J. Chem. Soc. Faraday II, **1974**, 70, 247.

[27] Blustin, P.H.: Chem. Phys. Let., **1975**, 35(1), 1.

[28] Maggiora, G.M; Petke, J.D.; Christoffersen, R.E.: Theor. Models Chem. Bonding, **1991,** 4, 65.

[29] Bent, H.A,: J. Chem. Educ., **1963**, 40, 446.

[30] Weinhold, F.: J. Chem. Educ., **1999**, 76(8), 1141.

[31] Buckingham, A. D.; Fowler, P. W. J. Chem. Phys. **1983**, 79, 6426.

[32] Umeyama, H.; Morokuma, K.: J.Am.Chem.Soc., **1977**, 99, 1361.

[33] Kollman, P.: J. Am. Chem. Soc., **1977**, 99(15), 4875.

[34] Hibbert, F.; Emsley, J.: In Advances in Physical Organic Chemistry; Bethell, D., Ed.; Academic Press: London, **1990**; Vol. 26.

[35] Marten, B.; Kim,K.; Cortis, C.; Friesner, R.A.; Murphy, R.B; Ringnalda, M.N.; Doree Sitkoff, D.; Honig, B.**:** J. Phys. Chem., 100 (28), 11775.

[36] Chabinyc, M.L.; Brauman J.I.: J. Phys. Chem. A; **1999**; 103(46); 9163.

[37] Wiberg, K.B.; Rablen, P.R.: J. Am. Chem. Soc., **1993**, 115, 9234.

[38] Galabov, B.; Bobadova-Parvanova, P.: J. Chem. Phys., **1999**, 103(34), 6793.

[39] Fliszar, S.; Vauthier, E.C.; Barone, V.: Adv. Quantum Chem. (**1999**), 36, 27.

[40] Su, Z.: J. Comput. Chem. (**1993**), 14(9), 1036.

[41] Chong, D.P.; Hu, C.-H.; Duffy, P.: Chem. Phys. Lett., **1996**, 249(5,6), 491; De Brito, A.N.; Correia, N.; Svensson, S.; Ågren, H.: J. Chem. Phys., **1991**, 95(4), 2965.

[42] Aldrich, P.D.; Kukolich, S.G.; Campbell, E.J.: J. Chem. Phys., **1983**, 78(6), 3521; Leung, H.O.: J. Chem. Phys., **1997**, 107(7), 2232; Howard, N.W.; Legon, A.C.; J. Chem. Phys., **1988**, 88(8), 4694.

[43] Cummins, P.L.; Bacskay, G.B.; Hush, N.S.; Halle, B.; Engström, S.: J. Chem. Phys., **1985**, 82(4), 2002.

[44] Ivanov, A.I.; Rebane, T. K.: Opt. Spectr., **1991**, 71(2), 146; Sham, T. K.: J. Chem. Phys., **1979**, 71(9), 3744.

[45] Aray, Y.; Gatti, C.; Murgich, J.: J. Chem. Phys., **1994**, 101(11), 9800; King, B.F.; Farrar, T.C.; Weinhold, F.: J. Chem. Phys., **1995**, 103(1), 348.

CHAPTER 7

7. TWO- AND THREE-DIMENSIONAL CLUSTERS OF UREA AND THIOUREA

In this chapter we will consider two and three-dimensional hydrogen-bonding clusters of urea and thiourea. To analyze the trends, individual H-bonding components of the total stabilization energy are separated. The enthalpy of sublimation is estimated as the sum of these energies at the infinite size limit. The obtained value is in accord with the experimental data, as opposed to the value obtained in Chapter 4 from the dimeric interactions. We will conclude that the cooperative effects of H-bonding interactions dictate the crystal structures of urea and thiourea.

7.1 Geometry of the clusters and H-bond partition energy

We have considered partially optimized (under the constraints described above) herringbone arrangements for primary agglomerates (one-dimensional clusters) of two types: chains and ribbons (Figure 7.1). We will use the notations **C** for chain and **R** for ribbons followed by the number of monomers in this linear agglomerate. The number of the agglomerates in the cluster is specified after in the second digit. For example, a cluster of 3 ribbons, each built of 2 molecules will be denoted as **R2x3**. Stabilization energies $E_{n,m}$ as calculated for the urea and thiourea clusters at the AM1, HF/D95**, and B3PW91/D95** levels are presented in Table 7.1. In the case of ribbons the repeating unit has two molecules. Consequently, clusters consisting of ribbons one monomer long present a special case. Molecules in these clusters form
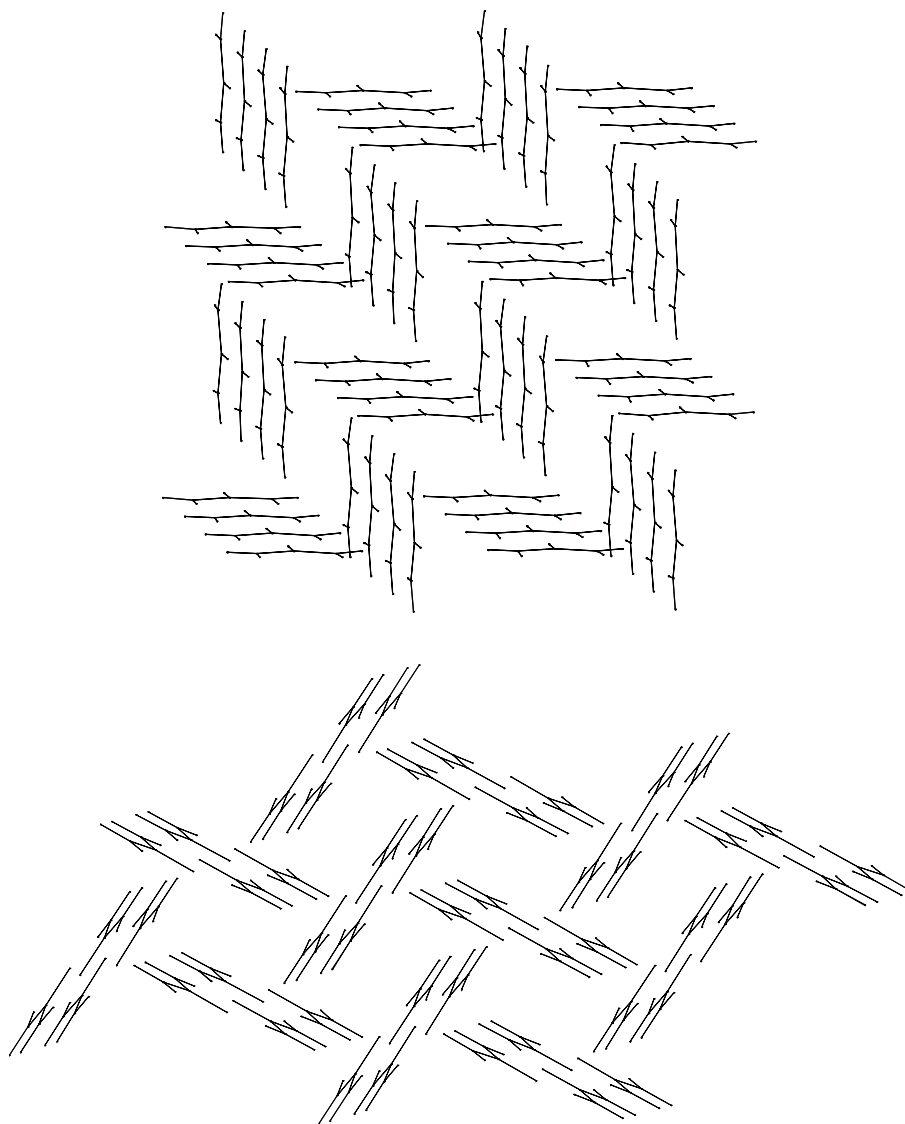
Figure 7.1. The cluster **C4x4x4**: chains of 4 monomers each, 4 chains in a layer, 4 layers in the structure (top), and **R4x4x3**: ribbons of 4 monomers each, 4 ribbons in a layer, 3 layers in the cluster (bottom).

H-bonds with only one of the two neighbors. Optimization of such a structure would

lead to a collapse. Therefore, we performed a single-point calculation using the

geometry optimized for clusters with two molecules in each ribbon. Moreover, for

clusters with an even number of ribbons there are two isomers possible, each with a

Table 7.1. HF/D95**, DFT/D95**, and AM1 results on urea and thiourea clusters: enthalpy of interaction, kcal/mol

	CNx1	CNx2	CNx3	CNx4	CNx5	CNx6	CNx7	CNx8	RNx1	RNx2	RNx3	RNx4	RNx5	RNx6	RNx7	RNx8
									HF/D95**, urea							
									0.00	1.93	-2.38	-0.40	-5.01			
1	0.00	-4.19	-7.35	-11.10	-14.41	-18.14	-21.47	-25.19	0.00	-4.91	-2.38	-6.56	-5.01			
2	-6.90	-21.66	-34.08	-47.54	-60.50	-73.76			-9.51	-21.62	-33.86	-45.65	-57.98			
3	-16.00	-42.60	-65.55						-17.96	-43.27	-62.15					
4	-25.62	-63.75							-26.79	-59.30	-90.48					
5	-35.41	-84.80							-35.55	-80.39						
									B3PW91/D95**, urea							
1									0.00	2.65	-0.98	1.36				
1	0.00	-3.92	-6.33	-10.16	-13.20				0.00	-3.03	-0.98	-4.59				
2	-6.17	-19.97	-31.00	-43.37	-55.21				-10.91	-23.58	-36.42	-48.69				
3	-14.89	-40.18	-61.11						-20.85	-47.31	-68.01					
4	-24.32	-60.88							-31.14	-65.20						
5	-34.03	0.00							-41.43							
									AM1, urea							
1									0.0	1.3	-4.1	-2.5	-8.2	-6.5	-12.2	-10.5
1	0.0	-4.2	-7.7	-11.6	-15.2	-19.1	-22.8	-26.7	0.0	-4.6	-4.1	-8.6	-8.2	-12.6	-12.2	-16.7
2	-6.1	-21.2	-34.3	-48.5	-62.0	-76.1	-89.6	-103.7	-8.8	-21.2	-33.6	-45.6	-58.3	-70.3	-83.0	-94.9
3	-13.5	-39.9	-63.2	-88.2	-112.1	-136.9	-160.9	-185.7	-17.0	-41.9	-61.4	-85.9	-105.5	-130.0	-149.6	-174.1
4	-21.4	-58.9	-92.5	-128.4	-162.7	-198.3	-232.8	-268.4	-25.4	-57.9	-89.7	-121.3	-153.8	-185.3	-217.8	-249.3
5	-29.4	-77.9	-121.9	-168.7	-213.4	-259.9	-304.9	-351.2	-33.8	-78.6	-117.9	-162.2	-201.7	-246.0	-285.5	-329.8
6	-37.5	-97.0	-151.4	-209.0	-264.2	-321.5	-377.0	-434.2	-42.1	-94.2	-146.3	-197.6	-250.0	-301.3	-353.8	-405.0
7	-45.7	-116.1	-180.9	-249.4	-315.1	-383.2	-449.2	-517.2	-50.5	-115.3	-174.6	-238.6	-298.2	-362.2	-421.8	-485.8
8	-53.9	-135.2	-210.5	-289.7	-366.0	-444.9	-521.5	-600.2	-58.9	-130.9	-202.9	-274.0	-346.4	-417.5	-490.0	-561.0
									HF/D95**, thiourea							
1									0.00	1.68	-4.92	-2.97	-10.04			
1	0.00	-4.15	-7.53	-11.31	-14.82	-18.58	-22.30	-25.87	0.00	-5.18	-4.92	-10.17	-10.04			
2	-4.04	-17.13	-27.26	-37.93	-47.85				-7.32	-20.07	-33.38	-45.65	-59.13			
3	-9.68	-31.77	-49.67						-13.92	-39.48	-57.71					
4	-15.89	-47.17							-20.76	-51.56						
5	-22.34	-62.50							-27.53	-71.29						
									AM1, thiourea							
1									0.0	1.5	-2.6	-1.0	-5.5	-3.9	-8.4	-6.8
1	0.0	-4.2	-8.3	-11.8	-16.0	-19.5	-23.7	-27.3	0.0	-2.8	-2.6	-5.6	-5.5	-8.5	-8.4	-11.4
2	-4.3	-17.5	-29.2	-40.6	-52.8	-64.0	-76.3	-87.5	-9.7	-21.6	-33.9	-45.5	-57.9	-69.4	-81.8	-93.4
3	-10.3	-33.0	-52.8	-72.9	-93.6	-113.3	-134.3	-153.9	-19.1	-43.2	-63.4	-87.0	-107.3	-131.0	-151.3	-174.9
4	-17.0	-48.9	-77.1	-106.0	-135.3	-163.6	-193.2	-221.4	-28.8	-61.1	-93.8	-125.5	-158.4	-190.1	-223.0	-254.7
5	-23.9	-65.1	-101.6	-139.3	-177.2	-214.1	-252.5	-289.2	-38.4	-83.2	-124.0	-168.2	-209.1	-253.3	-294.2	-338.3
6	-31.1	-81.3	-126.2	-172.7	-219.2	-264.8	-311.9	-357.2	-48.2	-101.3	-154.6	-206.9	-260.4	-312.6	-366.2	-418.4
7	-38.3	-97.5	-151.0	-206.2	-261.3	-315.6	-371.3	-425.3	-57.9	-123.5	-185.0	-249.8	-311.5	-376.2	-437.9	-502.6
8	-45.6	-113.8	-175.8	-239.7	-303.5	-366.5	-430.8	-493.4	-67.6	-141.6	-215.6	-288.5	-362.8	-435.6	-510.0	-582.8

different number of H-bonds. For example, four ribbons of one monomer each could form two H-bonds (1-2 and 3-4) or one H-bond (2-3). That is why we report two sets of results for each **R1xN** cluster in Table 7.1.

In order for semi-empirical and *ab-initio* results to be comparable, we had to correct HF and DFT values for counterpoise (CP) and zero-point vibration energy (ZPVE). Unfortunately, full optimization, necessary to obtain ZPVE, significantly distorts most of the clusters considered here. Only single chains, ribbons, and chain trimers have the symmetry elements which guarantee the existence of a stationary point with planar molecules, similar to the clusters optimized under constraints. We performed HF/D95** frequency calculations for these clusters and estimated ZPVE for the other clusters based on the assumption of additivity.

The stabilization energies are interpreted in Table 7.2-7.3 in two ways. First, the energies of the last H-bond as chains (ribbons) grow, were obtained using the formula:

$$\Delta E_m = (E_{n,m} - E_{n,m-1} - E_{n,1})/n$$

where m represents the number of monomers in single chain (ribbon), and n the number of chains (ribbons) in the cluster. Second, the interaction energies between the cluster and the last chain (ribbon) added to it were obtained using the formula:

$$\Delta E_n = (E_{n,m} - E_{n-1,m} - E_{1,m})/h$$

where h is the number of H-bonds between the last chain (ribbon) and the rest of the cluster. In the case of chains, $h=n$; in the case of ribbons $h=[n/2]$.

7.2 The effect of cluster growth in two dimensions on enthalpy of interaction and individual H-bonds

As one can conclude from comparison of the left and right sides of Table 7.1, in the case of the thiourea the total stabilization energies of the ribbon clusters are lower than those of the chain clusters at any size. For urea, however, chain clusters

Table 7.2. HF/D95**, DFT/D95**, and AM1 results on urea clusters: enthalpy of the last H-bond within the chain (ribbon), and the last interchain (interribbon) interaction, kcal/mol

N	CNx1	CNx2	CNx3	CNx4	CNx5	CNx6	CNx7	CNx8	RNx1	RNx2	RNx3	RNx4	RNx5	RNx6	RNx7	RNx8
	HF/D95**, last H-bond in chain								HF/D95**, last H-bond in ribbon							
2	-6.90	-6.64	-6.46	-6.34	-6.34	-6.25			-9.51	-9.32	-9.70	-9.67	-9.59			
3	-9.11	-8.37	-8.04						-8.45	-8.37	-8.63					
4	-9.61	-8.48							-8.83	-8.98	-8.65					
5	-9.79	-8.43							-8.75	-8.09						
	B3PW91/D95**, last H-bond in chain								B3PW91/D95**, last H-bond in ribbon							
2	-6.17	-6.07	-6.11	-5.76	-5.76				-10.91	-11.60	-11.49	-11.37				
3	-8.72	-8.15	-7.93						-9.93	-10.35	-10.20					
4	-9.43	-8.39							-10.29	-10.27						
5	-9.72								-10.28							
	AM1, last H-bond in chain								AM1, last H-bond in ribbon							
2	-6.13	-6.45	-6.33	-6.33	-6.31	-6.30	-6.29	-6.29	-8.80	-8.97	-8.48	-8.63	-8.40	-8.52	-8.36	-8.47
3	-7.40	-7.27	-7.07	-7.02	-6.98	-6.95	-6.94	-6.92	-8.22	-8.03	-7.88	-7.93	-7.81	-7.85	-7.77	-7.81
4	-7.84	-7.41	-7.20	-7.13	-7.08	-7.04	-7.02	-7.00	-8.39	-8.62	-8.09	-8.21	-8.03	-8.13	-8.00	-8.08
5	-8.03	-7.45	-7.25	-7.17	-7.11	-7.07	-7.05	-7.02	-8.34	-8.04	-8.03	-8.08	-7.96	-8.01	-7.93	-7.98
6	-8.12	-7.46	-7.28	-7.18	-7.12	-7.08	-7.06	-7.03	-8.38	-8.45	-8.08	-8.22	-8.03	-8.13	-8.00	-8.08
7	-8.18	-7.47	-7.29	-7.19	-7.13	-7.09	-7.07	-7.04	-8.36	-8.26	-8.06	-8.11	-8.00	-8.05	-7.97	-8.01
8	-8.21	-7.47	-7.30	-7.19	-7.14	-7.09	-7.07	-7.05	-8.38	-8.47	-8.08	-8.23	-8.02	-8.13	-8.00	-8.09
	HF/D95**, chain-chain								HF/D95**, ribbon-ribbon							
1										1.93	-4.31	1.98	-4.61			
1		-4.19	-3.16	-3.75	-3.31	-3.73	-3.33	-3.72		-4.91	2.53	-4.18	1.56			
2		-3.93	-2.76	-3.28	-3.03					-2.59	-2.74	-2.28	-2.82			
3		-3.53	-2.31							-3.67	-0.46					
4		-3.13								-2.86	-2.19					
5		-2.80								-3.10						
	B3PW91/D95**, chain-chain								B3PW91/D95**, ribbon-ribbon							
1										2.65	-3.63	2.34				
1		-3.92	-2.41	-3.83	-3.04					-3.03	2.05	-3.61				
2		-3.81	-2.43	-3.10	-2.83					-1.75	-1.93	-1.36				
3		-3.47	-2.01							-2.81	0.08					
4		-3.06								-1.46						
	AM1, chain-chain								AM1, ribbon-ribbon							
1										1.31	-5.41	1.61	-5.66	1.66	-5.71	1.67
1		-4.15	-3.52	-3.95	-3.60	-3.93	-3.61	-3.93		-4.62	0.52	-4.50	0.45	-4.49	0.44	-4.49
2		-4.47	-3.50	-4.04	-3.65	-4.00	-3.67	-3.99		-3.64	-3.58	-3.19	-3.87	-3.19	-3.88	-3.19
3		-4.27	-3.26	-3.84	-3.43	-3.78	-3.46	-3.77		-3.94	-1.22	-3.77	-1.26	-3.76	-1.27	-3.76
4		-4.03	-3.05	-3.64	-3.22	-3.58	-3.26	-3.56		-3.52	-3.24	-3.06	-3.54	-3.05	-3.56	-3.04
5		-3.82	-2.91	-3.48	-3.07	-3.42	-3.11	-3.40		-3.69	-1.87	-3.51	-1.93	-3.50	-1.93	-3.50
6		-3.66	-2.81	-3.35	-2.95	-3.29	-2.99	-3.28		-3.30	-3.33	-3.06	-3.43	-3.04	-3.45	-3.04
7		-3.53	-2.73	-3.25	-2.87	-3.20	-2.90	-3.18		-3.58	-2.20	-3.39	-2.26	-3.39	-2.27	-3.39
8		-3.42	-2.68	-3.17	-2.80	-3.12	-2.83	-3.10		-3.30	-3.28	-3.06	-3.38	-3.05	-3.40	-3.05

Table 7.3. HF/D95** and AM1 results on thiourea clusters: inctemental values for enthalpy of the last H-bond within the chain (ribbon), and the last interchain (interribbon) H-bond, kcal/mol

N	CNx1	CNx2	CNx3	CNx4	CNx5	CNx6	CNx7	CNx8	RNx1	RNx2	RNx3	RNx4	RNx5	RNx6	RNx7	RNx8
	HF/D95**, last H-bond in chain								HF/D95**, last H-bond in ribbon							
2	-4.04	-4.42	-4.06	-3.83	-3.64				-7.32	-8.28	-7.84	-8.13	-7.81			
3	-5.64	-5.24	-4.96						-6.60	-7.12	-6.47					
4	-6.21	-5.63							-6.84	-6.88						
5	-6.45	-5.59							-6.77	-7.28						
	AM1, last H-bond in chain								AM1, last H-bond in ribbon							
2	-4.32	-4.52	-4.21	-4.23	-4.16	-4.16	-4.12	-4.12	-9.72	-10.14	-9.58	-9.71	-9.38	-9.51	-9.28	-9.40
3	-5.99	-5.64	-5.13	-5.12	-4.97	-4.96	-4.89	-4.89	-9.38	-9.38	-8.96	-9.00	-8.79	-8.85	-8.72	-8.77
4	-6.66	-5.89	-5.34	-5.31	-5.13	-5.12	-5.03	-5.03	-9.69	-9.73	-9.28	-9.36	-9.12	-9.21	-9.04	-9.12
5	-6.97	-5.97	-5.42	-5.37	-5.18	-5.17	-5.07	-5.07	-9.65	-9.64	-9.22	-9.28	-9.05	-9.12	-8.97	-9.04
6	-7.14	-6.00	-5.47	-5.40	-5.20	-5.20	-5.09	-5.09	-9.72	-9.78	-9.31	-9.40	-9.15	-9.24	-9.08	-9.16
7	-7.24	-6.01	-5.49	-5.42	-5.22	-5.21	-5.10	-5.10	-9.71	-9.70	-9.29	-9.34	-9.12	-9.19	-9.04	-9.10
8	-7.30	-6.02	-5.51	-5.42	-5.23	-5.22	-5.11	-5.11	-9.74	-9.81	-9.33	-9.42	-9.16	-9.26	-9.09	-9.17
	HF/D95**, chain-chain								HF/D95**, ribbon-ribbon							
1									-5.18	0.26	-5.25	0.13				
1		-4.15	-3.39	-3.77	-3.51	-3.76	-3.71	-3.57	-5.42	-5.98	-4.95	-6.15				
2		-4.53	-3.04	-3.32	-2.94				-5.82	-4.31						
3		-4.14	-2.74						-5.02							
4		-3.85							-5.41							
	AM1, chain-chain								AM1, ribbon-ribbon							
1									1.50	-4.08	1.55	-4.46	1.62	-4.55	1.63	
1		-4.21	-4.05	-3.56	-4.19	-3.52	-4.21	-3.51	-2.82	0.23	-2.99	0.09	-2.98	0.04	-2.98	
2		-4.41	-3.69	-3.55	-3.95	-3.45	-4.00	-3.43	-2.16	-2.59	-1.84	-2.69	-1.82	-2.70	-1.82	
3		-4.12	-3.18	-3.26	-3.49	-3.12	-3.56	-3.09	-2.48	-0.55	-2.28	-0.59	-2.28	-0.60	-2.28	
4		-3.76	-2.79	-2.98	-3.10	-2.83	-3.17	-2.79	-1.78	-1.93	-1.48	-2.03	-1.45	-2.05	-1.45	
5		-3.44	-2.51	-2.75	-2.80	-2.60	-2.88	-2.55	-2.12	-0.79	-1.91	-0.83	-1.90	-0.83	-1.90	
6		-3.19	-2.31	-2.56	-2.58	-2.42	-2.66	-2.37	-1.66	-1.70	-1.38	-1.79	-1.35	-1.81	-1.35	
7		-2.99	-2.16	-2.41	-2.40	-2.28	-2.48	-2.23	-1.94	-0.91	-1.73	-0.95	-1.72	-0.96	-1.72	
8		-2.82	-2.05	-2.29	-2.27	-2.17	-2.34	-2.12	-1.60	-1.58	-1.33	-1.67	-1.31	-1.68	-1.30	

become more stable at size **3x3** at both HF and AM1 level.This result is in accord with the motif observed in crystal structure. By comparison, the linear clusters reported in Chapter 5 become more stable in chain structures starting with **C10** at HF, but not at AM1 level. To find a source for the stabilization of chain clusters we considered the energies of the different kinds of H-bonds separately. For this purpose we examined

the energy of the last H-bonds, as defined above, for clusters of different sizes. The results are reported in Tables 7.2-7.3 and in Figure 7.2.
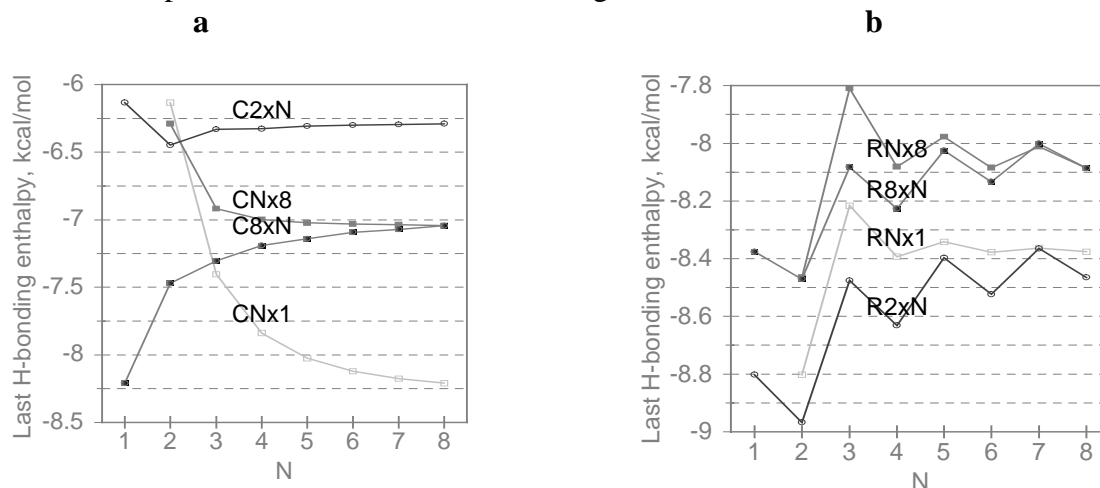
Figure 7.2. The last H-bond within the chains and ribbons for urea chain (a) and ribbon (b) clusters (AM1 results)

Examination of the Figure 7.2a shows that the last H-bond in chains becomes stronger as the chain grows (compare these values within the columns in Tables 7.2 and 7.3). However, in larger clusters this effect becomes much less pronounced (2% for **CNx8** vs. 11% for **CNx1** in the urea clusters and 4% vs. 21% respectively in the case of thiourea). From Figure 7.2b one may conclude that the last H-bond in ribbons, by contrast, becomes weaker as the ribbon grows. This effect also becomes less pronounced in larger clusters. For both chains and ribbons of the same length, the last H-bond becomes 5-10% weaker as the cluster grows in the other dimensions, increasing number of primary agglomerates in the cluster (compare the values within one row in Tables 7.2 and 7.3). As there are two molecules in the unit cell of a ribbon and two ribbons (chains) in the unit cell of a 2D cluster, this trend varies depending on whether the number of monomers in the cluster is even or odd.

The H-bonding interaction between chains of the same length (Figure 7.4)

follows trends similar to the ones observed within 1-D ribbons and transverse chains (see Section 5.6), with first H-bond being the most stable, second the least stable and converging to the intermediate limiting value. The H-bonds between the ribbons, however, seem to be converging to different values for even and odd numbers of ribbons in the cluster. The reasons for this phenomenon will be considered in the next Section. As chains and ribbons become longer, the H-bonds between them become considerably weaker, and convergence is not achieved at the size of eight monomers. To rationalize this counterintuitive trend, we will have to consider long-range electrostatic interactions.
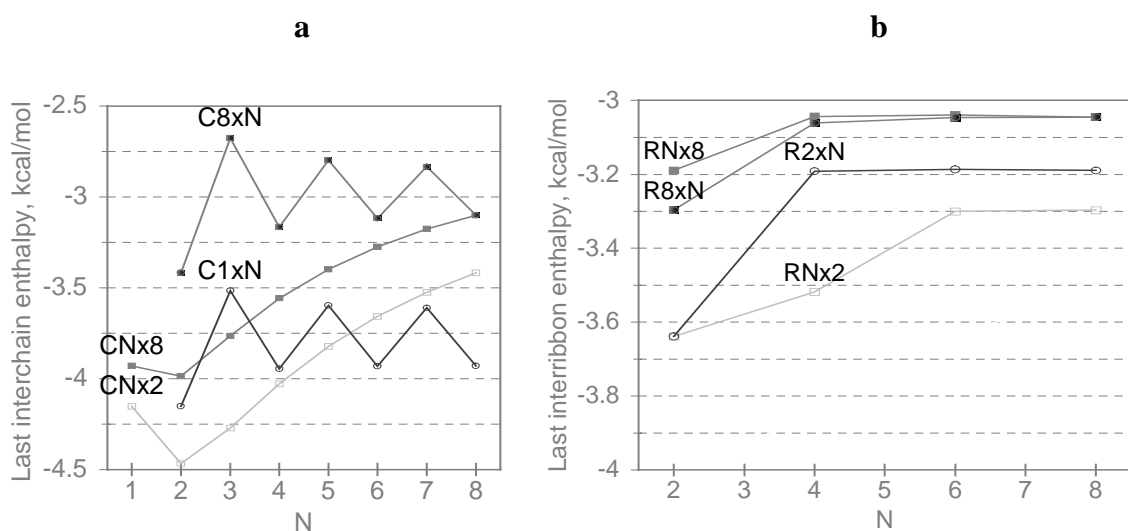
Figure 7.3. The last interchain (interribbon) interaction for urea chain (a) and ribbon (b) clusters (AM1 results).

Table 7.4. Incremental values for H-bonds in PC model (Mulliken HF/D95** point charges for monomer).

N	CNx1	CNx2	CNx3	CNx4	CNx5	CNx6	CNx7	CNx8	∞	RNx1	RNx2	RNx3	RNx4	RNx5	RNx6	RNx7	RNx8	∞
	last H-bond in chain									last H-bond in ribbon								
2	-4.85	-4.73	-4.59	-4.57	-4.53	-4.52	-4.50	-4.50	-4.41	-7.72	-7.68	-7.08	-7.25	-6.97	-7.11	-6.93	-7.04	-6.85
3	-5.61	-5.12	-4.91	-4.84	-4.78	-4.75	-4.73	-4.71	-4.62	-7.04	-6.56	-6.47	-6.43	-6.36	-6.35	-6.31	-6.31	-6.24
4	-5.84	-5.19	-4.97	-4.90	-4.83	-4.80	-4.77	-4.75	-4.64	-7.23	-7.26	-6.68	-6.83	-6.58	-6.70	-6.54	-6.64	-6.48
5	-5.95	-5.21	-5.00	-4.92	-4.85	-4.82	-4.79	-4.76	-4.65	-7.16	-6.67	-6.65	-6.58	-6.54	-6.52	-6.49	-6.48	-6.43
6	-6.00	-5.23	-5.02	-4.93	-4.86	-4.82	-4.79	-4.77	-4.66	-7.21	-7.31	-6.66	-6.85	-6.57	-6.71	-6.53	-6.65	-6.49
7	-6.02	-5.23	-5.03	-4.93	-4.90	-4.83	-4.80	-4.78	-4.67	-7.19	-6.68	-6.68	-6.61	-6.58	-6.55	-6.53	-6.52	-6.47
8	-6.06	-5.24	-5.04	-4.94	-4.92	-4.83	-4.80	-4.78	-4.68	-7.21	-7.34	-6.66	-6.86	-6.57	-6.72	-6.53	-6.65	-6.50
∞	-6.24	-5.42	-5.22	-5.12	-5.09	-4.96	-4.91	-4.88	-4.79	-7.18	-6.99	-6.65	-6.71	-6.55	-6.61	-6.51	-6.56	-6.48
	interchain H-bond									interribbon H-bond								
1										1.16	-4.98	1.37	-5.15	1.41	-5.19	1.42	-3.66	
1		-4.00	-3.55	-3.57	-3.64	-3.55	-3.53	-3.66	-3.51	-4.31	0.50	-4.23	0.45	-4.22	0.44	-4.22	-3.66	
2		-3.88	-3.28	-3.39	-3.40	-3.35	-3.31	-3.46	-3.33	-3.06	-2.64	-2.89	-2.85	-2.89	-2.88	-2.90	-2.79	
3		-3.59	-2.99	-3.14	-3.12	-3.08	-3.04	-3.18	-3.04	-3.22	-0.70	-3.18	-0.72	-3.19	-0.74	-3.18	-2.55	
4		-3.37	-2.80	-2.96	-2.92	-2.91	-2.86	-2.99	-2.85	-2.67	-2.32	-2.53	-2.48	-2.54	-2.50	-2.54	-2.45	
5		-3.20	-2.68	-2.83	-2.79	-2.78	-2.73	-2.85	-2.71	-2.89	-1.19	-2.84	-1.24	-2.85	-1.25	-2.85	-2.40	
6		-3.08	-2.59	-2.73	-2.69	-2.68	-2.63	-2.76	-2.61	-2.56	-2.24	-2.45	-2.36	-2.45	-2.38	-2.46	-2.37	
7		-2.98	-2.53	-2.65	-2.65	-2.59	-2.56	-2.69	-2.54	-2.75	-1.43	-2.69	-1.48	-2.70	-1.48	-2.70	-2.35	
8		-2.90	-2.48	-2.59	-2.62	-2.49	-2.50	-2.63	-2.48	-2.52	-2.21	-2.41	-2.32	-2.42	-2.33	-2.42	-2.34	
∞		-2.71	-2.29	-2.41	-2.43	-2.32	-2.33	-2.46	-2.31	-2.37	-2.09	-2.30	-2.16	-2.30	-2.16	-2.31	-2.26	

7.3 Point-charge model of interaction.

As discussed in Chapter 5 for ribbons, seemingly anticooperative behavior (weakening of H-bonds) could be attributed to the different number of the second neighbors (repulsive) interactions with respect to the number of the nearest neighbor (attractive) interactions. Likewise, the second neighbor interactions may be responsible for the anticooperative effects described in the previous Section. Due to the long range character of second neighbor interactions, one may expect electrostatic and polarization energy to be their major component. To examine the electrostatic component of H-bonding energy, we used a combination of atomic Mulliken point charges (PC) obtained in HF/D95** calculation of the urea monomer and the

geometry of AM1 optimized clusters. The results are presented in Table 7.4. As one can see, additive electrostatic energies follow general trends described above for the total energy of H-bonding interactions.

We used the geometry of the octamer to expand the cluster periodically in one and two dimensions and calculated the incremental value of H-bonds in the PC model. The value converged to 0.01 kcal/mol only after the molecules at 100Å from the central one were accounted for. The slow convergence of electrostatic energy is well known. These asymptotic limits for electrostatic interactions differ by about 0.2 kcal/mol from the values for the largest clusters considered here (**C8x8, R8x8**). The difference between these limits and the PC energy value a the finite size cluster can be used to correct ΔH values for all four types of H-bonds. The best estimated values for all methods are collected in Table 7.5.

Table 7.5. Best estimate for the enthalpy of H-bond formation and of sublimation. Dimeric values are shown for comparison.

	Urea			Thiourea	
	chains				
H-bond	AM1	HF/D95**	B3PW91/D95**	AM1	HF/D95**
Intrachain	-6.91	-8.75	-8.66	-5.11	-5.55
Interchain	-2.80	-3.38	-3.31	-2.12	-3.63
ΔHsub	-12.51	-15.51	-15.28	-9.35	-12.81
C2	-6.13	-6.85	-6.12	-4.32	-4.20
C1x2	-4.15	-4.46	-4.19	-4.21	-4.18
Sum of dimeric values	-10.28	-11.31	-10.31	-12.74	-12.56
Experiment	-21.	-21.	-21.		
	ribbons				
Intraribbon	-7.88	-10.23	-10.74	-9.17	-8.26
Interribbon	-2.88	-3.02	-1.62	-1.30	-5.19
ΔHsub	-10.76	-13.25	-12.36	-10.47	-13.45
C2	-8.80	-10.17	-11.57	-9.72	-7.78
C1x2	-4.62	-4.73	-2.85	-2.82	-5.15
Sum of dimeric values	-13.42	-14.90	-14.42	-12.54	-12.93
Experiment				-26.	-26.

Table 7.6. Total ΔH of interaction, and its components for urea 3D-clusters: AM1, PC and the difference (Δ).

	CNx4x4		Last H-bond within the chain				C4x4xN		Interchain H-bond		
N	AM1	PC	AM1	PC	Δ		AM1	PC	AM1	PC	Δ
1	-87.18	-84.29					-128.40	-101.73			
2	-275.90	-241.44	-6.35	-4.55	-1.79		-313.66	-256.54	-3.55	-3.32	-0.24
3	-474.05	-397.42	-6.94	-4.48	-2.46		-493.53	-407.31	-3.22	-3.07	-0.15
4	-674.59	-558.74	-7.08	-4.81	-2.27		-674.59	-558.74	-3.29	-3.11	-0.19
	RNx4x4		Last H-bond within the ribbon				R4x4xN		Interribon H-bond		
N	AM1	PC	AM1	PC	Δ		AM1	PC	AM1	PC	Δ
1	-54.46	-51.37					-121.27	-102.98			
2	-254.38	-202.53	-9.09	-6.24	-2.85		-284.61	-237.07	-2.63	-1.94	-0.69
3	-428.01	-349.73	-7.45	-5.99	-1.46		-448.91	-373.32	-2.69	-2.08	-0.61
4	-615.21	-504.93	-8.30	-6.49	-1.81		-615.21	-504.93	-2.81	-1.79	-1.02

7.4 Three-dimensional clusters

To evaluate the effect of the third dimension on H-bonding enthalpy we performed AM1 calculations for some 3D-clusters (Table 7.6). One can see that the last H-bond within both chains and ribbons displays oscillatory behavior, and for **4x4x4** clusters it is about 0.15 kcal/mol weaker than for corresponding 2D-clusters **4x4.** As in the case of 2D-clusters, the last H-bond becomes stronger for chains, and weaker for ribbons, as the chains (ribbons) grow. The interactions between primary agglomerates are also oscillatory and 0.15 weaker than in 2D-clusters. As 3D-clusters do not change the trends observed for 2D-clusters and are only available for clusters up to **4x4x4**, we will use values obtained for 2D-clusters to estimate the enthalpy of sublimation for urea and thiourea polymorphs.

7.5 Estimation of the enthalpy of crystal formation

The values collected in Table 7.5 for urea show that H-bonds within the primary agglomerates for chains are still weaker than for ribbons (in contrast to 1D-clusters). However, as the chains increase in size and in the number of H-bonds between them, they become more stable than ribbon structures. Yet H-bonds in thiourea chains are too weak for this to happen. H-bonding between primary agglomerates is stronger for ribbons of thiourea and for chains of urea. This is another factor in the distinction. The sublimation enthalpy comes to 15.5 kcal/mol. This far from the experimental value of 21 kcal/mol, but close to 3D-periodical HF result of 16.1 kcal/mol reported in Section 3.5.

Similar values, based on H-bonding enthalpy for the dimers, do not reproduce the experimentally found stability of the chain structure for urea or (in case of AM1) the experimentally found stability of the ribbon structure for thiourea. Hence, we can conclude that the cooperative effects of H-bonding interactions dictate crystal structures of these compounds.

7.6 Conclusions

We have reported the results of molecular and crystal orbital studies on hydrogen-bonded molecular crystals of urea and thiourea. Non-empirical quantum chemical methods were applied to compare the relative stability of polymorphic modifications. The periodical Hartree-Fock method, which underestimates dispersion energy, recovers about a half of the crystal sublimation enthalpy and reveals significant non-additive effects of hydrogen bonding in different directions. Cluster

calculations allow the study of individual components of the interaction energy due to the different kinds of H-bonds in these crystals. The extrapolated results of cluster calculations are in quantitative agreement with periodical results. Non-additive effects were found to be a reason for experimentally observed differences in crystal structures of urea and thiourea. Since these effects are not reproduced by standard empirical force fields, *ab initio* methods can be a useful tool in calculating the relative stability of different polymorphic modifications.

Even though it is probably not feasible to directly apply *ab initio* methods to predicting crystal structures in the nearest future, they may ultimately be an important part of the complex approach to this problem. The global search and initial selection of the candidates can be performed only using the empirical force fields. *Ab initio* methods can provide the qualitative understanding and quantitative data necessary to improve these force fields. Moreover, these methods may be used at the final step of the search, to reveal the most stable among possible crystal structures.

PUBLICATIONS

The results of this thesis were published (in part) in the following papers:

Sections 3.1, 3.2, 3.3: Cardenes-Jiron, G.I., Masunov, A., Dannenberg J.J: Molecular orbital study of crystalline *para*-benzoquinone. <u>J. Phys. Chem. A</u>; **1999**, <u>103</u>(35); 7042-7046.

Sections 4.1, 4.4, 4.6: Masunov, A., Dannenberg, J.J.: Theoretical study of urea. I. Monomers and dimers <u>J. Phys. Chem. A</u>, **1999,** <u>103</u>(1), 178 –184.

Section 4.6: Giribet, C.G.; Vizioli, C.V.; Ruiz de Azua, M.C.; Contreras, R.H.; Dannenberg, J.J.; Masunov, A., Proximity effects on nuclear spin-spin coupling constants, Part 2. The electric field effect on 1J(CH) couplings. <u>J. Chem. Soc., Faraday Trans</u>. **1996**, <u>92</u>(17), 3029-3033.

Section 5.7: Dannenberg, J.J.; Haskamp,L.; Masunov, A. Are Hydrogen Bonds Covalent or Electrostatic? A Molecular Orbital Comparison of Molecules in Electric Fields and H-Bonding Environments, <u>J. Phys. Chem. A</u>; **1999**; <u>103</u>(35); 7083-7086.

Sections 5.2,5.4,5.6: Masunov, A., Dannenberg, J.J.: Theoretical study of urea and thiourea. II. Higher oligomers <u>J. Phys. Chem. B</u>; **2000**, <u>104</u>(4); 806-810.

Section 6.5: Masunov, A., Dannenberg, J.J. A theoretical investigation of the C-H...O interaction between substituted phenylacetylenes and water. <u>J. Mol. Str. THEOCHEM</u> **1996**, <u>371</u>, 17-19.

Chapter 7: Masunov, A., Dannenberg, J.J.: Theoretical study of urea and thiourea. III. 2,3D-clusters. <u>J. Phys. Chem. A</u>; **2000**, to be submitted.